

Report No. CDOH-DTD-CU-93-7

**A CASE STUDY OF ELASTIC
CONCRETE DECK BEHAVIOR
IN A FOUR-SPAN PRESTRESSED
BRIDGE: FINITE ELEMENT
ANALYSIS**

Li Cao
John H. Allen
P. Benson Shing
Department of Civil, Environmental,
& Architectural Engineering
University of Colorado
Boulder, Colorado 80309-0428

Final Report
January 1993

Prepared in cooperation with the
U.S. Department of Transportation
Federal Highway Administration

Technical Report Documentation Page

1. Report No. CDOT-DTD-CU-93-7		2. Government Accession No.		3. Recipient's Catalog No.	
4. Title and Subtitle A Case Study of Elastic Concrete Deck Behavior in a Four-Span Prestressed Girder Bridge: Finite Element Analysis				5. Report Date January, 1993	
				6. Performing Organization Code	
7. Author(s) Li Cao, John H. Allen, P. Benson Shing				8. Performing Organization Rpt.No. Research Series CU/SR-93/1	
9. Performing Organization Name and Address University of Colorado at Boulder Dept. of Civil, Environmental, & Architectural Engineering Boulder, CO 80309-0428				10. Work Unit No. (TRAIS)	
				11. Contract or Grant No. DOT92-061	
12. Sponsoring Agency Name and Address Colorado Department of Transportation 4201 E. Arkansas Ave. Denver, Colorado 80222				13. Type of Rpt. and Period Covered Interim, 6/92 to 1/93	
				14. Sponsoring Agency Code 80.00	
15. Supplementary Notes Prepared in Cooperation with the U.S. Department of Transportation Federal Highway Administration					
16. Abstract <p>The feasibility of eliminating the top mat of steel reinforcement in a concrete bridge deck was investigated using a finite element model. The elimination of the top level of steel is possible because of the flexibility of the girders. Girder deflections reduce the magnitude of maximum tensile and compressive stresses in the transverse directions. It is desirable to eliminate or reduce the amount of steel present in the top of the deck because this steel is subjected to corrosion from deicing chemicals.</p> <p>The deck is supported on precast concrete girders which represents a more severe case than a deck supported on steel girders. A linear elastic finite element model was used to investigate the behavior of the bridge deck when loaded with a 92-kip tandem-axle truck with 24-kip axle weights. The analysis results confirm that the elimination of the top mat of reinforcing steel is feasible.</p> <p>This reinforcement technique is being used in one span of a bridge under construction in early 1993. The test structure has been instrumented with strain gages in the experimental and control sections in order to validate the finite element model.</p> <p>Implementation: This technique may be implemented after the full results of this study are available.</p>					
17. Key Words bridge deck, corrosion, reinforcement, strain gages			18. Distribution Statement No Restrictions: This report is available to the public through the National Technical Info. Service. Springfield, VA 22161		
19. Security Classif. (report) Unclassified		20. Security Classif. (page) Unclassified		21. No. of Pages 136	22. Price

**A CASE STUDY OF ELASTIC CONCRETE DECK
BEHAVIOR IN A FOUR-SPAN PRESTRESSED
GIRDER BRIDGE: FINITE ELEMENT ANALYSIS**

by

Li Cao

John H. Allen

P. Benson Shing

Report to the Sponsor:
Colorado Department of Transportation

January 1993
Department of Civil, Environmental,
& Architectural Engineering
University of Colorado
Boulder, CO 80309-0428
Research Series No. CU/SR-93/1

Abstract

The influence of girder flexibility on bridge deck behavior has not been considered in the design and analysis of bridge decks. Hence, the actual bending stresses in bridge decks may vary significantly from values predicted by the current AASHTO design code. Cracking in the top exposes the top mat of reinforcing bars to chloride attack. The response of a 420-foot-long, 52-foot-wide, four-span continuous precast girder highway bridge under truck loads is evaluated to explore the feasibility of eliminating the top reinforcing bars from bridge decks.

A linearly elastic finite element model is used to investigate the prototype deck behavior under a 92-kip truck with tandem 24-kip axles. It has been found that the maximum tensile and compressive stresses in the transverse direction are nearly equal and both less than 300 psi at the abutment end of the bridge. Near midspan of the bridge, the maximum tensile stresses in the transverse direction are less than 120 psi, which is only 40% of the peak stress near the abutment. The maximum top compressive stresses in the transverse direction, due to the positive moment, are less than 550 psi, which is, however, 80% greater than the maximum compressive stress at the abutment. The analysis results confirm the feasibility of eliminating the top reinforcing bars of concrete bridge decks.

Acknowledgements

The writers gratefully acknowledge the financial support and technical cooperation provided by the Colorado Department of Transportation for this study. However, opinions expressed in this report are those of the writers and do not necessarily represent those of the sponsor.

Contents

1	INTRODUCTION	1
2	FINITE ELEMENT MODELING OF SLAB-GIRDER DECKS	4
2.1	Modeling Approaches	4
2.2	Comparison of Models	5
2.3	Experimental Verification	8
2.3.1	Design of Texas Experimental Deck	8
2.3.2	Comparison between Analytical and Experimental Models	8
3	MODELING OF PROTOTYPE BRIDGE DECK	22
3.1	Description of Prototype bridge	22
3.2	Bridge Loadings	23
3.3	Finite Element Analysis	25
3.3.1	Mesh Refinement	26
3.3.2	Replacement of Solid Elements by Equivalent Beam Elements	28
3.3.3	Finite Element Models	30

4	ANALYSIS RESULTS	49
4.1	Load Group 1	50
4.2	Load Group 2	51
4.3	Load Group 3	53
4.4	Effect of Concrete Railings	55
4.5	Effect of Deck Cracking	56
5	CONCLUSIONS	71
	REFERENCES	74
	APPENDIX A: STRESS CONTOURS AT THE TOP OF BRIDGE DECK	76
	APPENDIX B: DEFLECTION DIAGRAMS OF THE BRIDGE DECK	107

List of Figures

2.1	Typical Section of a Slab-Girder Deck	12
2.2	Simply Supported T-Beam	12
2.3	T-Beam Analysis with Solid Elements	13
2.4	T-Beam Analysis with Solid & Beam Element	14
2.5	T-Beam Analysis with Shell & Beam Elements	15
2.6	Compressive Stresses at Top of T-Beam (psi): (a) Solid Elements; (b) Solid & Beam Elements; (c) Shell & Beam Elements.	16
2.7	Configuration of Texas Experimental Bridge Deck	17
2.8	Solid & Beam Element Model for Bridge Deck	18
2.9	Shell & Beam Element Model for Bridge Deck	19
2.10	Transverse Bending Stresses in the Slab (Solid & Beam Model and P=20 kips)	20
2.11	Comparison of Transverse Bending Stresses at Top of the Slab (P=10 kips)	21
3.1	Configuration of the Four-Span Prototype Bridge	33
3.2	Plan View of Truck Load Pattern	34
3.3	Truck Loads-Group 1	35
3.4	Truck Loads-Group 2	36

3.5	Truck Loads-Group 3	37
3.6	Element Refinement in Longitudinal Direction of a One-Span Bridge: (a) Element Mesh in Transverse Direction; (b) Element Mesh in Longitudinal Direction (10 Elements); (c) Element Mesh in Longitudinal Direction (20 Elements); (d) Element Mesh in Longitudinal Direction (30 Elements).	38
3.7	Transverse Bending Stresses at Top of the Deck along Loading Section	39
3.8	Element Refinement in Transverse Direction of a One-Span Bridge: (a) Element Mesh in Longitudinal Direction; (b) Coarse Mesh near Girder Supports; (c) Fine Mesh near Girder Supports.	40
3.9	Comparison of Transverse Bending Stresses at Top of the Deck along Loading Section	41
3.10	Element Mesh with Equivalent Beams Replacing the Deck: (a) Element Mesh in Transverse Direction; (b) Element Mesh with Beam Elements in Two Spans; (c) Element Mesh with Beam Elements in Three Spans.	42
3.11	Comparison of Transverse Bending Stresses at Top of the Deck along Critical Section	43
3.12	Comparison of Longitudinal Bending Stresses at Top of the Deck along Critical Section	44
3.13	Element Mesh for Load Group 1	45
3.14	Determination of Equivalent Solid Elements for Diaphragm: (a) Section of the Diaphragm ; (b) Equivalent Solid Element.	46
3.15	Element Mesh for Load Group 2	47
3.16	Element Mesh for Load Group 3	48

4.1	Transverse Bending Stresses at Top of the Deck along Critical Transverse Section (Load Group 1)	58
4.2	Longitudinal Bending Stresses at Top of the Deck along Critical Longitudinal Sections (Load Group 1)	59
4.3	Transverse Bending Stresses at Top of the Deck along the Transverse Section (42-ft. from the Abutment) (Load Group 2)	60
4.4	Longitudinal Bending Stresses at Top of the Deck along Critical Longitudinal Sections (Load Group 2)	61
4.5	Transverse Bending Stresses at Top of the Deck along Two Different Transverse Sections (Case E of Load Group 2)	62
4.6	Transverse Bending Stresses at Top of the Deck along Critical Transverse Section under Cases C & E of Load Group 2	63
4.7	Transverse Bending Stresses at Top of the Deck along Critical Transverse Section (Load Group 3)	64
4.8	Longitudinal Bending Stresses at Top of the Deck along Critical Longitudinal Sections (Load Group 3)	65
4.9	Critical Transverse Bending Stresses at Top of the Deck under Three Load Groups	66
4.10	Bridge Deck with Concrete Railings	67
4.11	Comparison of Transverse Bending Stresses at Top of the Deck along Critical Transverse Section with and without Railings (Case B of Load Group 2)	68
4.12	Cracked Transformed Section of the Bridge Deck	69
4.13	Comparison of Transverse Bending Stresses at Top of the Deck along Critical Transverse Section with and without Cracking (Case A of Load Group 3)	70

List of Tables

2.1	Deflections at the Mid-Span of T-Beam	6
2.2	Errors in Compressive Stress along the Top Central Line of the Flange	7
2.3	Errors in Compressive Stress along the Top Exterior Edge of the Flange	7
2.4	Deflection of the Interior Girder at Loading Section (in.) . . .	10
2.5	Transverse Bending Stresses at Gage Points (ksi) (Analytical Model: Solid & Beam Elements)	10
3.1	Maximum Transverse Bending Stresses with Different Meshes	27
3.2	Moment of Inertia of the Equivalent Beam	29
4.1	Maximum Stresses at the Top of the Deck(ksi) (Load Group 1)	50
4.2	Maximum Stresses at the Top of the Deck(ksi) (Load Group 2)	52
4.3	Maximum Stresses at the Top of the Deck(ksi) (Load Group 3)	54

Chapter 1

INTRODUCTION

Most bridges constructed in North America have a reinforced concrete slab over supporting girders. Generally, the design for reinforced concrete decks has been based upon the “Westergaard Theory” (Westergaard 1930) which assumes that a slab behaves as a continuum over fixed linear supports. The current AASHTO code slab design provisions (*Standard Specifications* 1989) are based upon empirical rules derived from earlier adaptations of the Westergaard Theory (*Standard Specifications* 1935; AASHTO Minutes 1957-1961).

Newmark (1949) investigated the behavior of bridge decks and recommended that the slab design moment should account for girder deflections. Nowadays, the influence of girder flexibility on bridge deck behavior is still not considered in the design and analysis of bridge decks. Because of girder deflections, the maximum elastic stress in a bridge deck due to truck loads may vary significantly from that predicted by the AASHTO design moments. Consequently, a bridge deck may be over-reinforced or under-reinforced.

Current bridge deck reinforcing practice is to place both an upper and a lower mat of reinforcing bars. According to the AASHTO Specifications (1989), the design bending moment has the same value for top and bottom

transverse bars. Directly above the bottom transverse bars are placed longitudinal bars. The area of bottom longitudinal reinforcement is set to be proportional to the area of bottom transverse reinforcement required by the AASHTO code. The upper mat contains a top layer of transverse reinforcing bars over a longitudinal layer of bars. The required area of top transverse bars is usually greater than the area of bottom transverse bars since greater top cover reduces the effective depth. The longitudinal bars in the upper mat are intended to control temperature and shrinkage cracks.

Recent experience has indicated that apparent shrinkage cracking has dramatically worsened. It seems that these cracks often occur over the upper transverse bars, permitting increased exposure to deleterious substances such as deicing chemicals. However, longitudinal cracks are not prevalent over the girders. Investigations on the behavior of bridge decks by Beal (1982) and Fang et al. (1990) have shown that the maximum negative bending moments, or top tensile stresses, are very low, much less than the maximum positive bending moments or stresses. Analysis of their work and other empirical evidence by Allen (1991) indicates that the tensile strength of deck concrete greatly exceeds the maximum top tensile stress induced by truck loads. However, this analysis applies only to the interior portions of the bridge span, where deflection of the girders is greatest. It is expected that the highest negative bending moments in the deck will occur in the vicinity of the supports.

The purpose of this research project is to investigate the response of a typical highway bridge deck under truck loads and determine the magnitude of stresses at the top of the bridge deck. The maximum tensile stress under truck loads will be compared to the cracking strength of deck concrete. This investigation is divided into two parts. The first part consists of the devel-

opment of a finite element model of the prototype bridge deck and stress analysis of the deck under truck loads. The second part of the investigation involves the instrumentation of the prototype bridge and monitoring the response of the prototype bridge subjected to a test truck and then actual highway loads.

This report describes the first part of the project. The essence of this investigation is to determine the maximum tensile stresses at the top and bottom of the prototype bridge deck using a linearly elastic finite element model, which has been chosen in view of the belief that flexural cracking is not prevalent in bridge decks. A special truck load was developed that is heavier than the prevalently used standard truck (HS20-44) for bridge design. The non-standard truck was chosen to provide a more conservative load condition for the finite element analysis.

Chapter 2

FINITE ELEMENT MODELING OF SLAB-GIRDER DECKS

2.1 Modeling Approaches

A typical bridge deck consists of a concrete slab supported by steel or concrete girders. The slab is often connected to girders by shear connectors, which transfer shear forces from the slab to girders. A typical section of a slab-girder deck is shown in Fig. 2.1. To investigate the stress state of a bridge deck, the most refined approach is to use the finite element method. In recent years, several researchers have proposed different finite element models for bridge decks (Razaqpur and Noful 1989; Fang et al. 1990; Lin et al. 1991; Mufie et al. 1991; Memari and West 1991).

In the analytical model proposed by Lin et al. (1991), the concrete slab, and the flanges and webs of steel girders are modeled by triangular plate elements. In their study, 3-D bar elements are used to simulate shear connectors, which combine the uniaxial and shear-slip behaviors. The 3-D bar

elements connect the nodes at the top of steel girders to those at the mid-plane of a slab. In the analytical model proposed by Fang et al. (1990), two layers of solid elements are used to represent a concrete slab, and steel girders are modeled with 3-D beam elements, which are connected to the concrete slab by rigid links. This analytical model was validated by laboratory tests conducted on a one-span three-girder deck.

2.2 Comparison of Models

To compare the different modeling approaches, a simply supported T-beam with a concentrated load at the mid-span has been analyzed by three different finite element models. One model is using 3-D solid elements for both the flange and the web of the T-beam. This model can be considered as the most accurate among the three. For the other two models, solid and shell elements are used, respectively, to model the flange, 3-D beam elements are used for the web, and rigid links are used to connect the flange to the web to form a composite beam. Rigid links, which are simulated by beam elements of very high stiffness, connect the bottom nodes of the flange to the beam elements.

A structural analysis program, SAP90 (Wilson et al. 1989), running on a personal computer has been selected for the computation. SAP90 has evolved from finite element analysis programs SAPIV, SAPV, and SAP80, and has proven to be reliable and versatile for structural analysis. The element library of SAP90 contains four types of elements. These are beam, eight-node solid, four-node shell, and plane quadrilaterals elements. The solid element is an 8-node brick element with conforming and non-conforming deformation modes. To avoid shear locking, the non-conforming solid element is used in our finite element models. The shell element is a 4-node element formulation which

Table 2.1: Deflections at the Mid-Span of T-Beam

Model	Deflection($\times 10^{-3}$ in.)
Beam Theory	1.039
Solid Elements	1.079
Solid & Beam Elements	1.108
Shell & Beam Elements	1.073

has a combination of membrane action and plate bending behavior. The plate bending behavior does not include any effect of shear deformation. The preprocessor and post-processor of SAP90 are able to generate element meshes and color-coded stress contour plots that are easy to read.

The geometric configuration of the simply supported T-beam with a concentrated load at the mid-span is shown in Fig. 2.2. The three different finite element models used for the T-beam are shown in Figs. 2.3 through 2.5.

Deflections at the mid-span of the T-beam computed with the different models are shown in Table 2.1. It is found that all three models give results that are very close to the solution obtained with the simple beam theory which neglects the shear-lag phenomenon.

Computed stress variations at the top of the flange are shown in Fig. 2.6. It is found that all three finite element analysis models are able to capture the shear-lag developed in the flange of the T-beam. Considering that the results obtained with the solid elements (Fig. 2.3) are accurate and using them as the comparison standard, errors in the bending stresses at the top of the T-beam obtained with the solid & beam and shell & beam models are computed and shown in Tables 2.2 and 2.3. Here, Section 1 is the loading section and located at the mid-span of the T-beam. It can be seen that

Table 2.2: Errors in Compressive Stress along the Top Central Line of the Flange

Section	1	2	3	4	5	6	7
Distance from Mid-Span (in.)	0.0	7.5	15	22.5	30	37.5	45
Solid & Beam (% error)	-19.56	-0.74	+20.14	+2.53	+4.33	+8.66	+40.88
Shell & Beam (% error)	+46.43	-4.46	+16.87	-0.06	+1.71	+6.99	+39.37

Table 2.3: Errors in Compressive Stress along the Top Exterior Edge of the Flange

Section	1	2	3	4	5	6	7
Distance from Mid-Span (in.)	0.0	7.5	15	22.5	30	37.5	45
Solid & Beam (% error)	+0.46	+2.26	+3.75	+1.66	-0.17	+0.76	+5.99
Shell & Beam (% error)	+6.42	+4.19	+1.27	+0.4	+0.18	+6.5	+9.48

the last two models produce results that are very close to those obtained with solid elements. Usually, better results are at sections away from the restrained edges and supports.

From the stress analysis of a simply supported T-beam, it is verified that solid elements and shell elements connected to 3-D beam elements via rigid links are able to represent the bending behavior of a composite beam reasonably well.

2.3 Experimental Verification

A one-span, slab-girder bridge deck that was tested at the University of Texas at Austin (Fang et al. 1990) is used to compare the solid & beam and shell & beam models.

2.3.1 Design of Texas Experimental Deck

The one-span, slab-girder bridge deck tested at the University of Texas at Austin was 49-ft long, and three W36X150 girders were spaced at a center-to-center distance of 7 ft., as shown in Fig. 2.7. The thickness of the concrete slab was 7.5 in. One half of the concrete slab was a precast concrete panel with a design concrete compressive strength of 6,000 psi, and the other half was a cast-in-place concrete slab with a design concrete compressive strength of 3,600 psi. The concrete deck was subjected to four-point wheel loads as shown in Fig. 2.7. The concrete deck was loaded to failure.

As shown in Fig. 2.7, there was a strain gage at the top of the deck near one of the wheel loads (point A). There were two strain gages at bottom of the deck. One was near the interior girder (point B) and another was near the exterior girder (point C). These three strain gages measured the transverse bending stresses in the deck.

2.3.2 Comparison between Analytical and Experimental Models

Because of the symmetry of the deck configuration and loading conditions, only one half of the experimental bridge deck that consisted of a cast-in-place concrete slab is analyzed. The difference in mechanical properties between

the cast-in-place concrete slab and the precast panel is ignored. The mechanical properties of the cast-in-place concrete are specified as follows: the modulus of elasticity $E_c = 4,095$ ksi, in accordance with the ACI recommendation (1989) that $E_c = 57,000\sqrt{f'_c}$, where $f'_c = 5,160$ psi (based on cylinder tests), and the Poisson's ratio is assumed to be 0.2. Steel girders have a modulus of elasticity of 29,000 ksi and a shear modulus of 11,154 ksi. The finite element model with solid and beam elements is shown in Fig. 2.8, and the model with shell and beam elements is shown in Fig. 2.9. In the former, two layers of solid elements are used for the concrete slab, and rigid links are connected to the nodes at the bottom of the slab. This arrangement is similar to the modeling approaches used by Fang et al. (1990). For the convenience of comparison, the two analytical models have the same mesh configuration in plan view.

There is a diaphragm at the mid-span of the experimental deck, which enhanced the lateral stability of the girders. This condition is simulated by restraining the lateral movements of the girders at the mid-span.

When each of the concentrated loads was increased from 5 to 20 kips, there was no cracking observed in the experimental deck. The analysis and test results on the deflection of the interior girder at the loading section are shown in Table 2.4. It is found that the deflection of the interior girder obtained with the solid & beam model is very close to the test result. For the shell & beam model, the computed deflection of the interior girder is quite good, but it is not as close to the test result as that obtained with the solid & beam model.

Table 2.5 shows the transverse bending stresses obtained by experiment and by the solid & beam model. The comparison of these stresses, when each of the wheel loads on the deck equals 20 kips, is shown in Fig. 2.10. It can

Table 2.4: Deflection of the Interior Girder at Loading Section (in.)

Load P (kips)	Test	Solid&Beam	Shell&Beam
5	0.032	0.033	0.038
10	0.068	0.065	0.075
15	0.100	0.098	0.113
20	0.135	0.130	0.151

Table 2.5: Transverse Bending Stresses at Gage Points (ksi) (Analytical Model: Solid & Beam Elements)

Load P (kips)	Point A (Top)		Point B (Bott.)		Point C (Bott.)	
	Test	Analysis	Test	Analysis	Test	Analysis
5	0.099	0.092	0.020	0.023	0.011	0.015
10	0.171	0.185	0.051	0.046	0.023	0.030
15	0.284	0.277	0.065	0.069	0.045	0.044
20	0.379	0.369	0.106	0.093	0.061	0.059

be seen that the transverse stresses in the concrete slab obtained with the solid & beam model are very close to the test results.

Figure 2.11 shows the comparison of the transverse bending stresses at the top of the deck obtained with the solid & beam and shell & beam models, respectively, for P equal to 10 kips. It can be seen that the stresses in the deck obtained with the shell & beam model are quite different from those obtained with the solid & beam model. The shell & beam model does not give stresses that are close to test results.

From the comparison of numerical and test results, it can be concluded that a finite element model with solid and beam elements is better suited

for the stress analysis of bridge decks than a model with shell and beam elements.

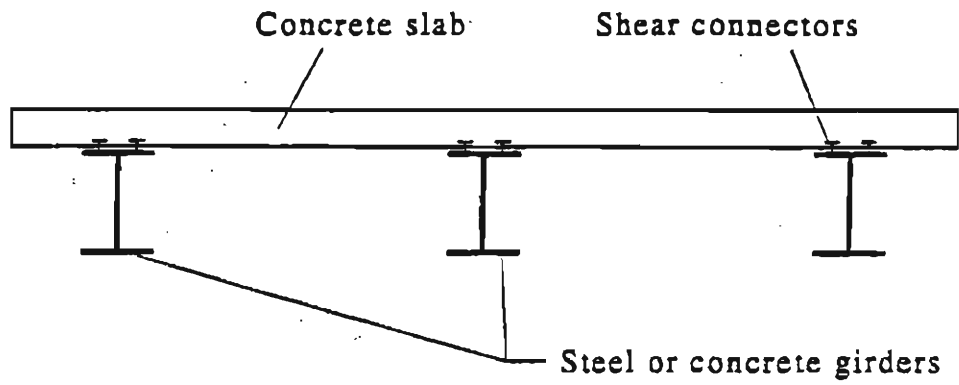


Figure 2.1: Typical Section of a Slab-Girder Deck

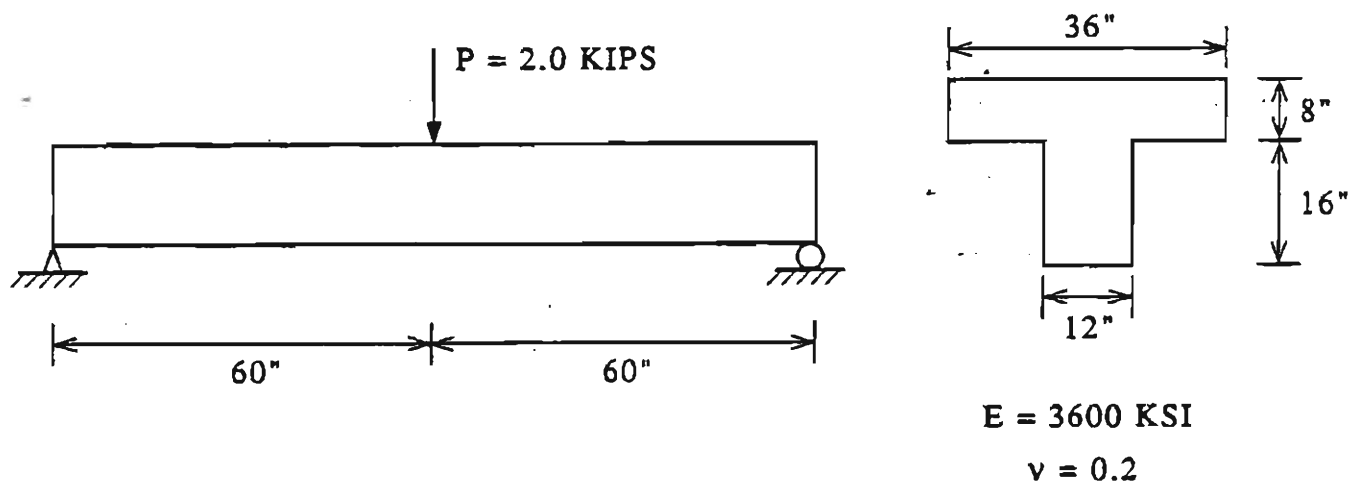


Figure 2.2: Simply Supported T-Beam

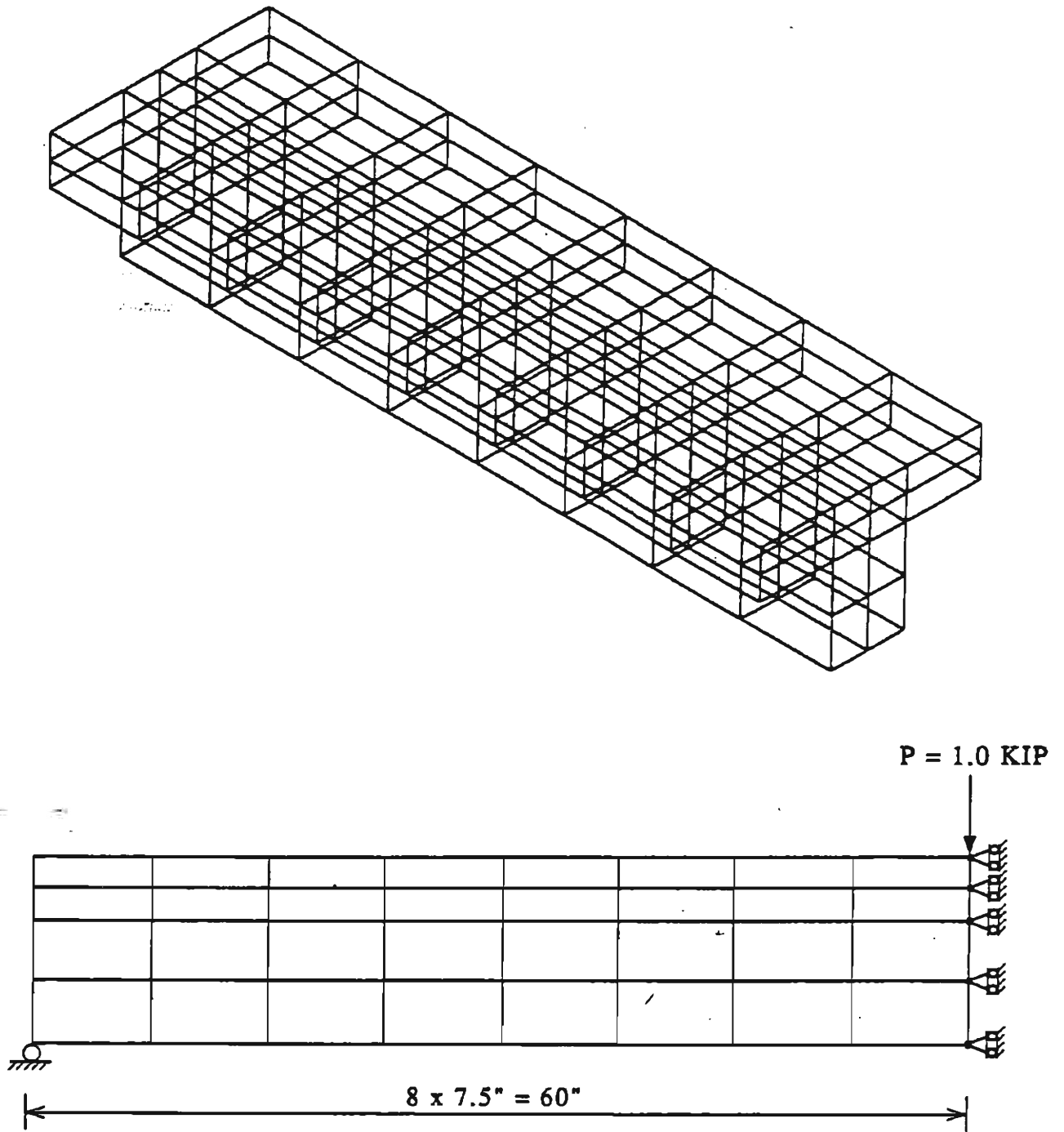


Figure 2.3: T-Beam Analysis with Solid Elements

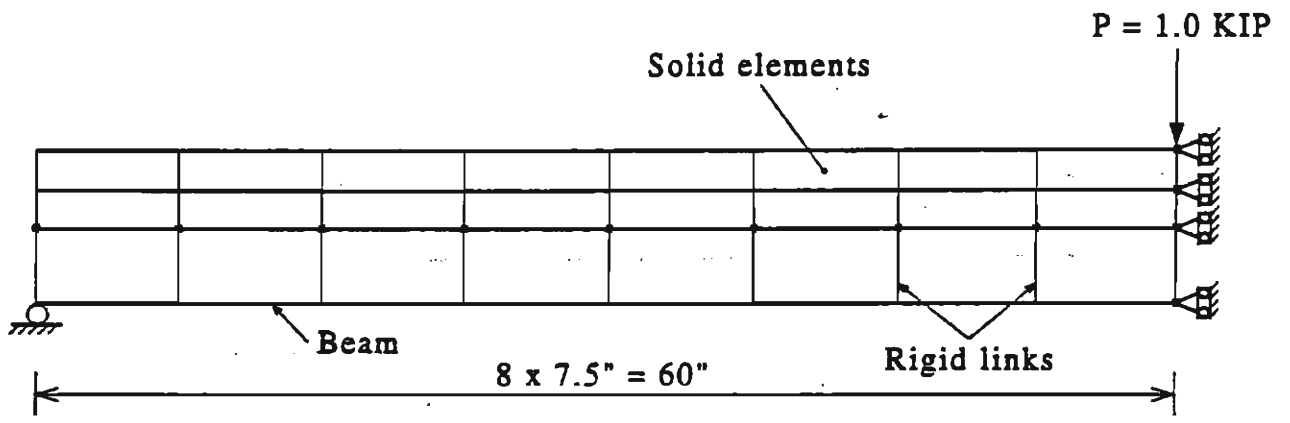
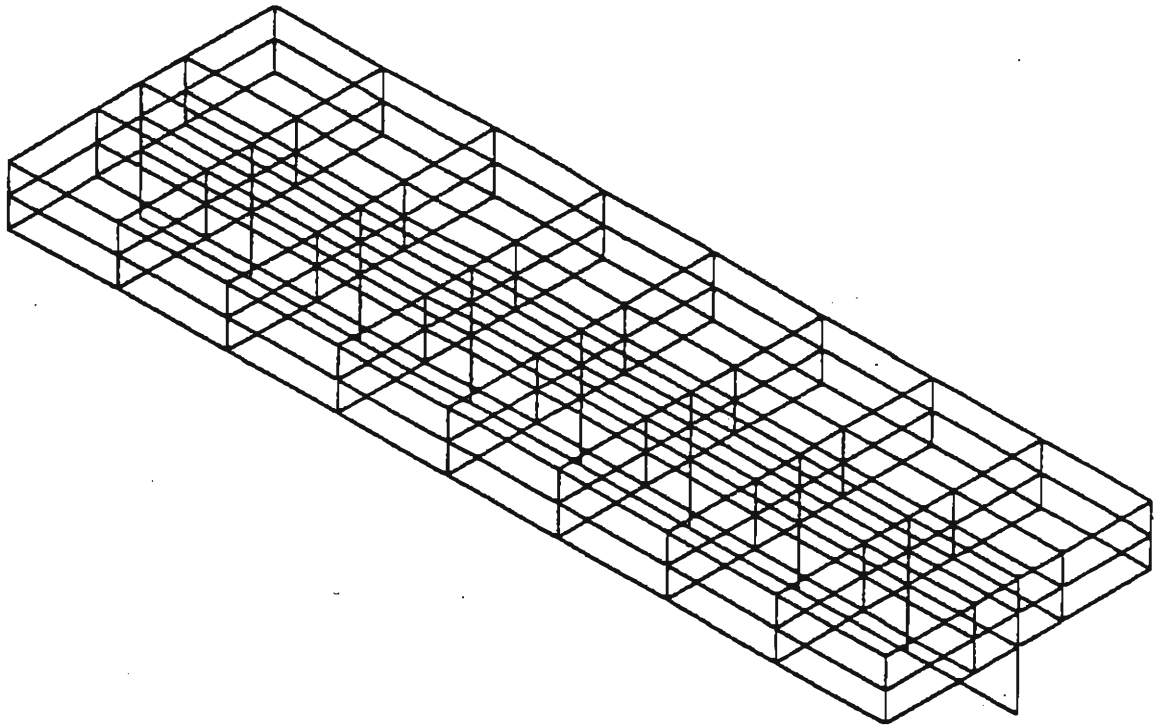


Figure 2.4: T-Beam Analysis with Solid & Beam Element

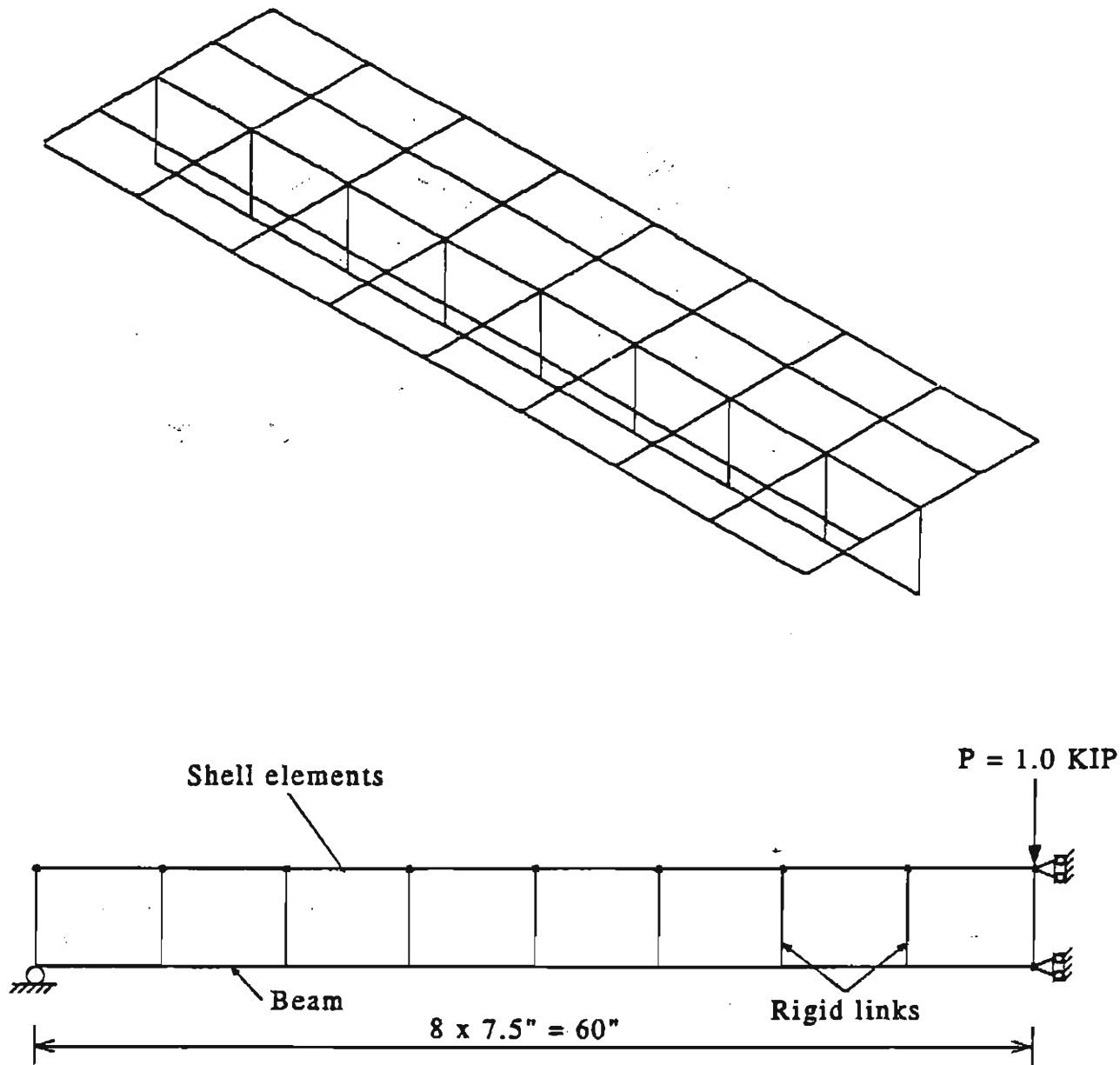
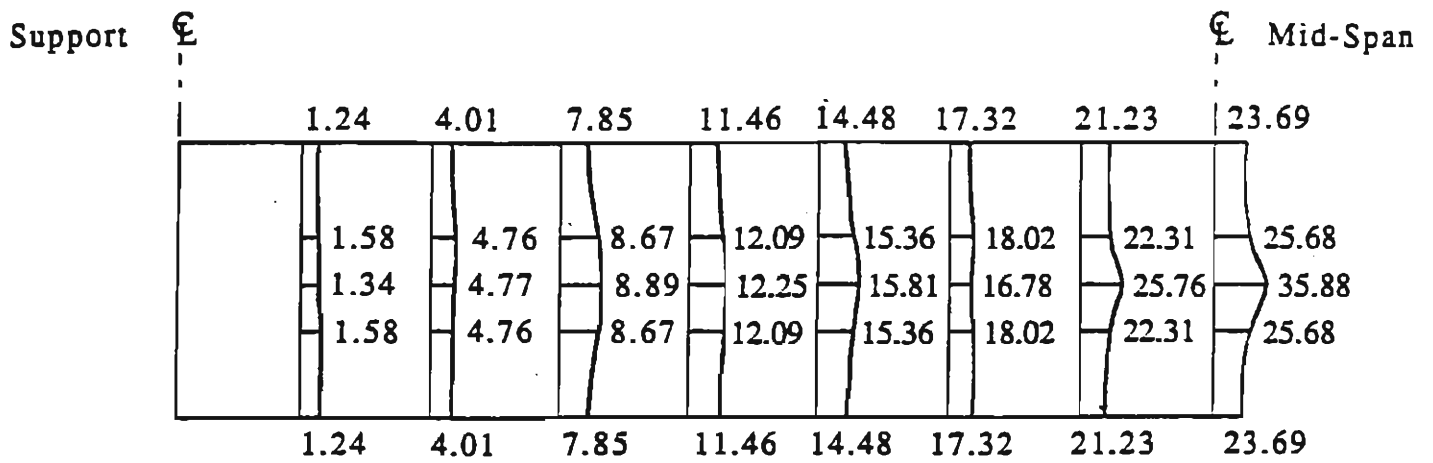
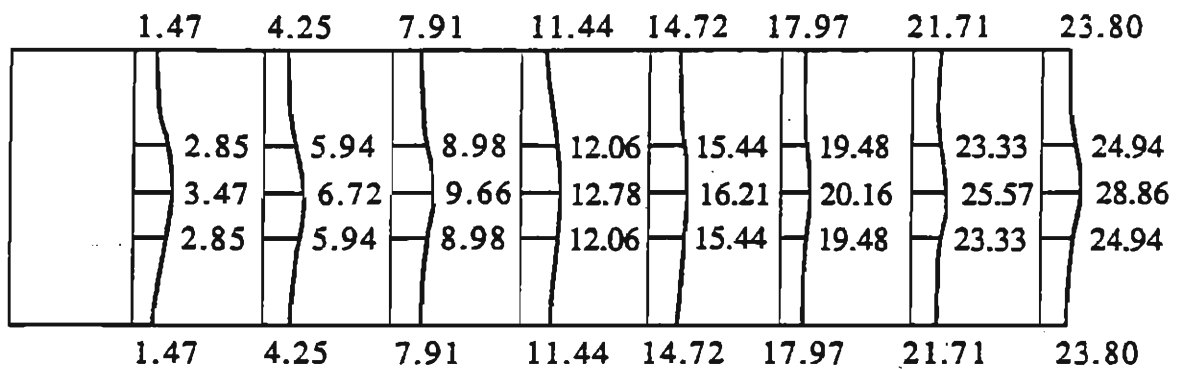


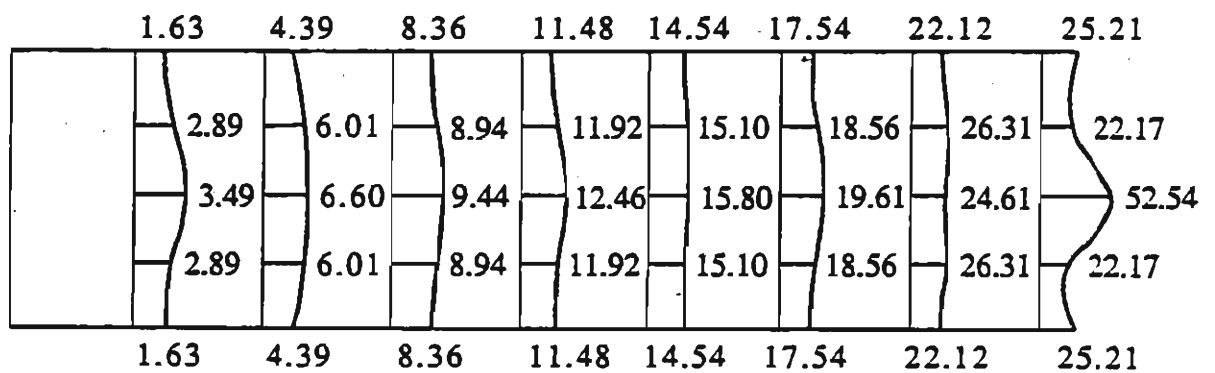
Figure 2.5: T-Beam Analysis with Shell & Beam Elements



(a)



(b)



(c)

Figure 2.6: Compressive Stresses at Top of T-Beam (psi): (a) Solid Elements; (b) Solid & Beam Elements; (c) Shell & Beam Elements.

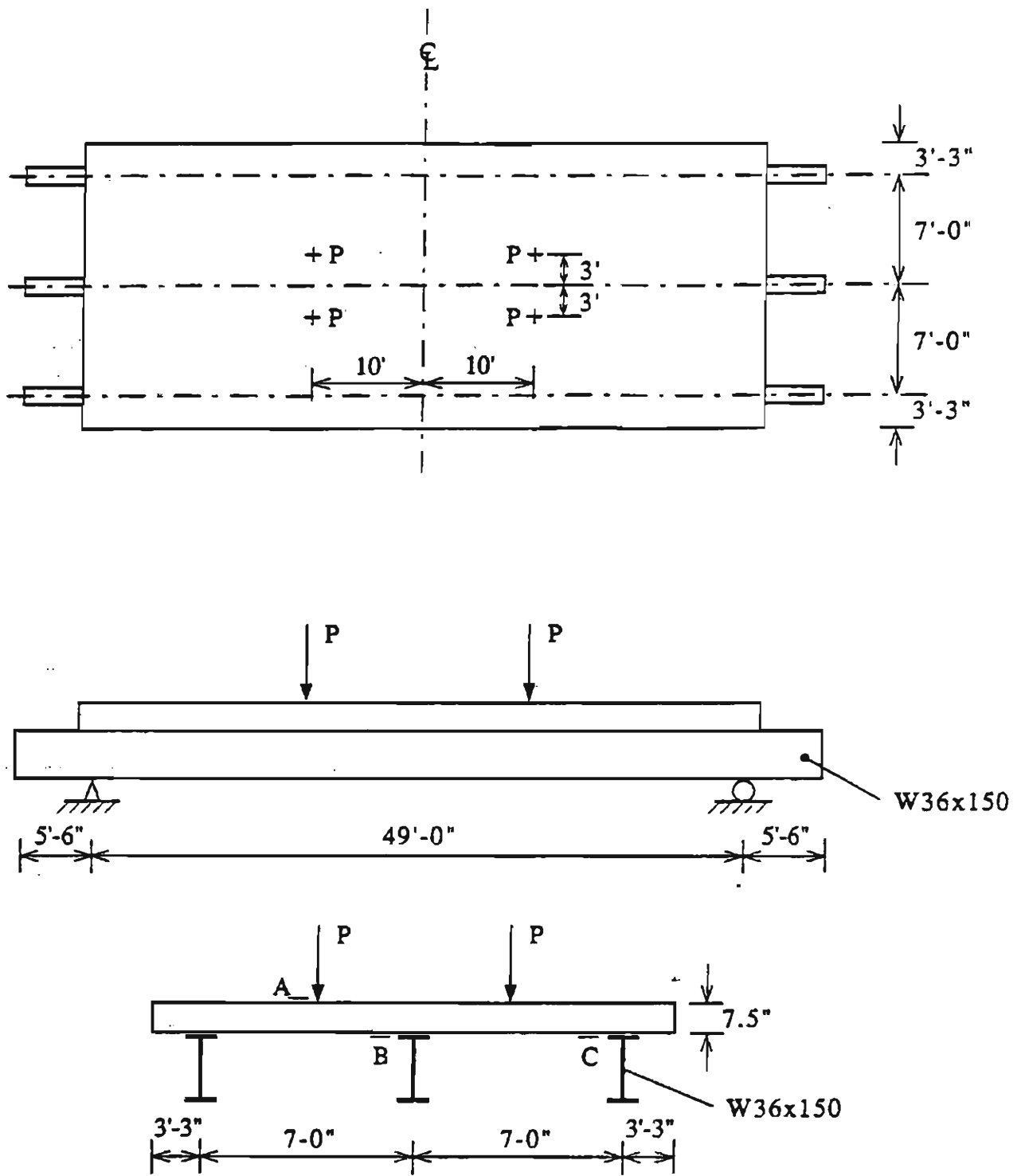


Figure 2.7: Configuration of Texas Experimental Bridge Deck

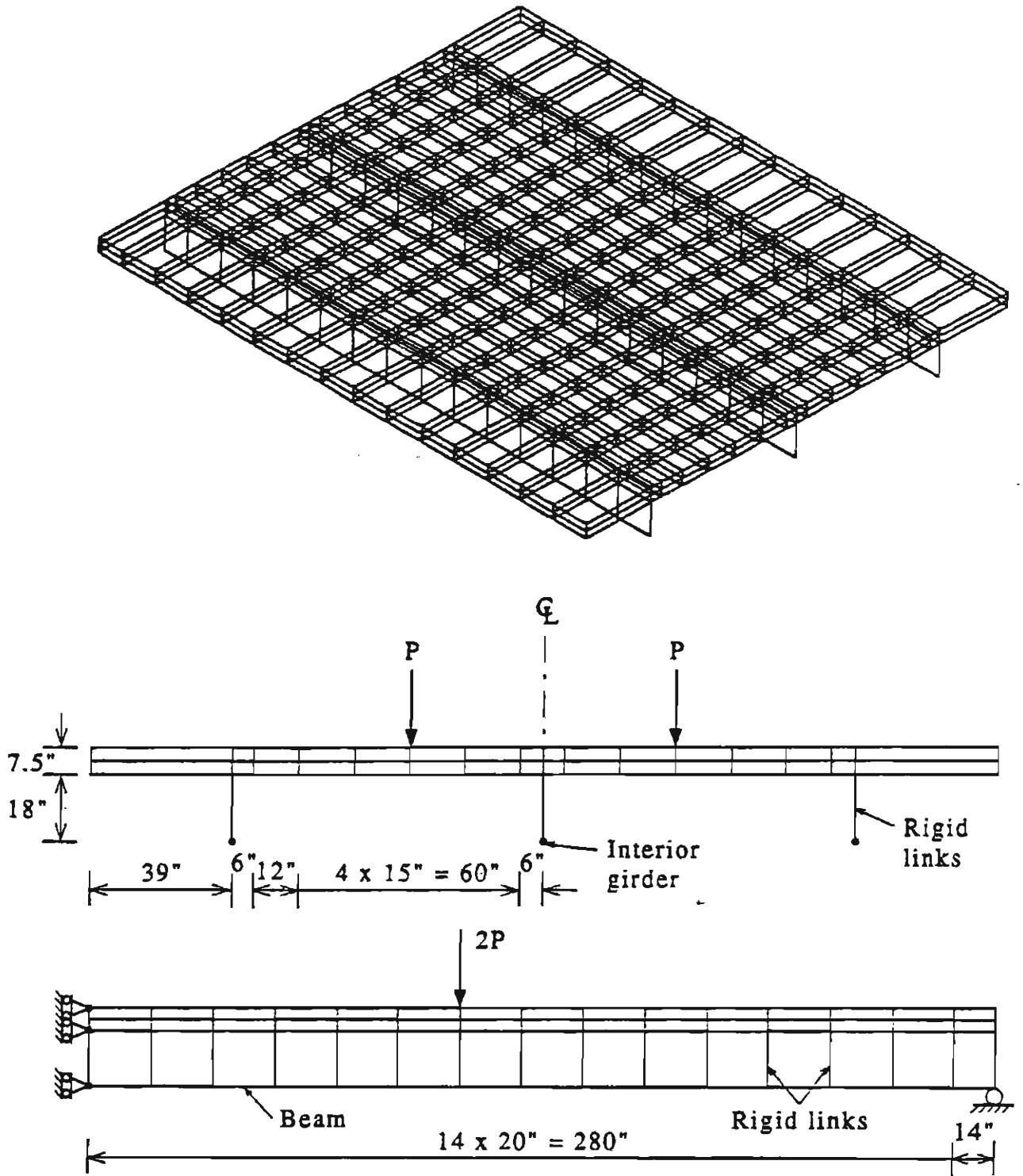


Figure 2.8: Solid & Beam Element Model for Bridge Deck

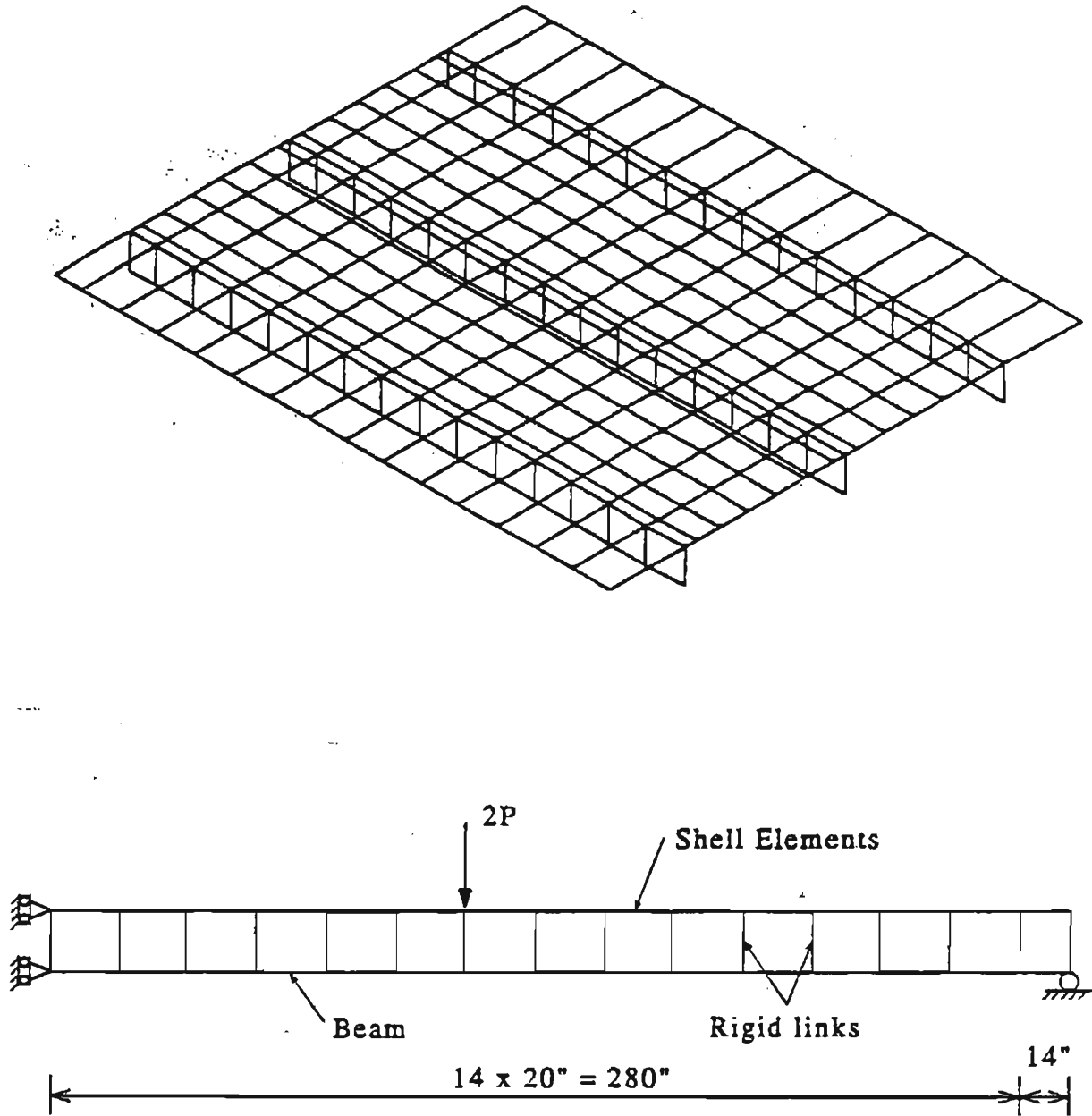


Figure 2.9: Shell & Beam Element Model for Bridge Deck

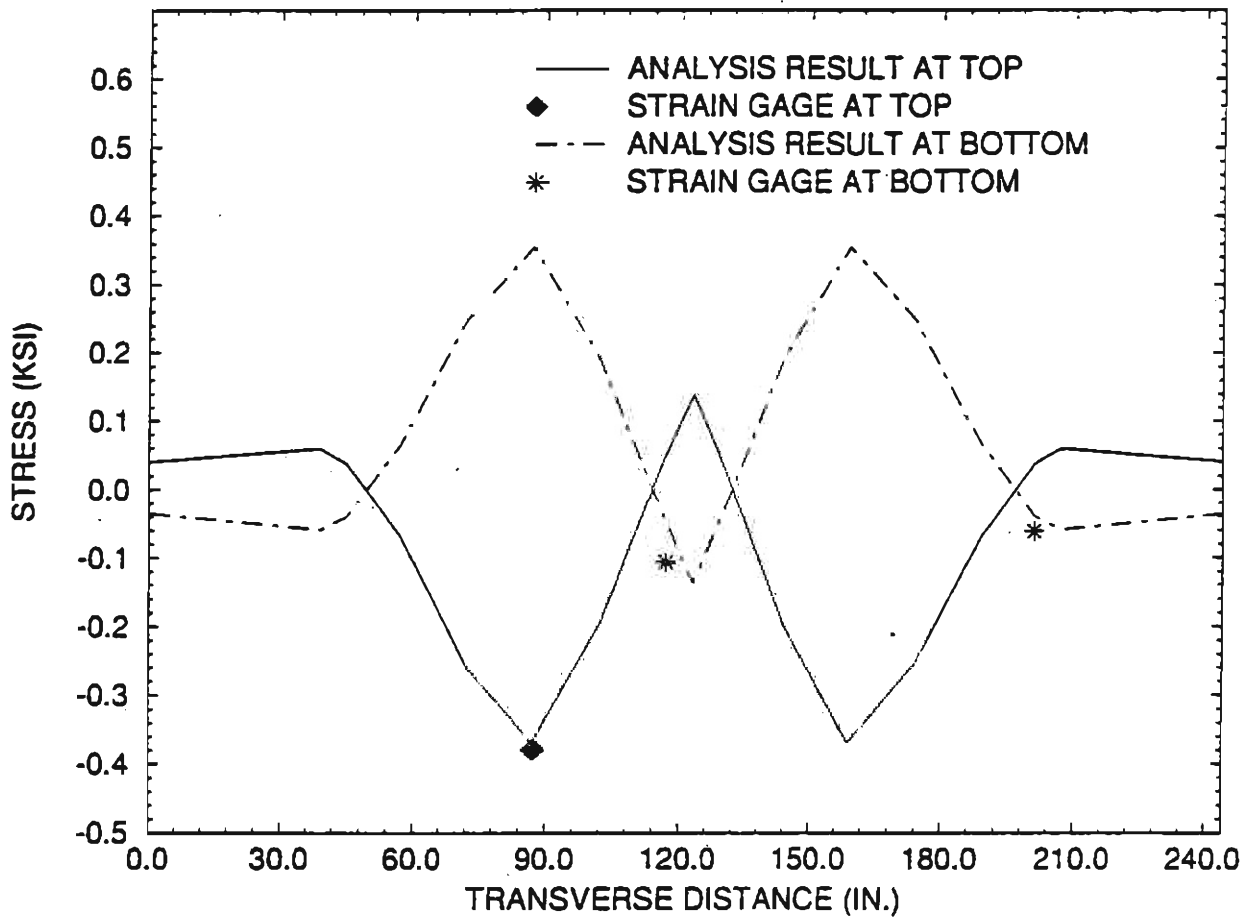


Figure 2.10: Transverse Bending Stresses in the Slab (Solid & Beam Model and P=20 kips)

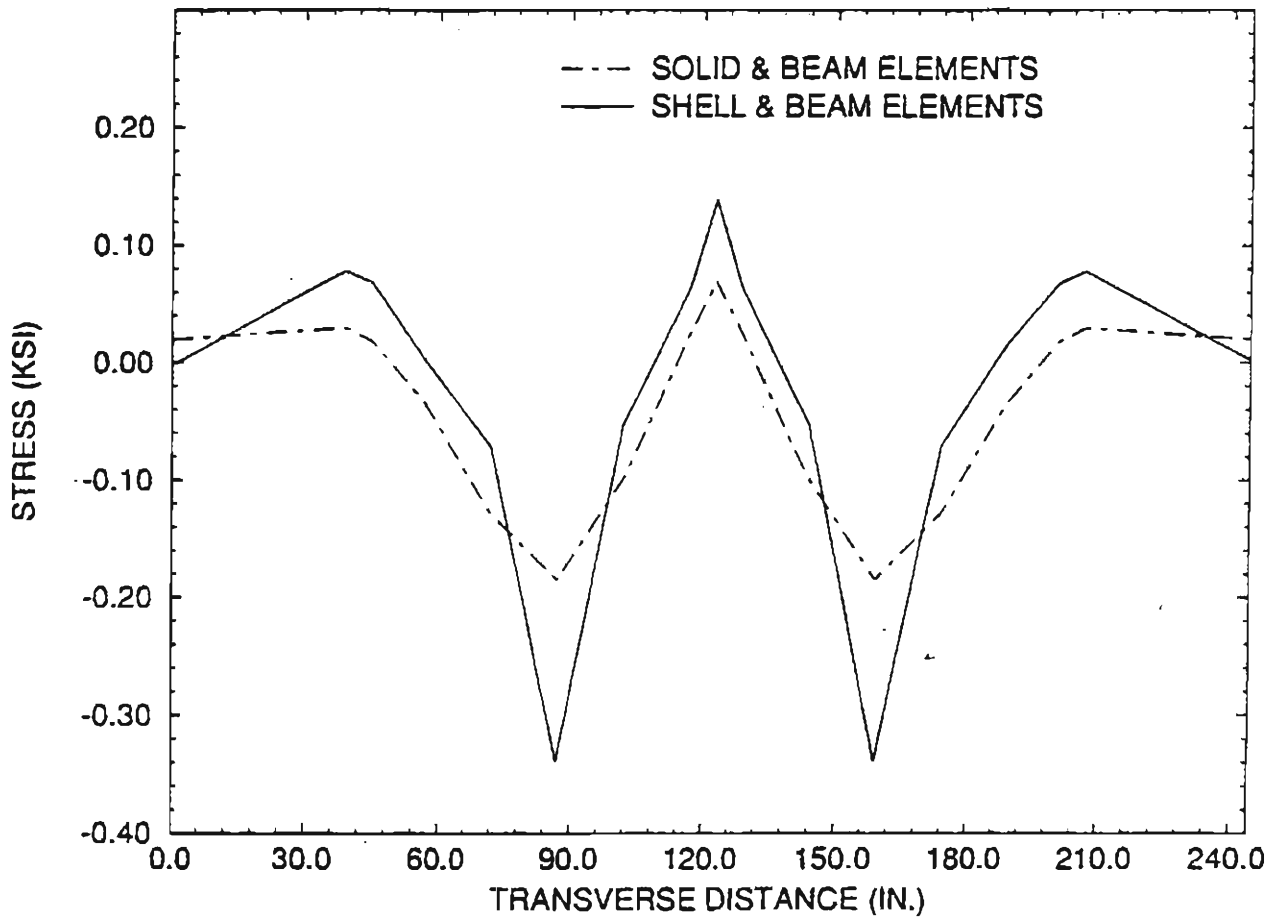


Figure 2.11: Comparison of Transverse Bending Stresses at Top of the Slab (P=10 kips)

Chapter 3

MODELING OF PROTOTYPE BRIDGE DECK

3.1 Description of Prototype bridge

The prototype bridge selected for this project is located on Colorado State Route 224 over the South Platte River near Commerce City. It is a 420-ft long and 52-ft wide bridge. The superstructure consists of four equal continuous spans. The supporting girders are standard precast Colorado Type G-54 girders spaced at approximately eight feet on center. The deck thickness for the prototype bridge is 8.0 in. to comply with the new design requirement adopted by the Colorado Department of Transportation. In the finite element model, a 7.5-in thick deck was used, based on the preliminary bridge design. The analysis results from the finite element model with the thinner deck are expected to be conservative. The configuration of the four-span bridge is shown in Fig. 3.1.

The prototype bridge deck has an eight-degree angle of skew. Because

the angle of skew is small, it is ignored in the stress analysis.

The specified 28-day concrete strength for the prototype bridge deck is 4,500 psi. Thus, the flexural tensile strength of the deck concrete is expected to vary from 470 psi to 805 psi ($7\sqrt{f'_c} \sim 12\sqrt{f'_c}$) (ACI 1992). Usually, the compressive strength of deck concrete obtained from field tests greatly exceeds the specified design strength. Test results indicate that bridge deck concrete used in Colorado often attains a 28-day strength of 6,000 psi if the design compressive strength is 4,500 psi. Consequently, the actual average tensile strength of deck concrete may be in the range of 542 psi to 930 psi. Therefore, it is conservative to assume that no deck cracking will be induced by truck loads if the maximum tensile stress is less than 470 psi.

3.2 Bridge Loadings

The current AASHTO Specifications (1989) for the design of bridge decks adopt an empirical equation that was first incorporated into the eighth edition published in 1961. This empirical design equation has approximately the same value of moment as that calculated by earlier editions of the code for the modified military load. These earlier editions are an adaptation of the "Westergaard Theory". The modified military load consists of two 24-kip axles spaced four-feet apart. According to these earlier editions of the AASHTO Specifications, the design moment for the HS20 truck would be calculated using two 16-kip axles instead of a single 32-kip axle. The slab design moment for the modified military load is 50% larger than that for the HS20 truck. This change from the earlier editions concealed the fact that military axles rather than the HS20 truck is used for the slab design.

As shown in Fig. 3.2, the truck load selected for our model includes the

tandem 24-kip axles from the modified military truck load. A front axle of 12 kips is selected, which is 25 percent of the total load of the tandem axle group. The weight of the front axle for the conventional AASHTO H-truck is also 25 percent of the rear axles. The total weight of the front and rear tandem axles of this model truck corresponds to an AASHTO H-30 truck. This load is also representative of a typical tandem axle dump truck. A 32-kip trailing axle as used for the standard HS20 truck is also used on our model truck. The axle and wheel spacing of the model truck are similar to that of the standard HS20 truck. The resulting model truck weighs 92 kips, which is 28 percent more than a conventional HS20 truck.

For the stress analysis, it has been decided that the model truck will be in three different longitudinal positions on the bridge. The first position is close to the abutment. The deflection of girders is smallest in this position. It is expected that the critical section of transverse tensile stresses will occur beneath the 24-kip axles. The trailing axle (32 kips) and the front axle (12 kips) will be not used in this load case, since these axle loads in the span are thought to increase the girder deflection and, thereby, decrease the top transverse tensile stresses. This assumption has been verified by analysis. Along the transverse direction, the wheels of either one or two trucks are positioned at five different locations, as illustrated in Fig. 3.3. For the load case where the top tensile stresses are maximum, the truck position is incrementally moved closer and farther from the abutment to obtain the longitudinal position causing the maximum top transverse tensile stresses.

The second longitudinal truck position is near the mid-span of the deck, approximately at the location of maximum moment in the girders. This causes the maximum deflection as well as differential deflections between the girders. One or two trucks are placed transversely in five positions, as

illustrated in Fig. 3.4.

The third longitudinal truck load position is in the vicinity of the pier. The bridge is continuous in this region so that the front axle and trailing axle are included, as shown in Fig. 3.5.

In all three truck load groups, it is expected that the positions of wheel loads in the transverse direction will cause severe transverse tensile stresses in the bridge deck.

3.3 Finite Element Analysis

For the elastic stress analysis of a four-span bridge deck, it is impossible to use solid elements to model both the concrete slab and the girders due to the limitation of the computer capacity. As shown earlier, using solid elements for the concrete slab and 3-D beam elements for the girders is a suitable approach. This analytical model produces quite accurate results for stresses. In the finite element model adopted here, two layers of solid elements are used to model the concrete slab and rigid links are used to connect the nodes at the bottom of the slab to the centroids of the girders which are represented by 3-D beams. The area and moment of inertia of each girder of the prototype bridge are 631 in.^2 and $242,585 \text{ in.}^4$, respectively.

There is a concrete diaphragm at the mid-span of each span. The diaphragm is modeled by beam elements which are connected to the centroids of the girders. These beam elements have a 24-in.-high and 8-in.-wide rectangular section. The connection between the diaphragm and the slab is not considered in the analytical model.

An impact factor of 1.3 is applied to the truck loads in the analysis, based on the AASHTO Specifications. The modulus of elasticity and the Poisson's

ratio are taken to be 3,600 ksi and 0.2, respectively.

3.3.1 Mesh Refinement

There are two main considerations in the finite element analysis of structures. One is the selection of a suitable element mesh. The other is the limitation of the computer capacity. When selecting an element mesh, places of stress concentration and high stress gradient require refined meshes. The general approach of selecting a finite element mesh is to select a coarse mesh for places where the solution is known to be smooth and a fine mesh for places where the stress is expected to vary rapidly.

In this study, the most important consideration is the maximum tensile stresses produced by transverse negative bending moments. Usually, these stresses occur at the top of the deck in the vicinity of supporting girders. Therefore, a suitable mesh should be chosen to obtain accurate stresses at these sites. The strategy used here to select a mesh is to vary element sizes in the longitudinal and transverse direction independently, and a suitable element size is determined by the convergence of these stresses.

(1) Mesh Refinement in the Longitudinal Direction

To determine an appropriate mesh, the four-span bridge deck is reduced into a simply supported one-span bridge deck with a span length of 399 in. and seven equally spaced girders with the same stiffness. The 7.5-in thick concrete slab is modeled with two layers of solid elements. The concrete slab between two girders is discretized into seven solid elements, which represent a quite fine mesh in the transverse direction of the deck. Furthermore, with the mesh in the transverse direction fixed, it is divided into 10, 20 and 30 elements, respectively, in the longitudinal direction. Such arrangements lead to element aspect ratios (length/thickness) of 10.64, 5.32 and 3.55, respectively. The

Table 3.1: Maximum Transverse Bending Stresses with Different Meshes

Longitudinal Divisions	Element Aspect Ratio	Max. Tensile Stress (ksi)	% Error with Respect to 30 Elements
10 Elements	10.64	0.467	17.54
20 Elements	5.32	0.545	3.73
30 Elements	3.55	0.566	0.0

procedure of refining the mesh in the longitudinal direction is shown in Fig. 3.6.

With two 50-kip point loads applied at the mid-span of the deck, stresses are computed with the different meshes. The transverse bending stresses at the top of the deck along the loading section are shown in Fig. 3.7. The maximum transverse bending stresses at the top of the deck obtained with the different meshes are compared in Table 3.1, where the maximum transverse tensile stress obtained with 30 elements is used as the comparison standard. Based on the results in Table 3.1, it is estimated with a quadratic interpolation that using an element aspect ratio not greater than 6.67 can lead to good results in stress analysis.

(2) Mesh Refinement in the Transverse Direction

It is necessary to determine the number of elements be used between a wheel load and a girder, and in areas of high stress gradients. The simply supported one-span bridge deck is investigated using two different meshes in the transverse direction, as shown in Fig. 3.8. There are 30 solid elements in the longitudinal direction of the deck for both cases. There is only one solid element between a wheel load and a girder for the coarse mesh, and two solid elements for the fine mesh.

Analysis results obtained with the coarse mesh indicate that the maximum transverse compressive and tensile stresses do not occur beneath the point loads or above the girders. This means that stresses at these sites are greatly distorted. When the fine mesh is used, such phenomenon of stress distortion virtually disappears. Transverse bending stresses at the top of the deck along the loading section, as illustrated in Fig. 3.9, clearly indicate that using the fine mesh will dramatically change the computed stresses in areas of high stress gradients. Hence, it is apparent that there should be at least two solid elements between a wheel load and a girder for stress analysis. Based on these considerations, a mesh of eight elements in the transverse direction between each pair of girders has been chosen.

3.3.2 Replacement of Solid Elements by Equivalent Beam Elements

Because the computer capacity is limited, it is impossible to represent the entire four-span bridge slab with solid elements. A strategy for simplification is to use equivalent beams to account for the effect of the slab-girder composite in three spans, and have a fine mesh in the end span. The equivalent beam has a 54-in.-high and 42.2-in.-wide rectangular section, whose moment of inertia is equal to that of a composite T-beam section consisting of one girder and a concrete slab, which has a width equal to the center-to-center distance between two girders. The moment of inertia of the equivalent beam is 553,792 in.⁴, and the procedure of calculating it is shown in Table 3.2.

To examine the effect of this modification, the four-span bridge deck is analyzed with two different models. One is using the equivalent beams to model two spans, with the slab in the remaining two spans modeled by solid elements. The other is using the equivalent beams to model three spans,

Table 3.2: Moment of Inertia of the Equivalent Beam

Components	$A_i(\text{in.}^2)$	$I_i(\text{in.}^4)$	$y_i(\text{in.})$	$A_i y_i$	$Y_i(\text{in.})$	$A_i Y_i^2$	$I_i + A_i Y_i^2$
Slab	709	3,322	3.75	2,658	14.3	144,932	148,255
Girder	631	242,585	34.17	21561	16.07	162,953	405,538
Total	1,340	—	—	24,219	—	—	553,792

Note:

A_i — Area of the i th component of the composite section;

I_i — Moment of inertia of the i th component of the section;

y_i — Distance between the centroid of the i th component of the section and the top of the slab;

Y_i — Distance between the centroid of the i th component of the section and the neutral axis of the equivalent beam.

with the slab in the remaining one span modeled by solid elements. These two different models are subjected to the same truck loads, which are located close to the pier, as shown in Fig. 3.10.

The transverse and longitudinal bending stresses at the top of the deck along critical sections obtained with the two different models are compared in Fig. 3.11 and Fig. 3.12, respectively. The critical section for transverse bending stresses is located 8 ft. away from the pier. It can be seen that the two models give similar bending stresses in the transverse and longitudinal directions of the deck. It is clear that the whole bridge deck can be simplified into a one-span deck that is modeled by solid and beams elements, while the rest is modeled by the equivalent beams. Such a simplification allows one to use a fine mesh in the vicinity of critical sections.

3.3.3 Finite Element Models

From the above results, it is decided that using eight solid elements between each pair of girders will be a fine enough mesh for the stress analysis. For most of the load cases, this arrangement will provide at least two solid elements between a point load and a girder. There is only one load case where a wheel load is placed closer than two elements from a girder. For this load case, the stress distortion is thought to be unimportant since it will occur right above the flange of a girder, which in reality will reduce the maximum stress produced by the finite element analysis. Therefore, a total of 50 solid elements will be used in the transverse direction, with eight solid elements used for each of the six transverse spans.

The mesh along the longitudinal direction will have different refinements based on the locations of the axle loads. A fine mesh will be used for critical areas where the axle loads are applied, and a coarse mesh will be used for the rest of the deck. Totally, 24 solid elements will be used in the longitudinal direction of the deck in each model.

For all three load groups, a fine mesh is located in the vicinity of the 24-kip axle loads. In this region, the length of the elements is 24 in., which leads to an element aspect ratio (length/thickness) not greater than 6.67.

The mesh used for the stress analysis of the deck under Load Group 1 is shown in Fig. 3.13. From the left side of the mesh, the first solid element has a length of 30 in. It accounts for the stiffness of the concrete diaphragm above the abutment. This effect is simulated by using equivalent solid elements which have the same in-plane bending stiffness as that of the diaphragm. The depth of the diaphragm is 62 in., and that of the equivalent solid elements is 7.5 in. Both have the same length of 30 in. The modulus of elasticity is

assumed to be 3,600 ksi for the diaphragm. Hence, the modulus of elasticity for the equivalent solid elements is determined to be 29,760 ksi, as shown in Fig. 3.14.

In the longitudinal direction, six small solid elements are used in the region of the fine mesh, and the rest of the deck is modeled by seventeen solid elements. The length of each span of the bridge used in the analysis is 102 ft. for the convenience of discretizing the mesh. This is slightly less than the prototype span length of 103 ft. This difference is thought to be so small that it can be ignored in the stress analysis.

The mesh used for the stress analysis of the deck under Load Group 2 is shown in Fig. 3.15. In the longitudinal direction, six small solid elements are used in the region of the fine mesh, and the rest of the deck is modeled with eighteen solid elements. The lengths of these elements vary so that the axle loads can be located at the desired nodes. The element aspect ratios of these elements vary from 6.4 to 25.6. The length of each span of the bridge used in the analysis is 102 ft. For this case, the distance between the rear axle and the trailing axle of the truck is 12 ft. This arrangement is thought to cause the maximum deflection of girders, because the trailing axle load is close to the mid-span.

The mesh used for the stress analysis of the deck under Load Group 3 is shown in Fig. 3.16. There are two solid elements with a high modulus of elasticity (which is 29,760 ksi) to account for the stiffness of the concrete diaphragm above the pier. Each of the solid elements has a length of 25.5 in. The depth of the diaphragm is 62 in., and that of the equivalent solid elements is 7.5 in. The length of the diaphragm is 51 in. The approach used to determine the modulus of elasticity for the equivalent solid elements is the same as that for Load Group 1. In the longitudinal direction, twelve small

solid elements are used in the region of the fine mesh, including two solid elements for the diaphragm, and the rest of the deck is modeled with twelve solid elements. The length of each span of the bridge used in the analysis is 103 ft. The distance between the rear axle and trailing axle of the truck is 12 ft. This arrangement is expected to cause the minimum deflection of girders, because the trailing axle load is close to the pier.

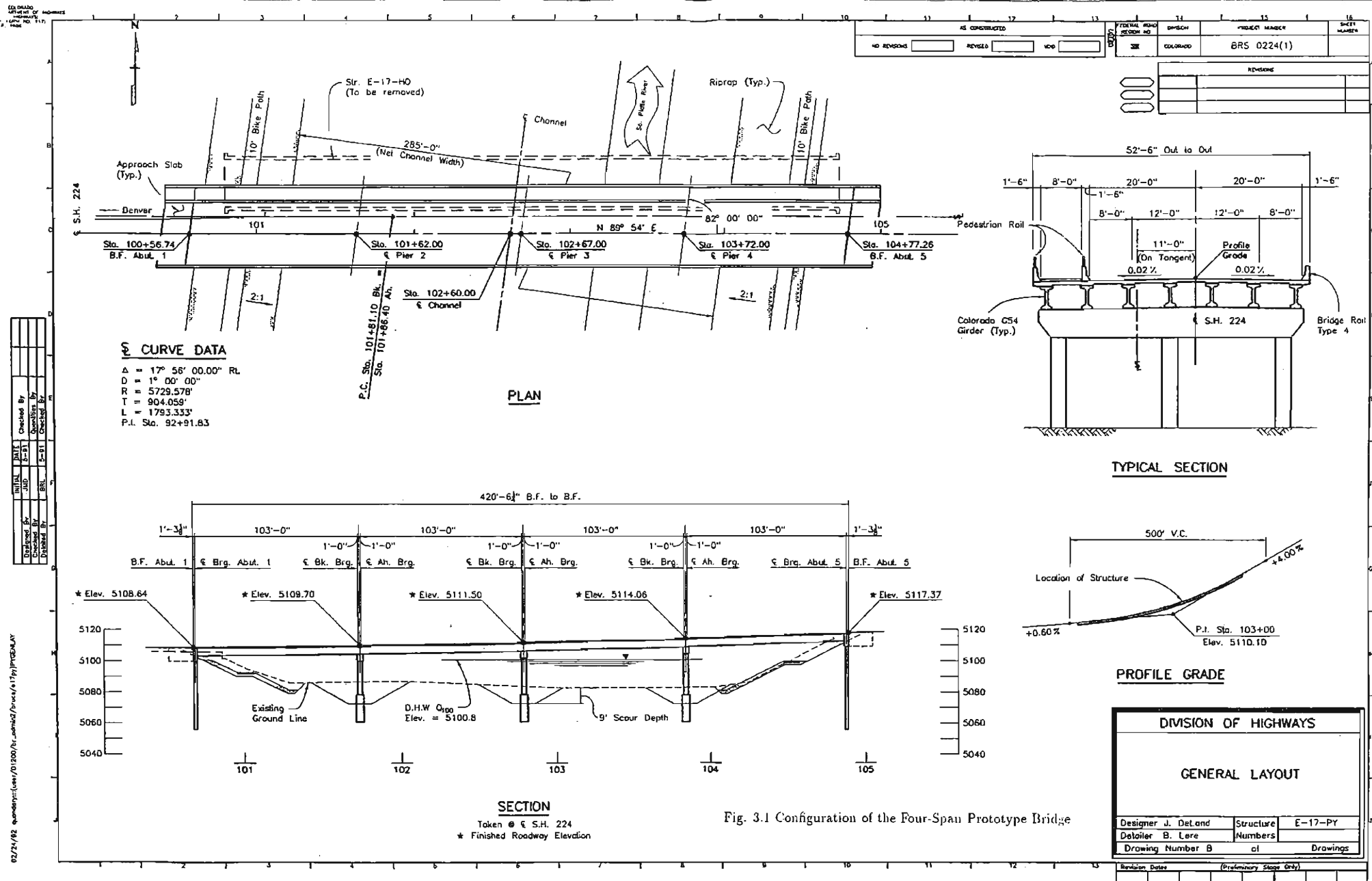


Fig. 3.1 Configuration of the Four-Span Prototype Bridge

02/24/82 e:\pwr\caw\01000\1r_smb\2\brw\617\p\CDMVA

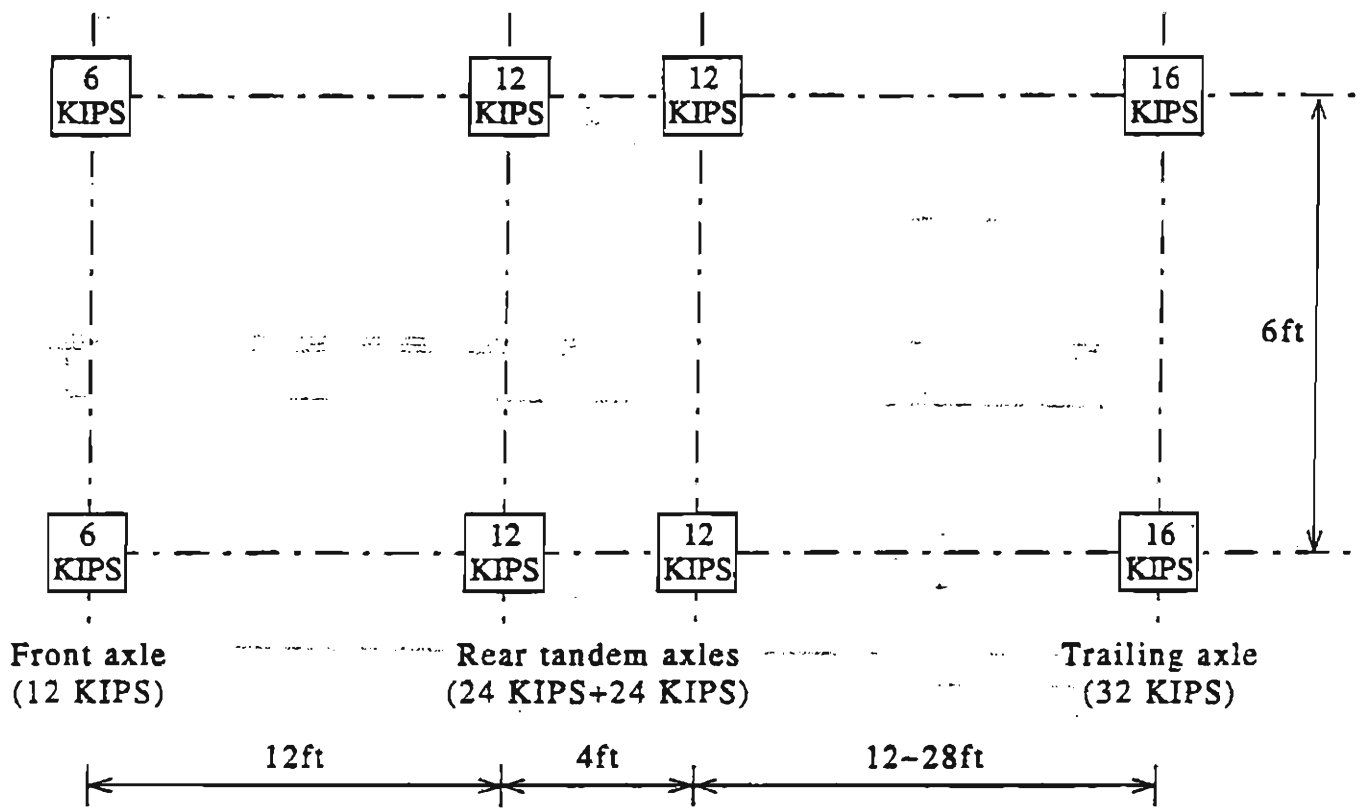


Figure 3.2: Plan View of Truck Load Pattern

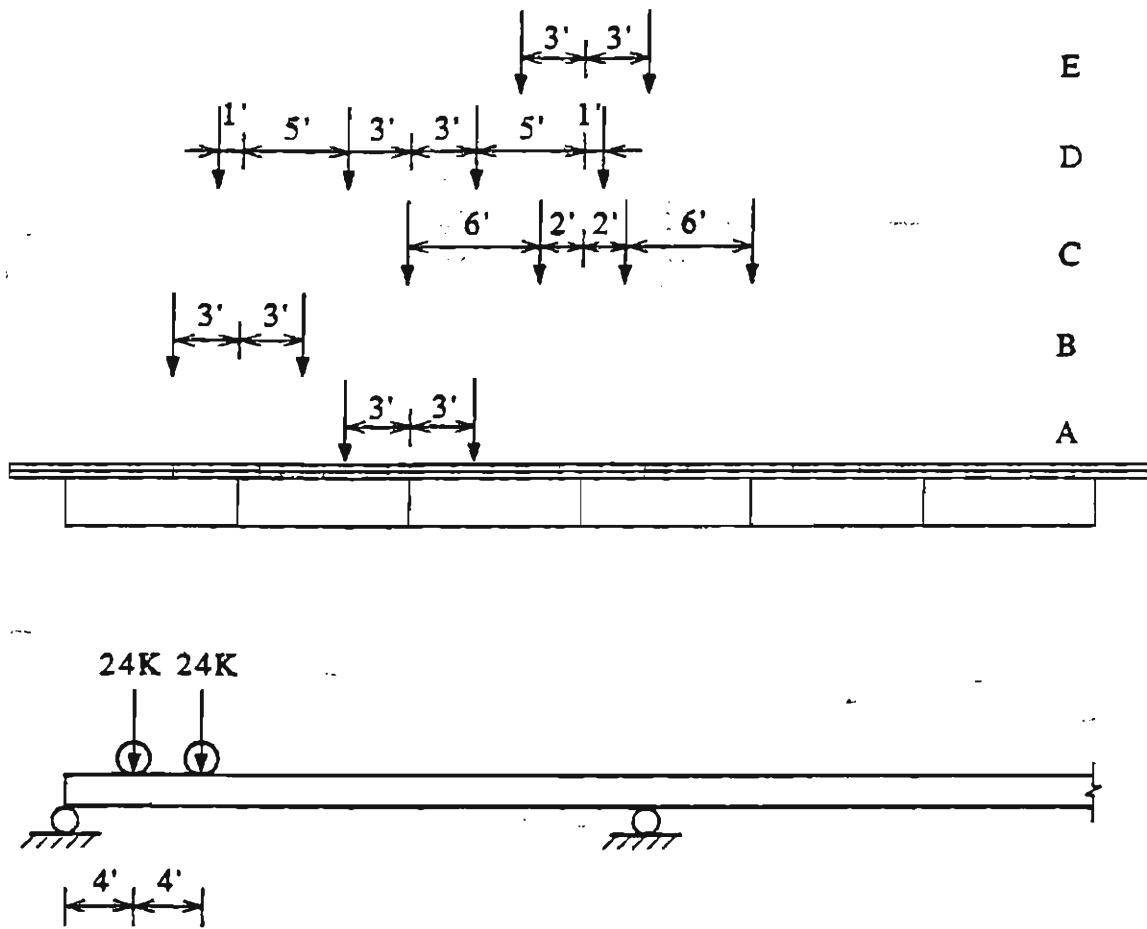


Figure 3.3: Truck Loads-Group 1

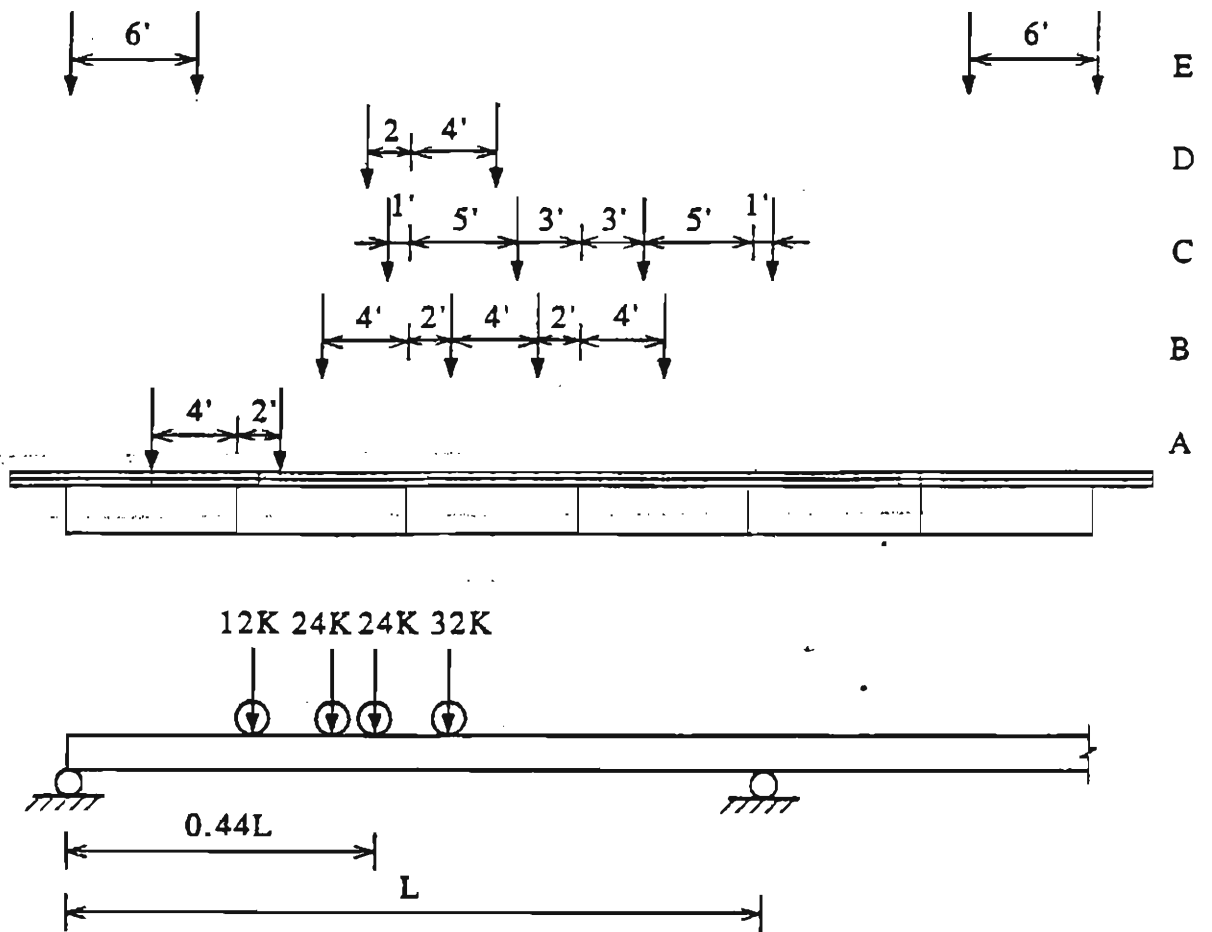


Figure 3.4: Truck Loads-Group 2

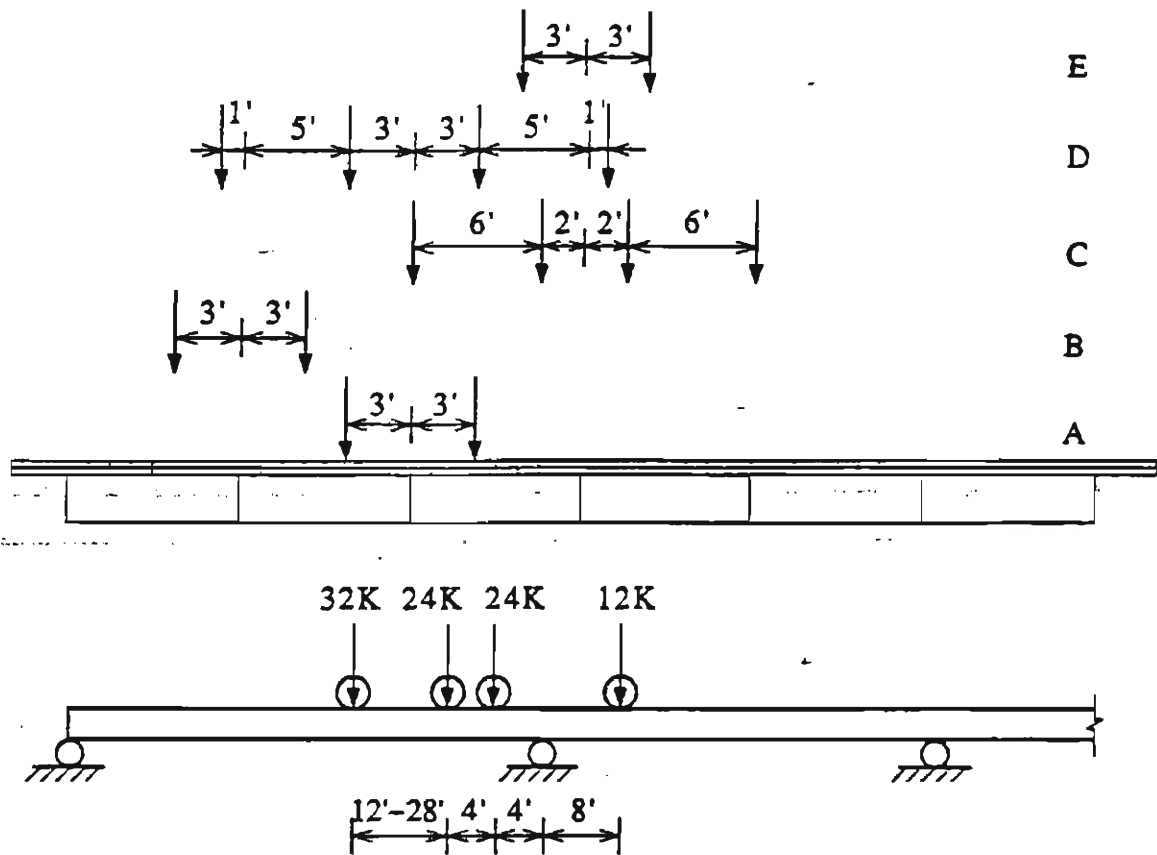


Figure 3.5: Truck Loads-Group 3

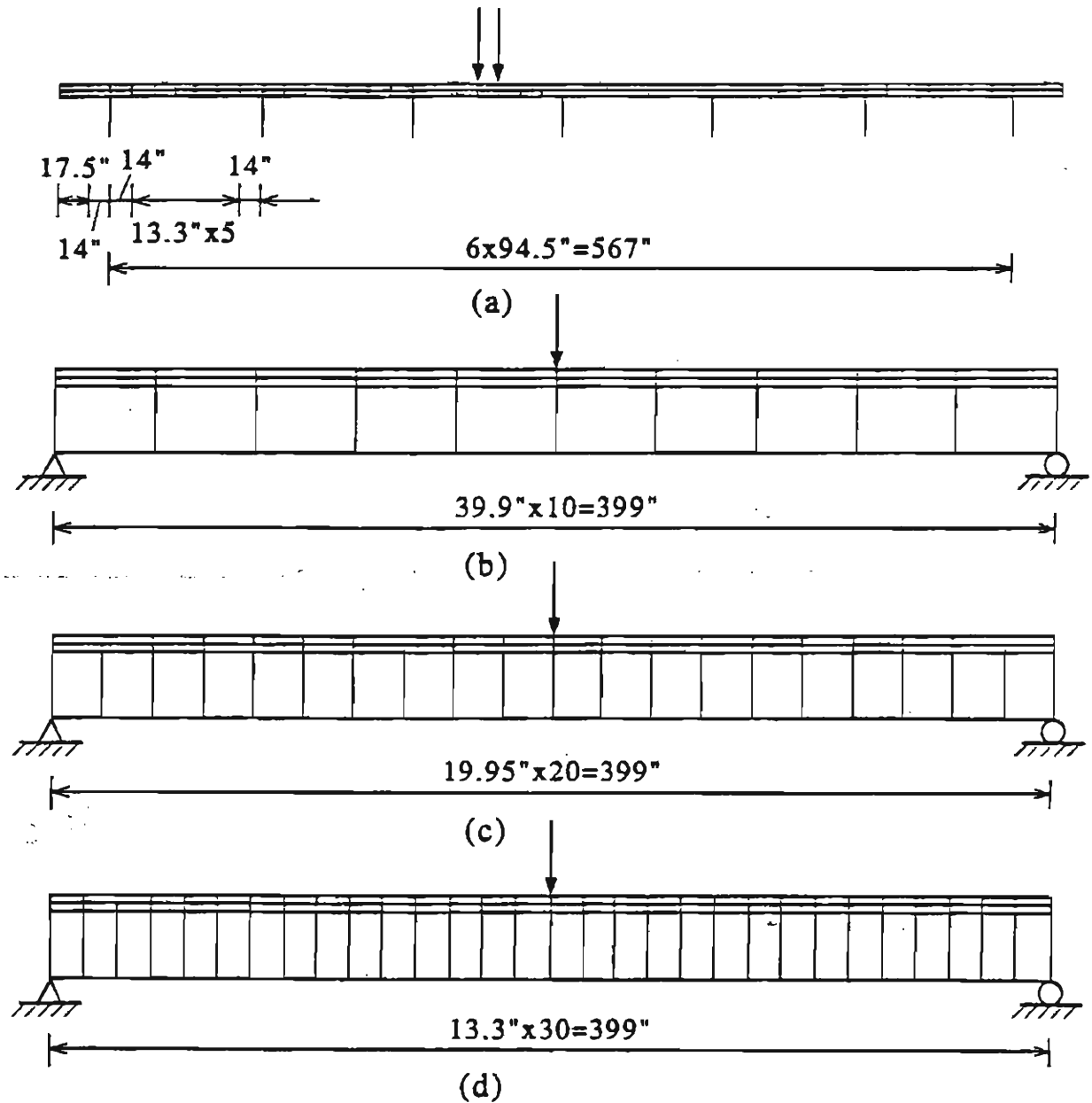


Figure 3.6: Element Refinement in Longitudinal Direction of a One-Span Bridge: (a) Element Mesh in Transverse Direction; (b) Element Mesh in Longitudinal Direction (10 Elements); (c) Element Mesh in Longitudinal Direction (20 Elements); (d) Element Mesh in Longitudinal Direction (30 Elements).

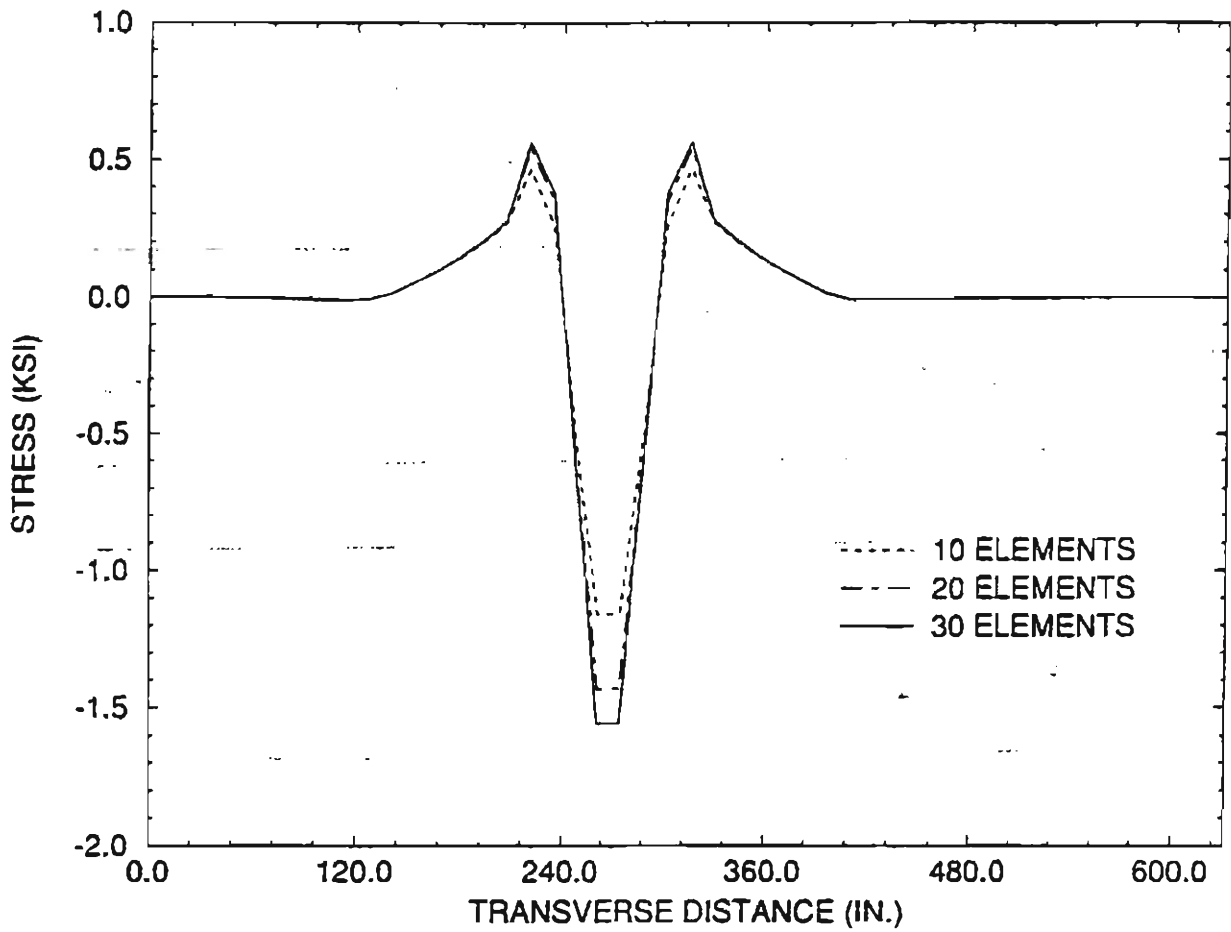


Figure 3.7: Transverse Bending Stresses at Top of the Deck along Loading Section

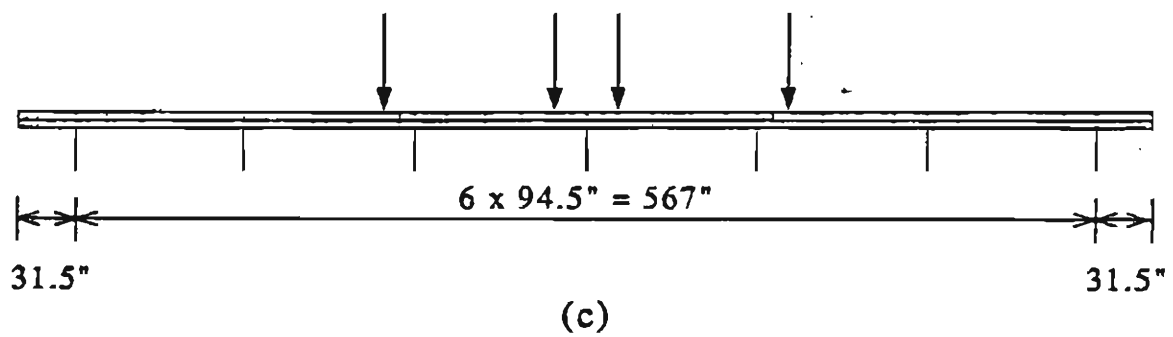
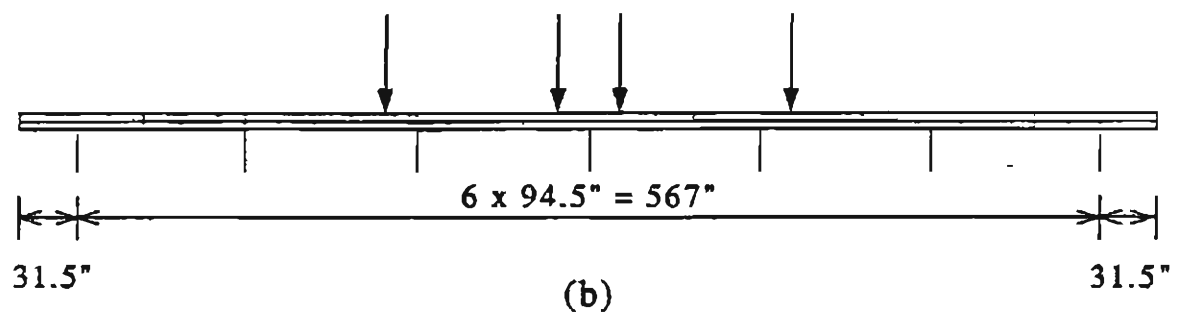
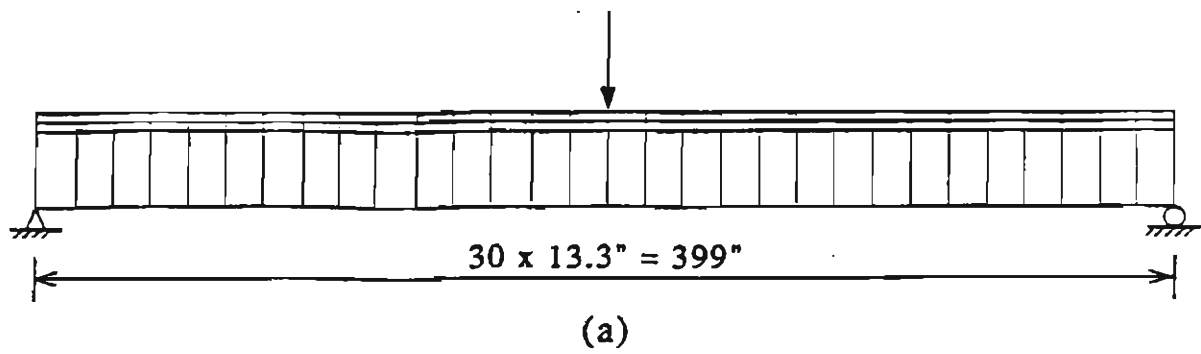


Figure 3.8: Element Refinement in Transverse Direction of a One-Span Bridge: (a) Element Mesh in Longitudinal Direction; (b) Coarse Mesh near Girder Supports; (c) Fine Mesh near Girder Supports.

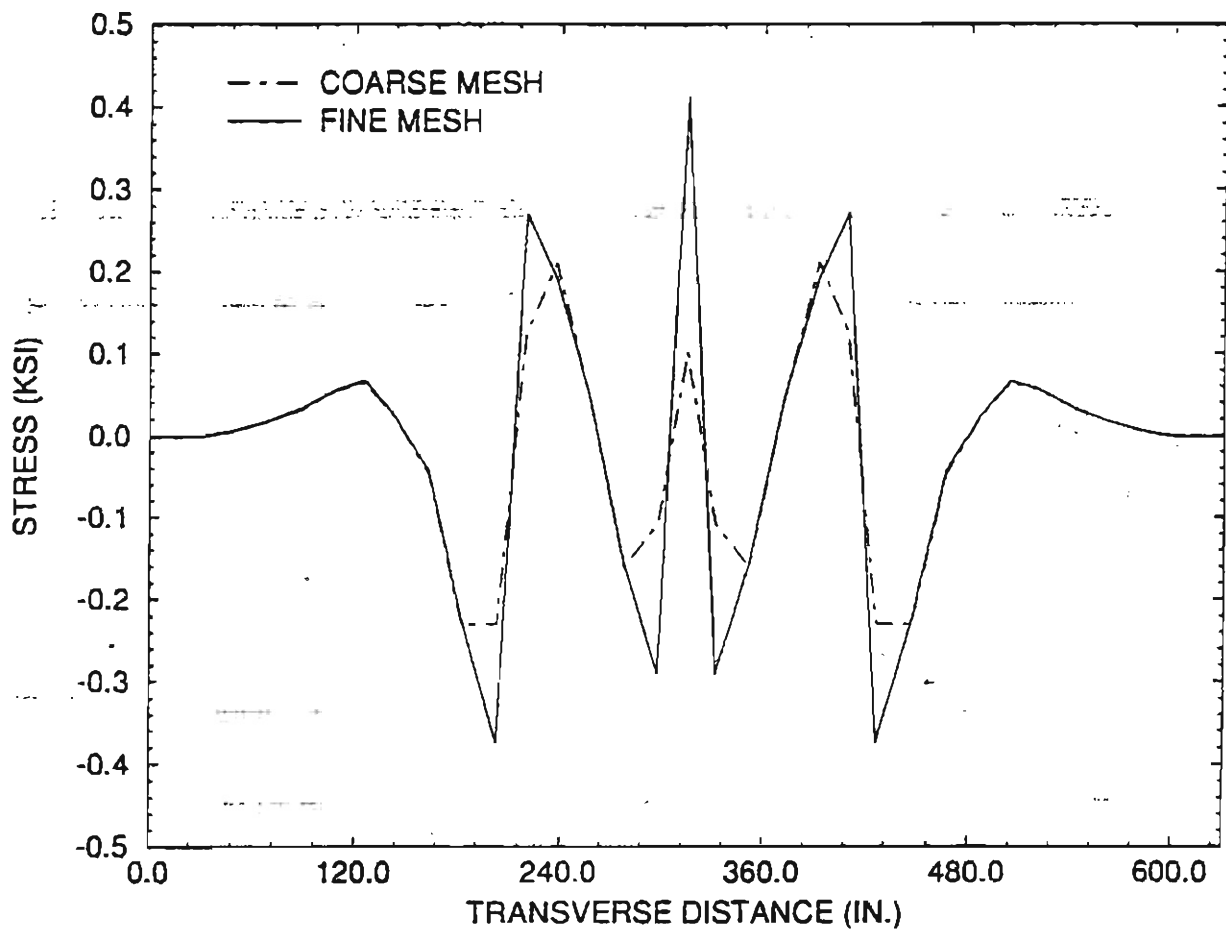


Figure 3.9: Comparison of Transverse Bending Stresses at Top of the Deck along Loading Section

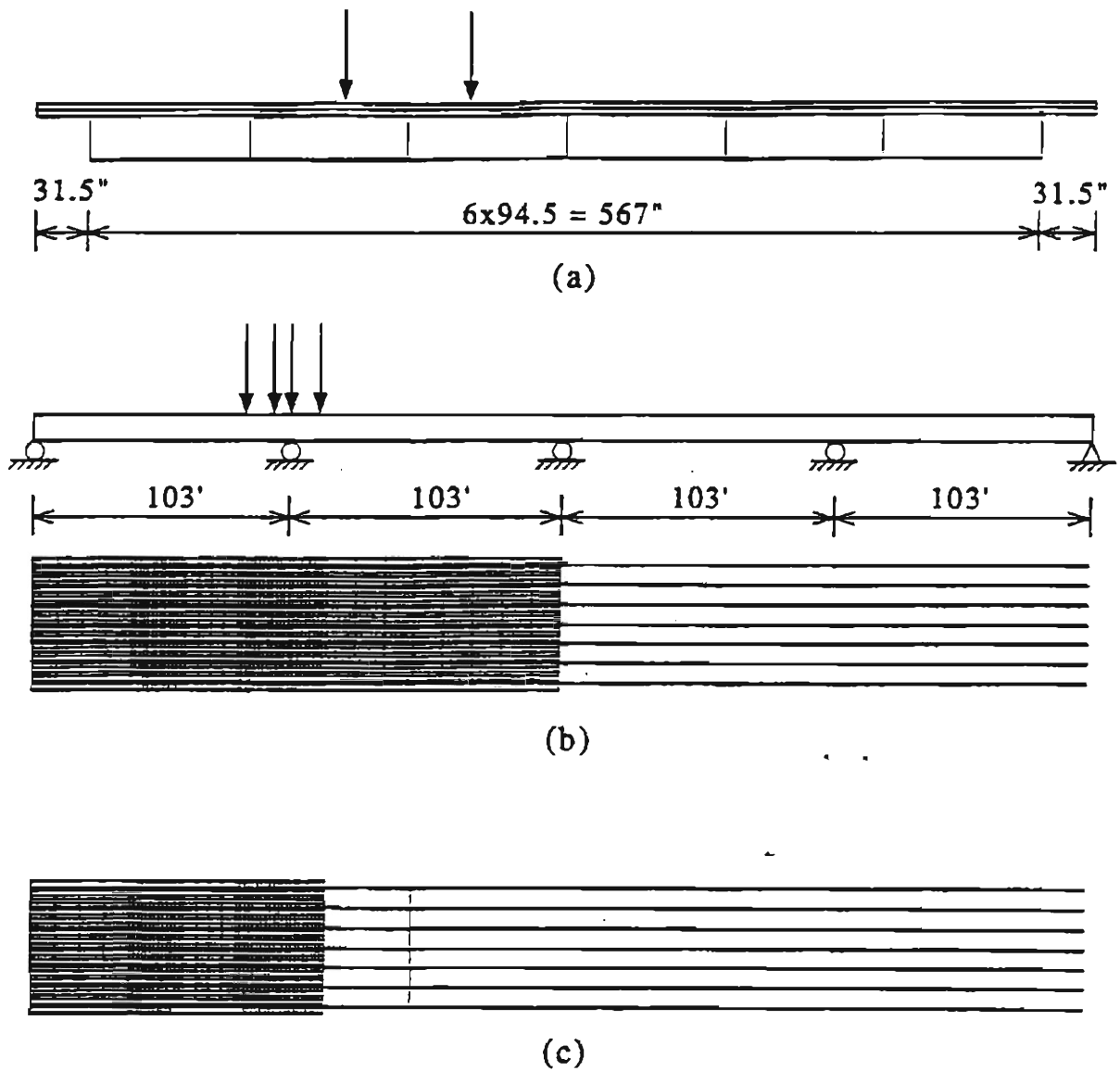


Figure 3.10: Element Mesh with Equivalent Beams Replacing the Deck: (a) Element Mesh in Transverse Direction; (b) Element Mesh with Beam Elements in Two Spans; (c) Element Mesh with Beam Elements in Three Spans.

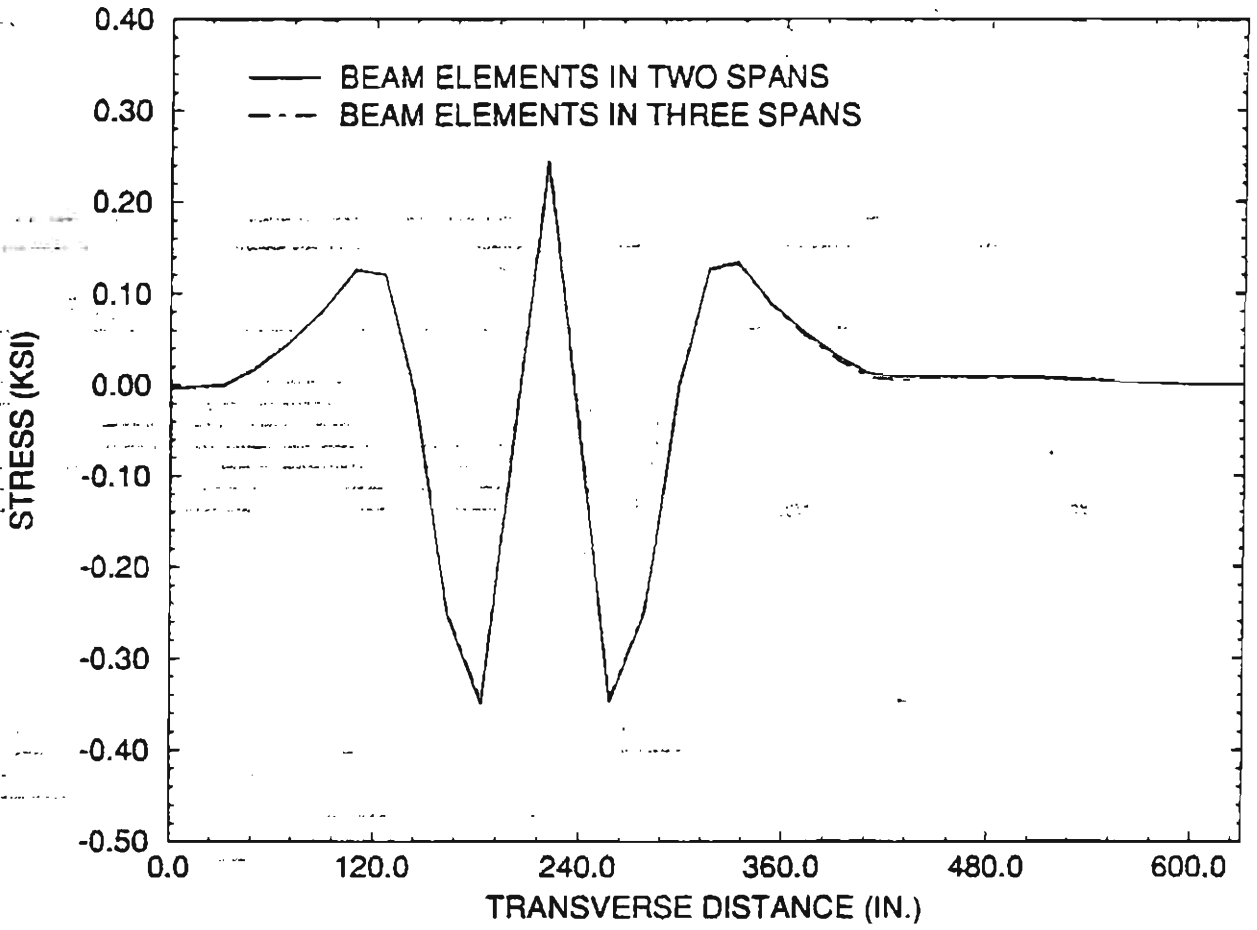


Figure 3.11: Comparison of Transverse Bending Stresses at Top of the Deck along Critical Section

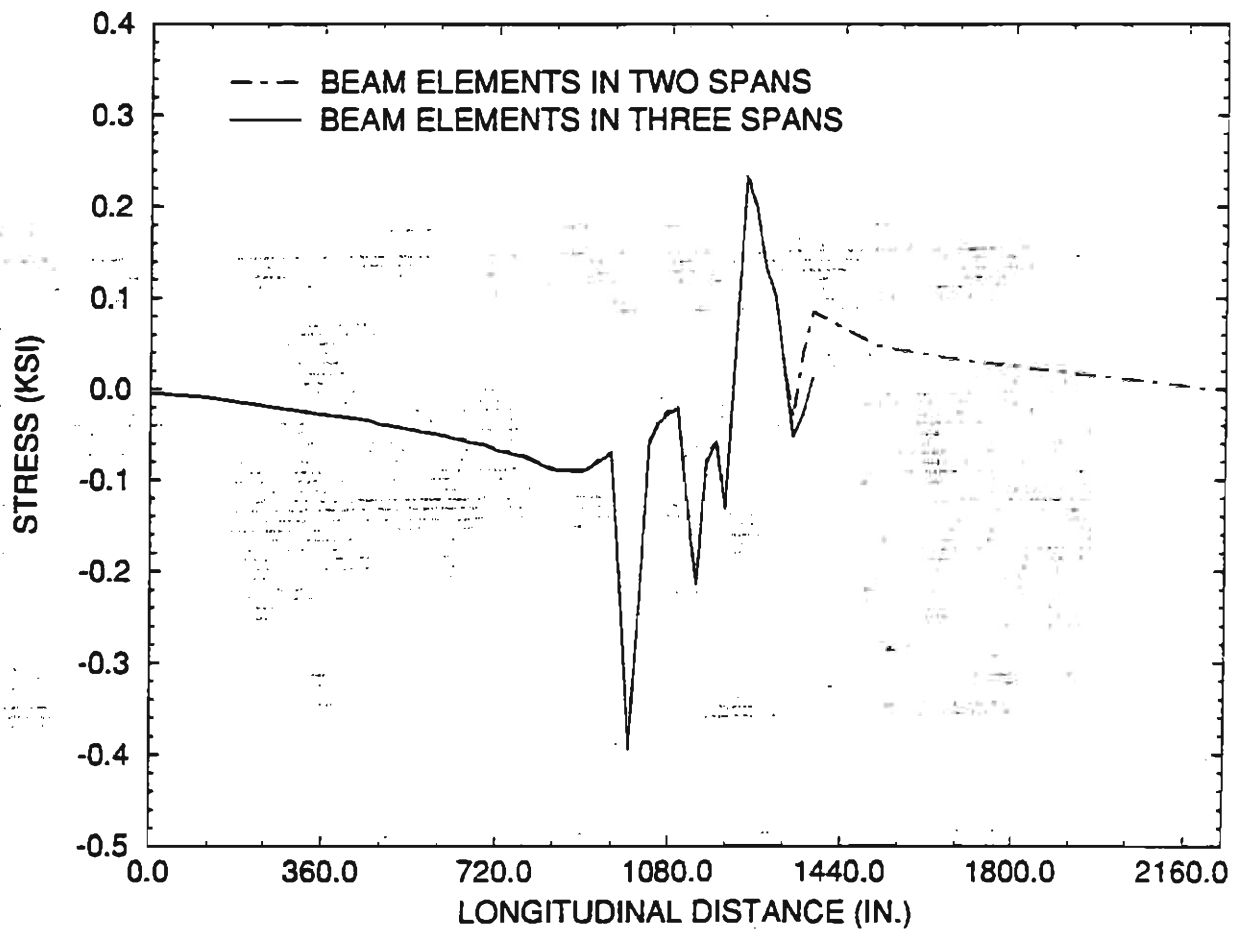


Figure 3.12: Comparison of Longitudinal Bending Stresses at Top of the Deck along Critical Section

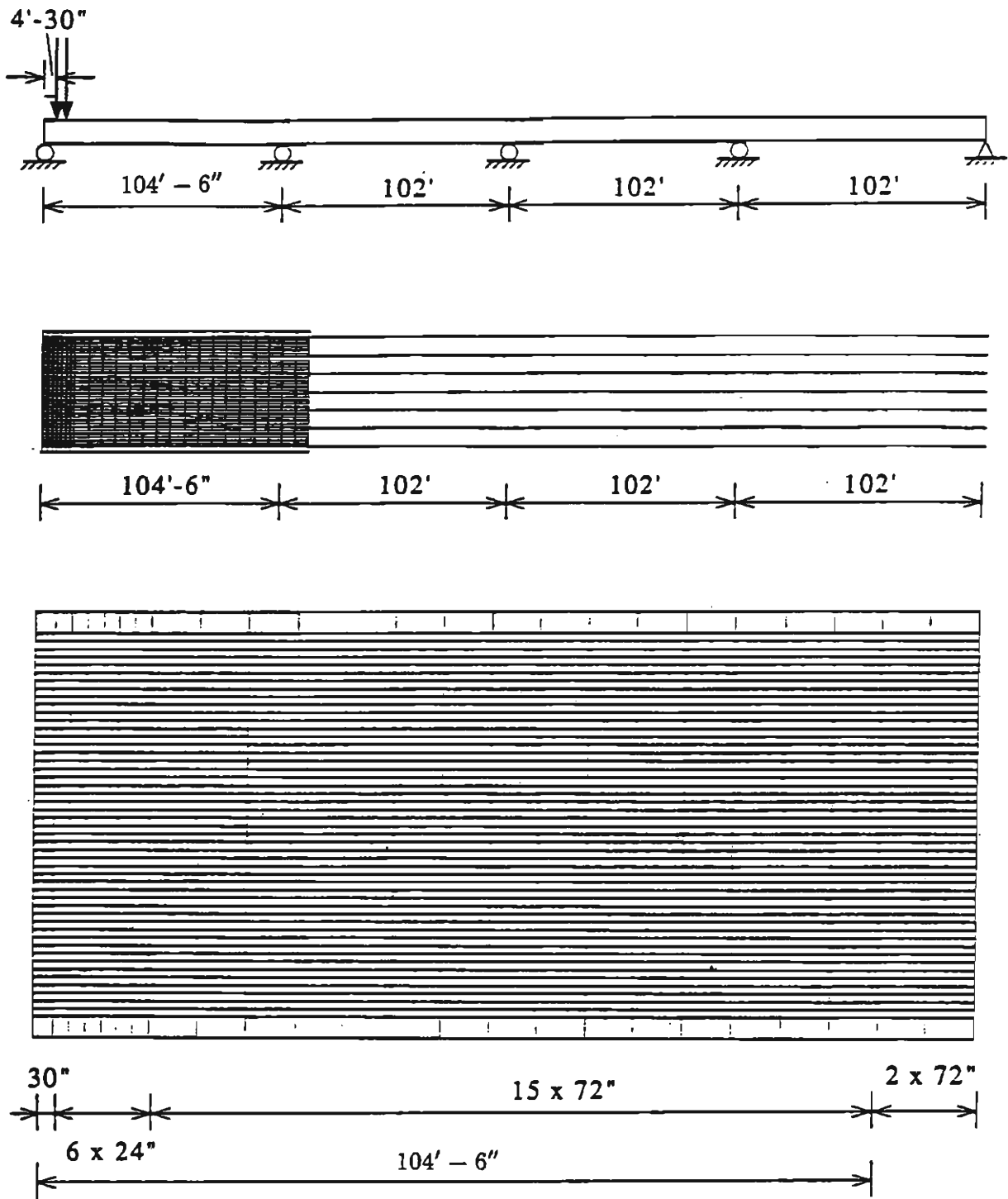


Figure 3.13: Element Mesh for Load Group 1

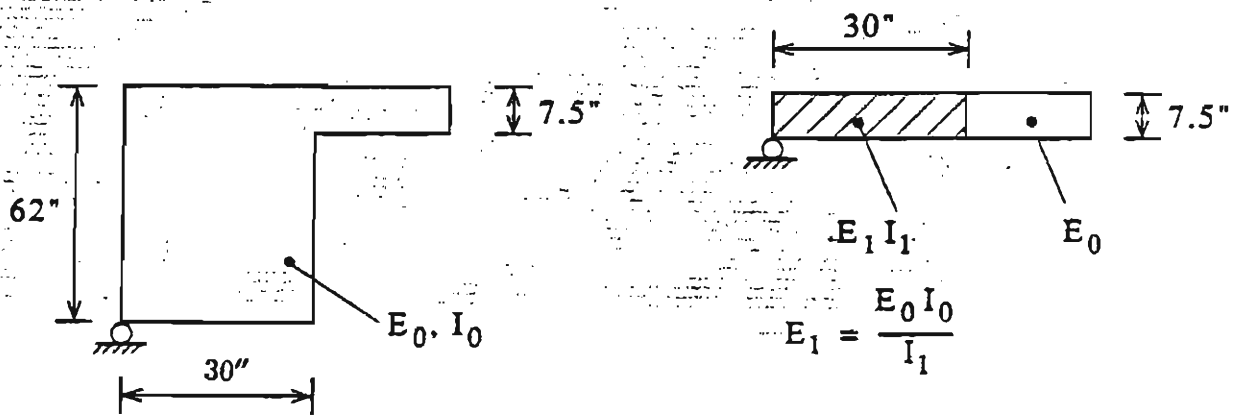


Figure 3.14: Determination of Equivalent Solid Elements for Diaphragm: (a) Section of the Diaphragm ; (b) Equivalent Solid Element.

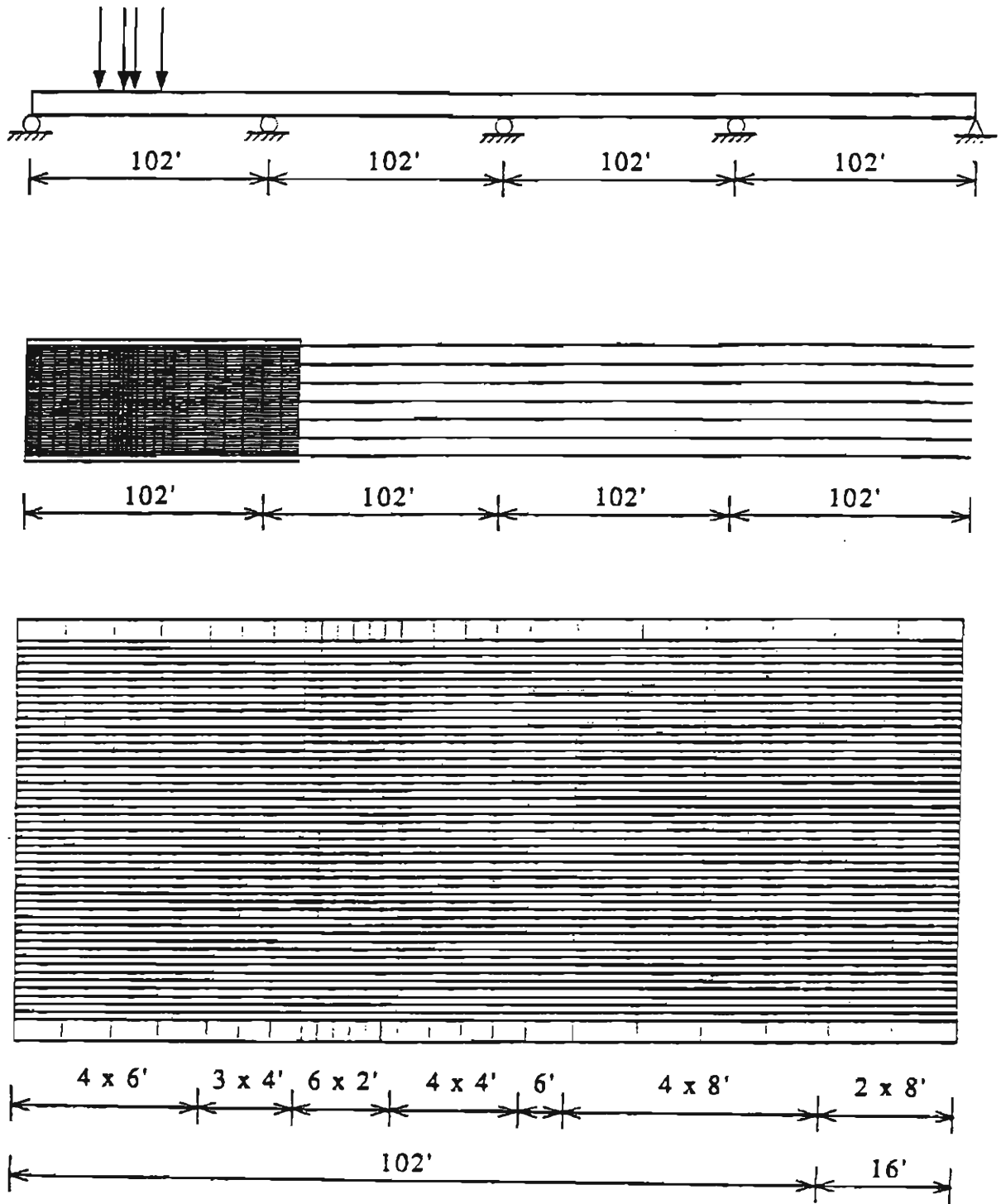


Figure 3.15: Element Mesh for Load Group 2

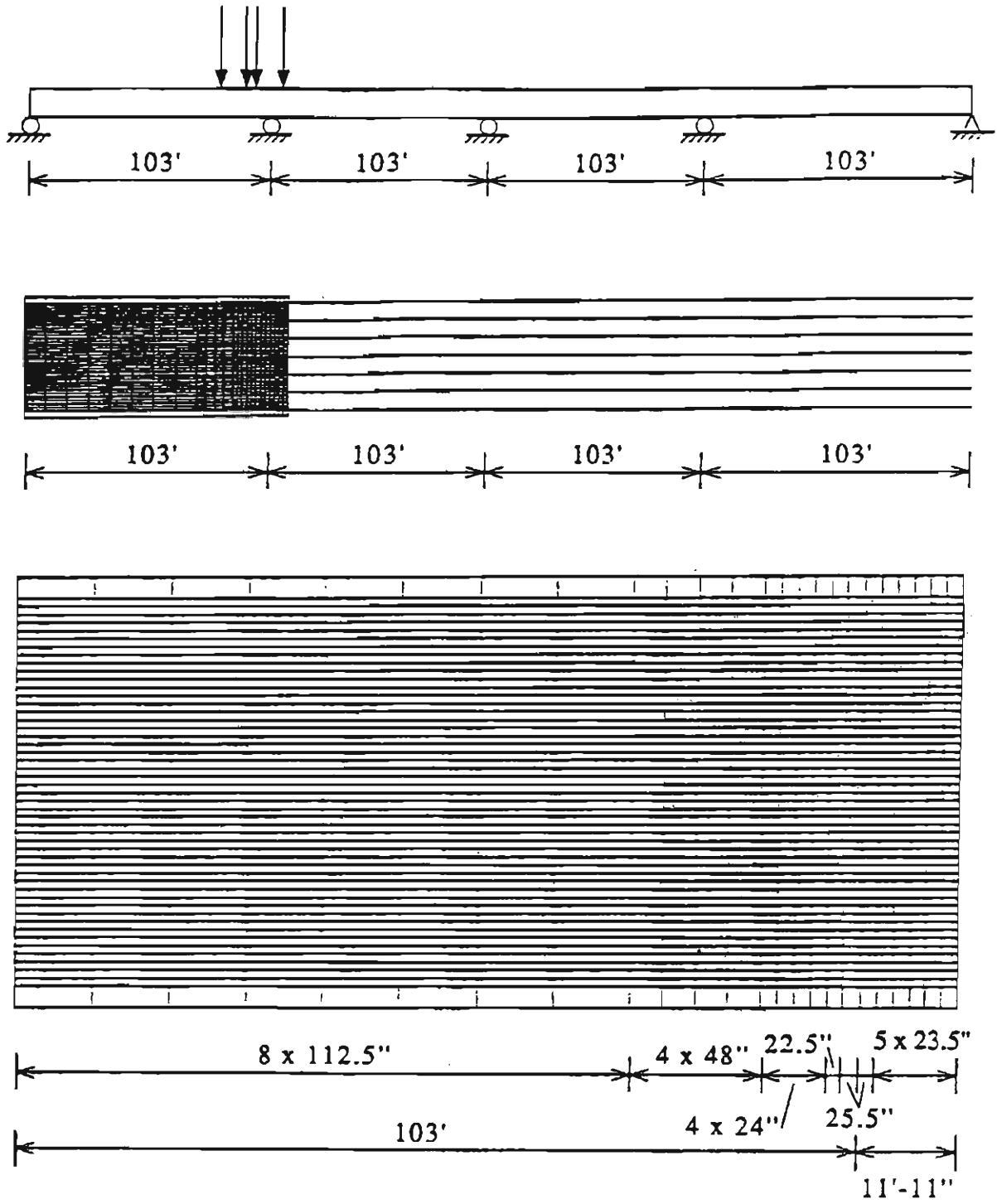


Figure 3.16: Element Mesh for Load Group 3

Chapter 4

ANALYSIS RESULTS

The bridge deck under the fifteen truck load cases is analyzed by means of the finite element models presented in Chapter 3, and the corresponding bending stresses along the transverse and longitudinal directions of the bridge deck are determined.

For the prototype bridge deck, the width of the flange of a girder is 2.33 ft. and the center-to center distance between two girders is 7.89 ft. Therefore, the clear span of the slab between each pair of girders is 5.56 ft. According to the AASHTO Specifications, the transverse bending moment of the slab induced by a HS20 truck is 3780 ft-lb/ft. If the reduction factor of 0.8 is considered due to the continuity of the slab, this bending moment becomes 3024 ft-lb/ft. Consequently, for a 7.5-in thick deck, the maximum tensile stress is 323 psi. It becomes 420 psi when the impact factor of 1.3 is used. This value can be used to compare with the maximum tensile stresses obtained with the finite element method.

It should be emphasized that because a distributed wheel load is treated as a concentrated load, the stresses computed at the nodes where concentrated loads are applied will be greater than those in the actual deck.

Table 4.1: Maximum Stresses at the Top of the Deck(ksi) (Load Group 1)

CASE	Transverse		Longitudinal	
	Max. Tensile	Max. Compressive	Max. Tensile	Max. Compressive
A	0.271	0.276	0.055	0.185
B	0.274	0.286	0.056	0.197
C	0.234	0.196	0.018	0.189
D	0.286	0.256	0.029	0.208
E	0.271	0.276	0.056	0.183

4.1 Load Group 1

The transverse and longitudinal bending stresses at the top of the deck under Load Group 1 are shown in Fig. 4.1 and Fig. 4.2. The critical section for the transverse bending stresses under the five load cases is 6 ft. away from the abutment, located between the two 24-kip axle loads. The critical section for the longitudinal bending stresses depends on the locations of wheel loads, which is usually beneath the wheel loads. Since the axle loads are close to the support, little longitudinal bending moment is developed in the bridge deck. Consequently, the longitudinal bending stresses are relatively small. The maximum bending stresses at the top of the deck under the five cases of Load Group 1 are shown in Table 4.1.

It is found that the top bending stresses under the five load cases are less than 300 psi. Case D has the maximum top transverse tensile stress equal to 286 psi. This value is only 68.1 percent of the maximum tensile stress obtained with the AASHTO design moment. The top longitudinal compressive stresses are less than 210 psi, and the top longitudinal tensile

stresses are relatively small.

Since Case D causes the maximum transverse bending stress, the 24-kip axle loads corresponding to this case are moved back and forth by 2 ft., towards and away from the abutment. When the tandem axles move 2 ft. towards the abutment with respect to the original location, the maximum transverse tensile stress at the top of the deck is reduced to 255 psi. Moving the tandem axles 2 ft. away from the abutment with respect to the original location reduces the maximum tensile stress to 280 psi. This shows that the original location of the 24-kip tandem axle loads produces the maximum transverse tensile stress at the top of the deck.

4.2 Load Group 2

The transverse and longitudinal stresses at the top of the deck under Load Group 2 are shown in Fig. 4.3 and Fig. 4.4. It can be seen that transverse tensile stresses above the girders are greatly reduced with respect to the previous case because of the significant deflections of the girders. The critical section for the top transverse bending stresses under Cases A, B, C and D is 42 ft. away from the abutment, located between the two 24-kip axle loads. For Case E, the maximum top tensile transverse stress occurs beneath the 32-kip axle load, which is 56 ft. away from the abutment. The critical sections for the longitudinal bending stresses are different for each case, usually located at the wheel loads. Since axle loads are located near the mid-span of the deck, the top longitudinal compressive stresses are very large. The maximum bending stresses at the top of the deck under the five cases of Load Group 2 are shown in Table 4.2.

It is found that the top transverse tensile stresses are less than 120 psi,

Table 4.2: Maximum Stresses at the Top of the Deck(ksi) (Load Group 2)

CASE	Transverse		Longitudinal	
	Max. Tensile	Max. Compressive	Max. Tensile	Max. Compressive
A	0.116	0.475	0.138	0.454
B	0.114	0.521	0.157	0.486
C	0.079	0.467	0.147	0.457
D	0.084	0.499	0.079	0.345
E	0.222	0.220	0.134	0.378

about 60 percent less than those under Load Group 1, except for Case E, where the maximum tensile stress is 222 psi. The top transverse compressive stresses are less than 550 psi, about 80 percent greater than that under Load Group 1, and 24 percent greater than the expected bending stress (420 psi) resulting from the AASHTO design moment. The top longitudinal compressive stresses are less than 500 psi, and the top longitudinal tensile stresses are around 150 psi. Both are larger than those under Load Group 1.

Case E is an unusual loading condition that is intended to produce the maximum top tensile stress from the "hogging" of the deck due to truck loads placed at the exterior edges of the deck. It is interesting to look at the top transverse stress variations along two different sections under load Case E, as shown in Fig. 4.5. One is between the two 24-kip axle loads (42 ft. away from the abutment), where the top transverse tensile stress at the center of the deck is 148 psi. The other is beneath the 32-kip axle load (56 ft. away from the abutment), and the stress at the same transverse location is 222 psi. The difference between these top transverse tensile stresses at the two sections is 74 psi. Obviously, this difference is caused by differential deflections among

the girders. The significance of girder deflection was further explored by combining the effects of load Cases C & E. If the bridge deck is subjected to Cases C and E at the same time, the differential girder deflections are significantly reduced and the maximum top transverse tensile stress is 223 psi, which is still less than that under Load Group 1. The top transverse bending stresses under the combination of the two load cases are shown in Fig. 4.6. This combination of loads dramatically reduces the maximum top transverse compressive stress of load Case C from 467 psi to 320 psi. In other words, the transverse positive bending moment is changed by about 31.5 percent due to the differential girder deflection.

4.3 Load Group 3

The transverse and longitudinal bending stresses at the top of the deck under Load Group 3 are shown in Fig. 4.7 and Fig. 4.8. It can be seen that the transverse stress variations are similar to those under Load Group 1, because of small deflections of the girders near the pier. The critical section for the top transverse bending stresses under the five load cases is .8 ft. away from the pier, which is beneath one of the two 24-kip axle loads. The maximum top longitudinal compressive stresses occur beneath the wheel loads. The maximum top longitudinal tensile stresses occur along the nodes above a girder between the two wheel loads. Since the axle loads are applied at both sides of the pier, very large longitudinal tensile stresses are developed in the vicinity of the support. The maximum bending stresses at the top of the deck under the five cases of Load Group 3 are shown in Table 4.3.

It can be seen that the top transverse bending stresses are less than 300 psi, and Case D has the maximum top transverse tensile stress equal to 239.2

Table 4.3: Maximum Stresses at the Top of the Deck(ksi) (Load Group 3)

CASE	Transverse		Longitudinal	
	Max. Tensile	Max. Compressive	Max. Tensile	Max. Compressive
A	0.210	0.247	0.534	0.17
B	0.212	0.287	0.565	0.18
C	0.209	0.177	0.733	0.19
D	0.239	0.250	0.564	0.20
E	0.209	0.275	0.530	0.17

psi. The maximum top transverse tensile stress for Load Group 3 is 84% of that for Load Group 1. The top longitudinal compressive stresses are less than 200 psi, and the top longitudinal tensile stresses are larger than 500 psi. Removing the 32-kip axle load of Case D causes the maximum top transverse tensile stress to increase slightly.

Analysis of the bridge deck under the three different load groups shows that the girder flexibility greatly reduces the transverse negative bending moments in the bridge deck. The critical top transverse bending stresses with respect to the different longitudinal locations of axle loads are compared in Fig. 4.9. It can be seen that the transverse tensile stresses at the top of the deck will decline when the axle loads move farther away from the supports.

Considering that the design tensile strength of deck concrete is usually above 470 psi (Section 3.1), one can conclude that the transverse tensile stresses at the top of the deck induced by the fifteen load cases are not likely to cause deck cracking. The maximum tensile stress developed is 286 psi, which is only 61 percent of the expected design tensile strength of deck concrete. Furthermore, it should be mentioned that the above analyses do

not consider the influence of the flanges of the girders, and should, therefore, be conservative.

Analysis results indicate that the maximum transverse tensile stress at the bottom of the slab can be as high as 520 psi, which is greater than the expected tensile strength of deck concrete. Hence, cracks can develop in regions of positive moment. This effect is investigated in Section 4.5.

4.4 Effect of Concrete Railings

There are three lines of concrete railings at the top of the prototype bridge deck, which are monolithically connected to the concrete slab. The concrete railings used here conform to Colorado Railing Standard Type 4. In the previous computations, the effect of the concrete railings was not taken into account.

To investigate the effect of the concrete railings, solid elements are used to model the concrete slab and girders, as well as the railings of a simply supported one-span bridge deck, which has the same configuration as the four-span bridge. The finite element mesh for the one-span bridge deck is shown in Fig. 4.10. The concrete diaphragm at the mid-span of the bridge is modeled with beam elements, which are attached to the nodes of the solid elements modeling the girders. Placing the axle loads at the mid-span of the bridge deck produces maximum differential deflections among the girders. Hence, Case B of Load Group 2 is used to compare the stress analyses with and without the concrete railings.

A one-span bridge without railings is first analyzed. Railings are then added to the bridge, and the analysis is repeated. The transverse bending stresses at the top of the deck along the critical section (42 ft. away from the

abutment) obtained with and without the concrete railings are shown in Fig. 4.11. It can be observed that the top transverse tensile stress in the vicinity of the interior railing is increased from 89 psi to 157 psi, an increase of 76.4 percent, when the railings are present. However, it is still only 33% of the expected tensile strength (470 psi) of deck concrete. Stresses at those nodes that are far away from the interior railing have little change. Because the concrete railings increase the longitudinal bending stiffness, the longitudinal bending stresses in the deck are slightly reduced. Hence, it may be important to consider the effect of the concrete railings in the stress analysis for those nodes that are close to the interior railing. It is not necessary to consider this effect if the nodes are far away from the railings. If the axle loads are close to the supports, it is not necessary to consider this effect, because the differential deflections of the girders are small to start with.

4.5 Effect of Deck Cracking

In previous computations, it is assumed that no cracking occur at the bottom of the bridge deck. This may not be true since the maximum transverse tensile stresses at the bottom of the slab can be close to the tensile strength of deck concrete as shown by previous computations. Deck cracking is most likely to occur at the bottom of the slab beneath the wheel loads, and propagates in the longitudinal direction with the movement of truck loads. This will reduce the bending stiffness of the slab section.

To investigate the effect of deck cracking, a simplified method is used to model deck cracking in the finite element model. It is assumed that cracks will occur at the bottom of the slab under the wheel loads. The bending stiffness of a cracked section is calculated. The modulus of elasticity of the

solid elements at the cracked sections is modified to simulate the reduction of the bending stiffness at these sections. Case A of Load Group 3, in which the axle loads are close to the pier, is used to compare the stress analyses with and without deck cracking. The modeling of deck cracking is shown in Fig. 4.12.

For a one-foot wide concrete slab, the area of steel reinforcement is 0.6764 in.². Therefore, the moment of inertia of an uncracked section is 421.9 in.⁴, and that of a cracked section is 167 in.⁴. Consequently, the modulus of elasticity for the solid elements at a cracked section is 1,424 ksi, while that at an uncracked section is assumed to be 3,600 ksi. The shift of the neutral axis is neglected here.

The transverse bending stresses at the top of the deck with and without deck cracking are shown in Fig. 4.13. It is found that the maximum transverse bending stress at the top of the deck is increased from 210 psi to 303 psi, which is an increase of 44 percent.

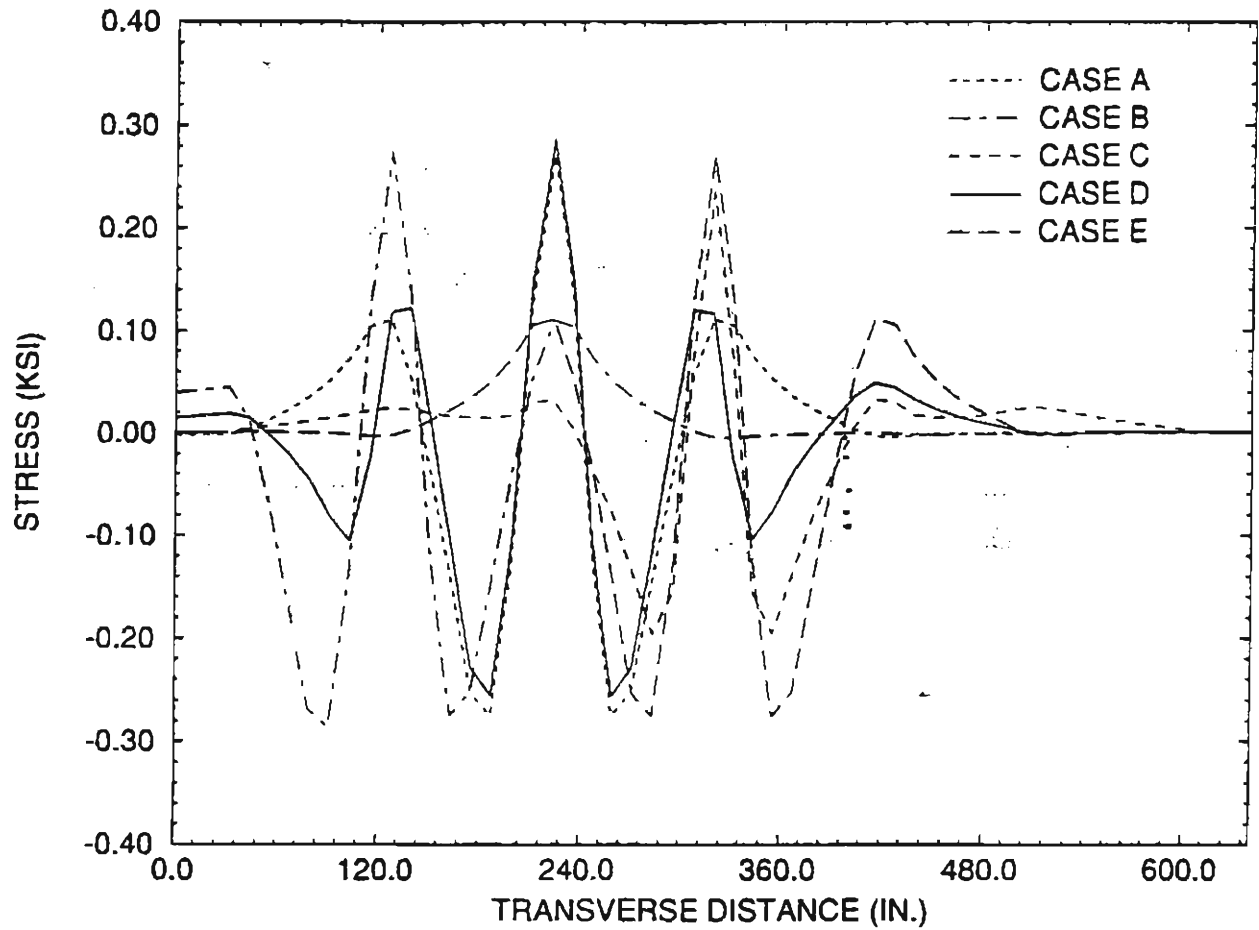


Figure 4.1: Transverse Bending Stresses at Top of the Deck along Critical Transverse Section (Load Group 1)

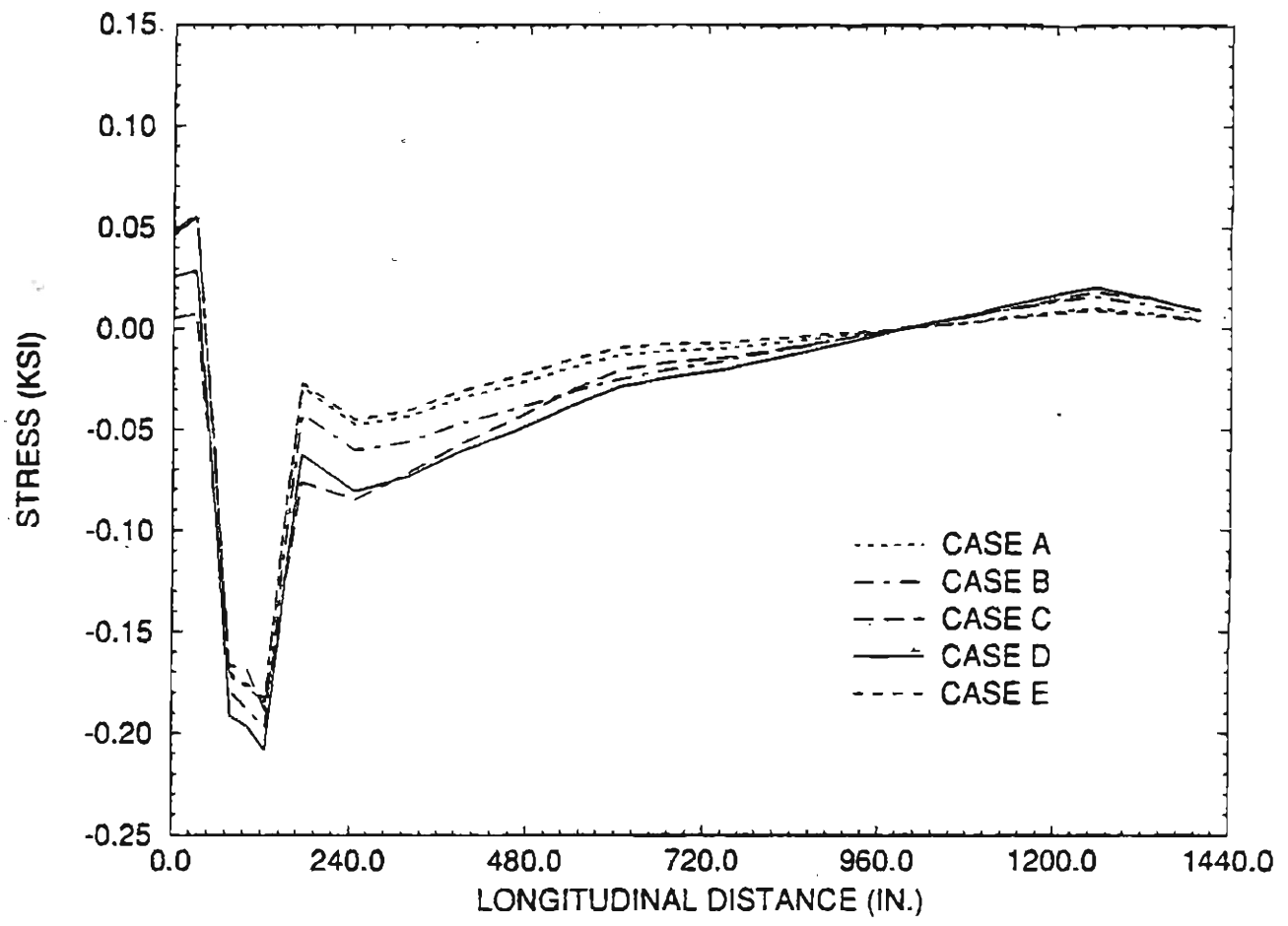


Figure 4.2: Longitudinal Bending Stresses at Top of the Deck along Critical Longitudinal Sections (Load Group 1)

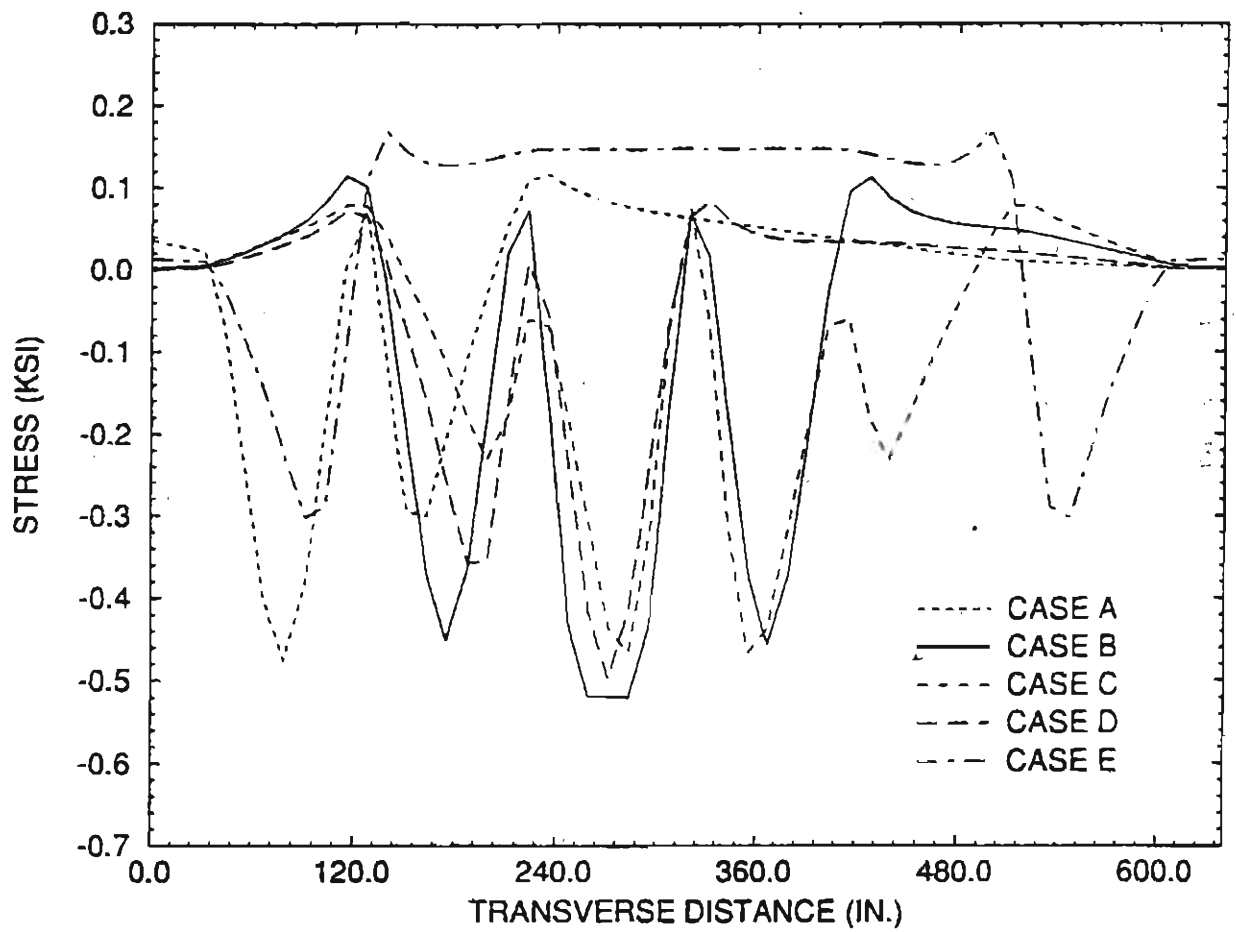


Figure 4.3: Transverse Bending Stresses at Top of the Deck along the Transverse Section (42-ft. from the Abutment) (Load Group 2)

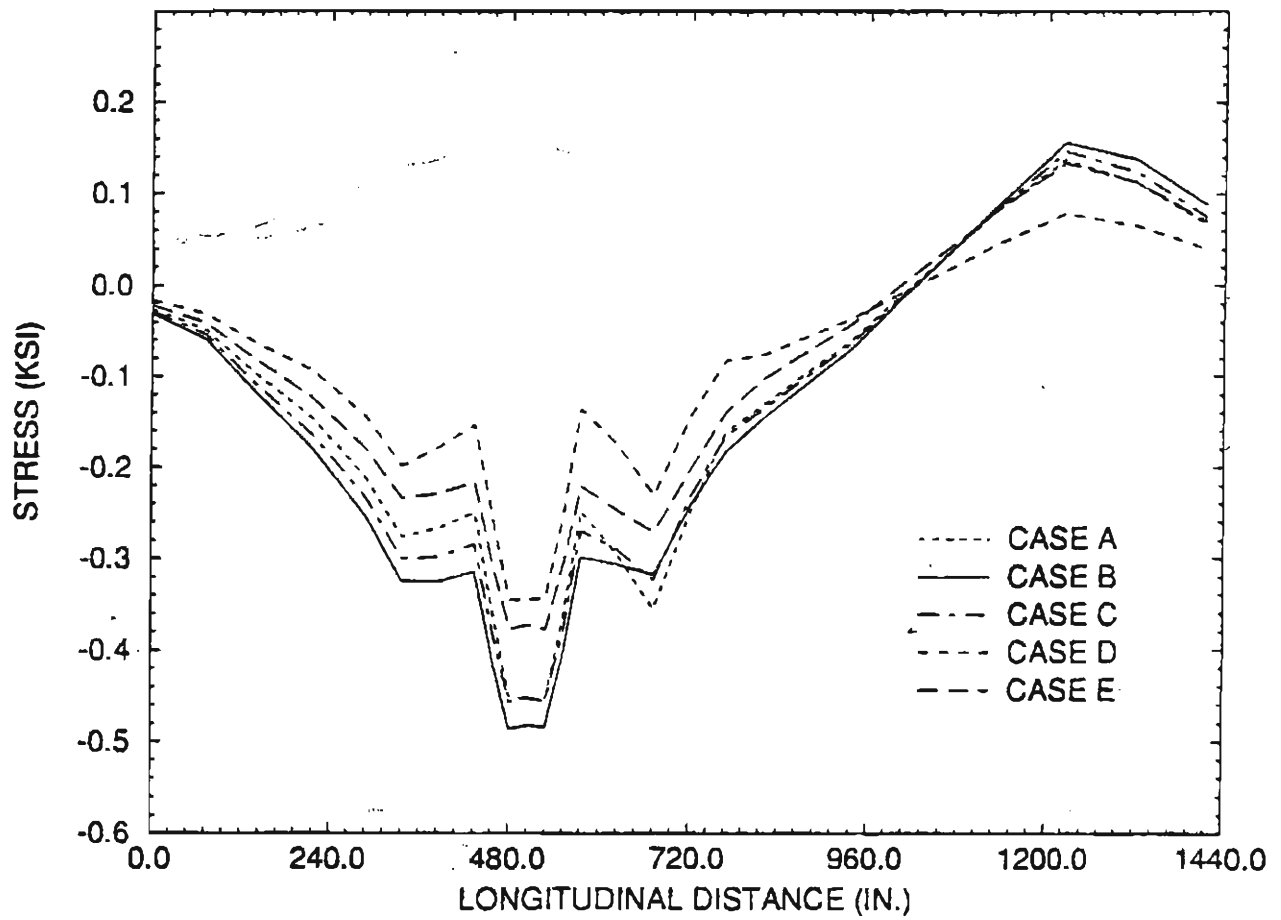


Figure 4.4: Longitudinal Bending Stresses at Top of the Deck along Critical Longitudinal Sections (Load Group 2)

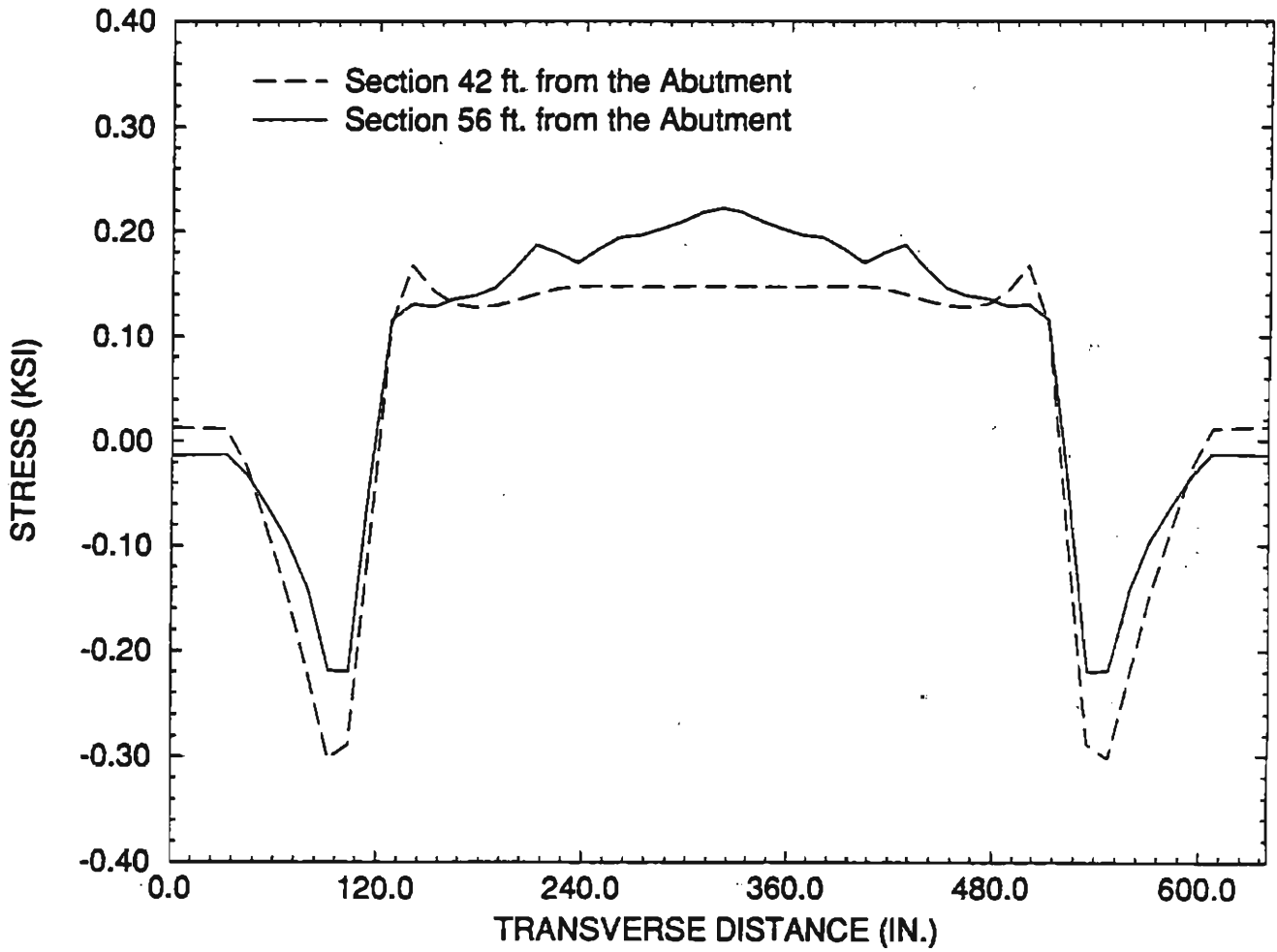


Figure 4.5: Transverse Bending Stresses at Top of the Deck along Two Different Transverse Sections (Case E of Load Group 2)

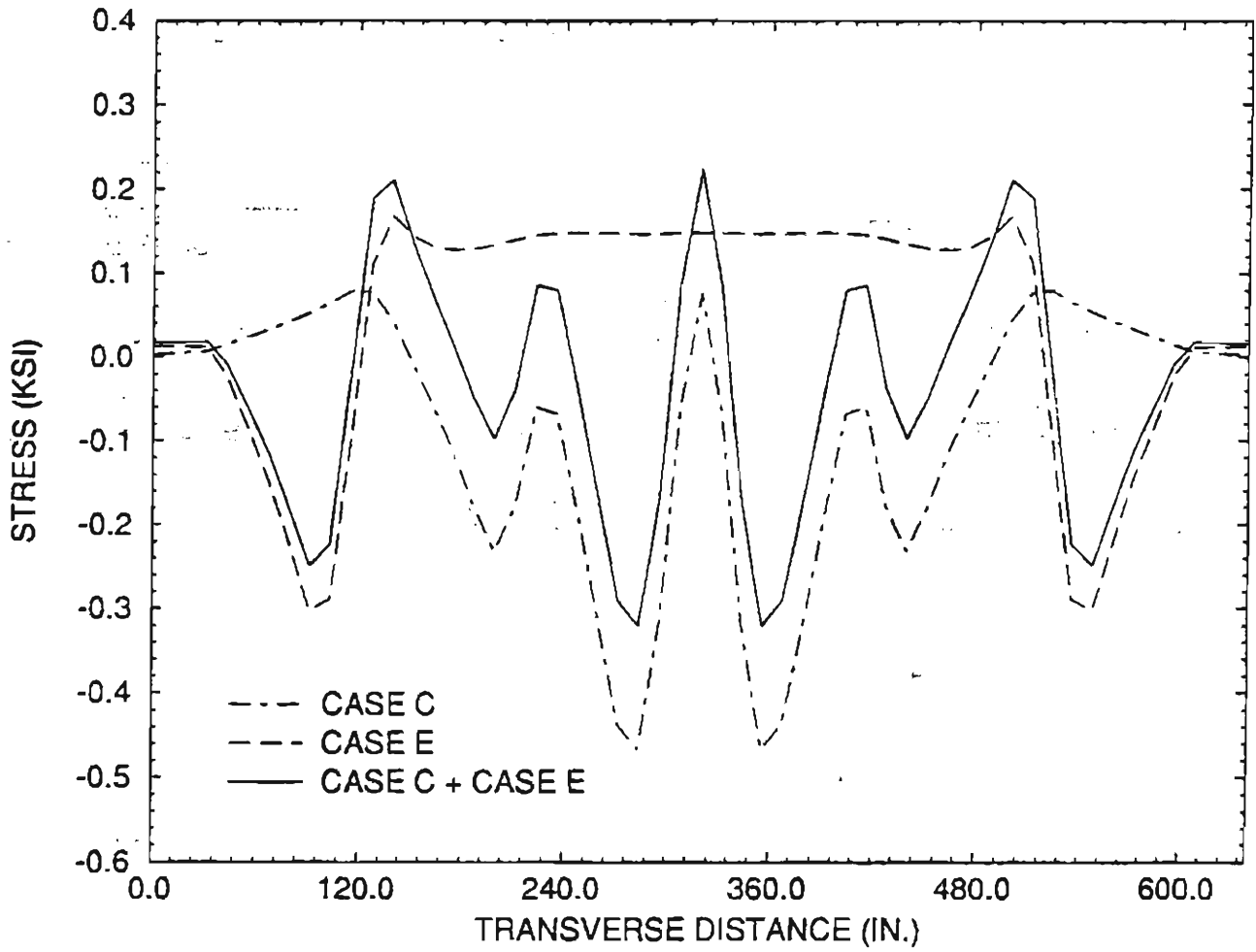


Figure 4.6: Transverse Bending Stresses at Top of the Deck along Critical Transverse Section under Cases C & E of Load Group 2

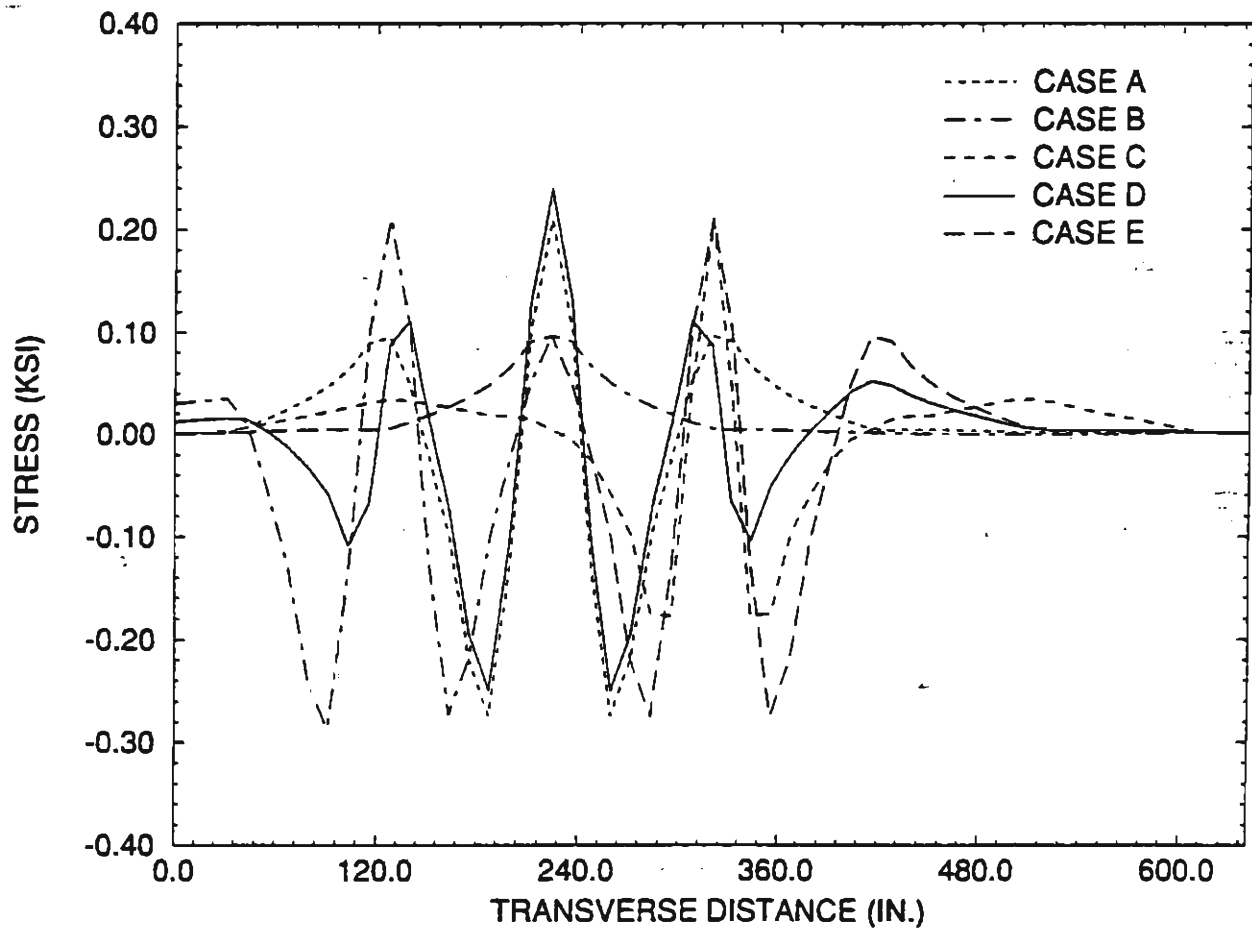


Figure 4.7: Transverse Bending Stresses at Top of the Deck along Critical Transverse Section (Load Group 3)

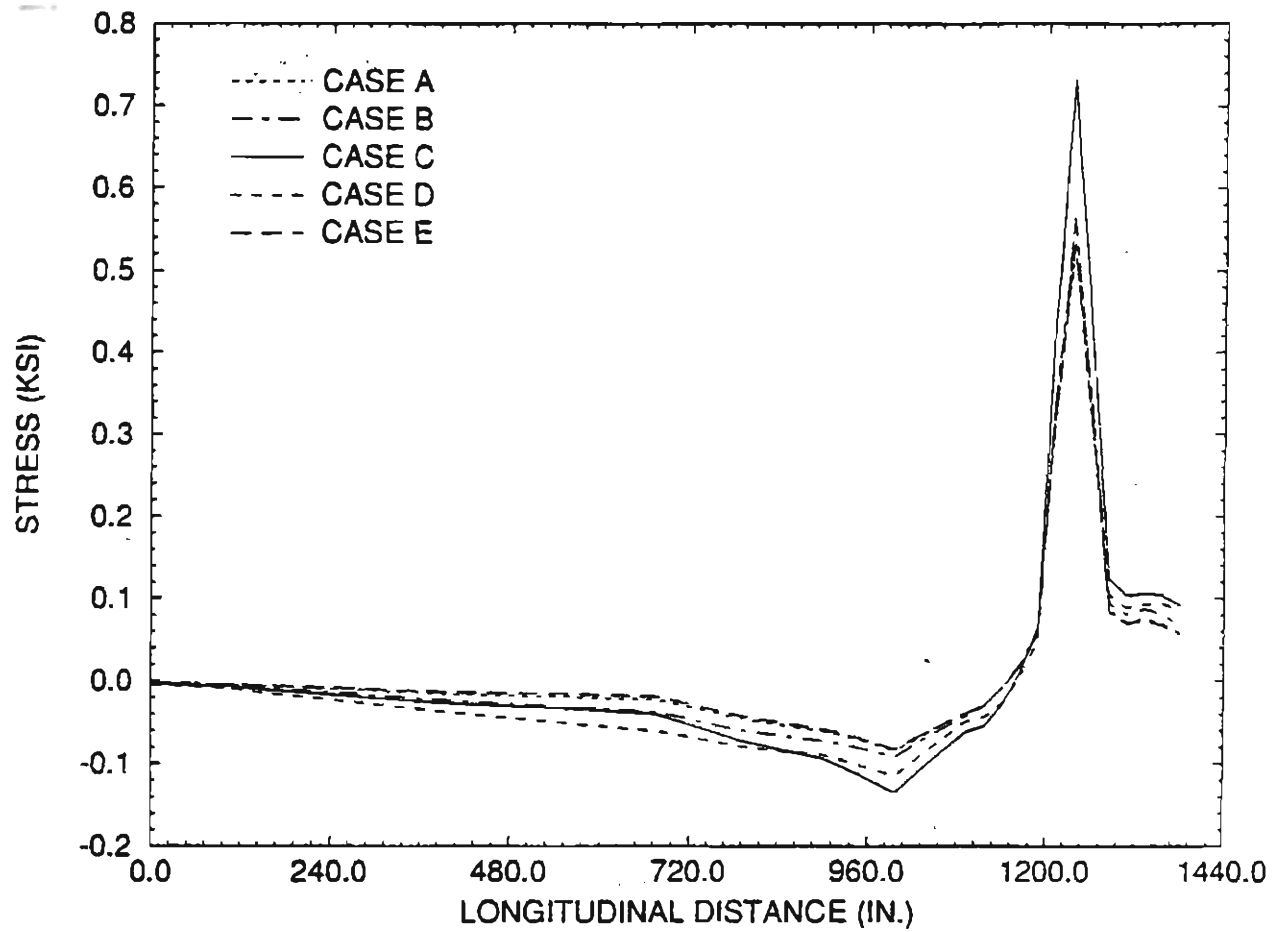


Figure 4.8: Longitudinal Bending Stresses at Top of the Deck along Critical Longitudinal Sections (Load Group 3)

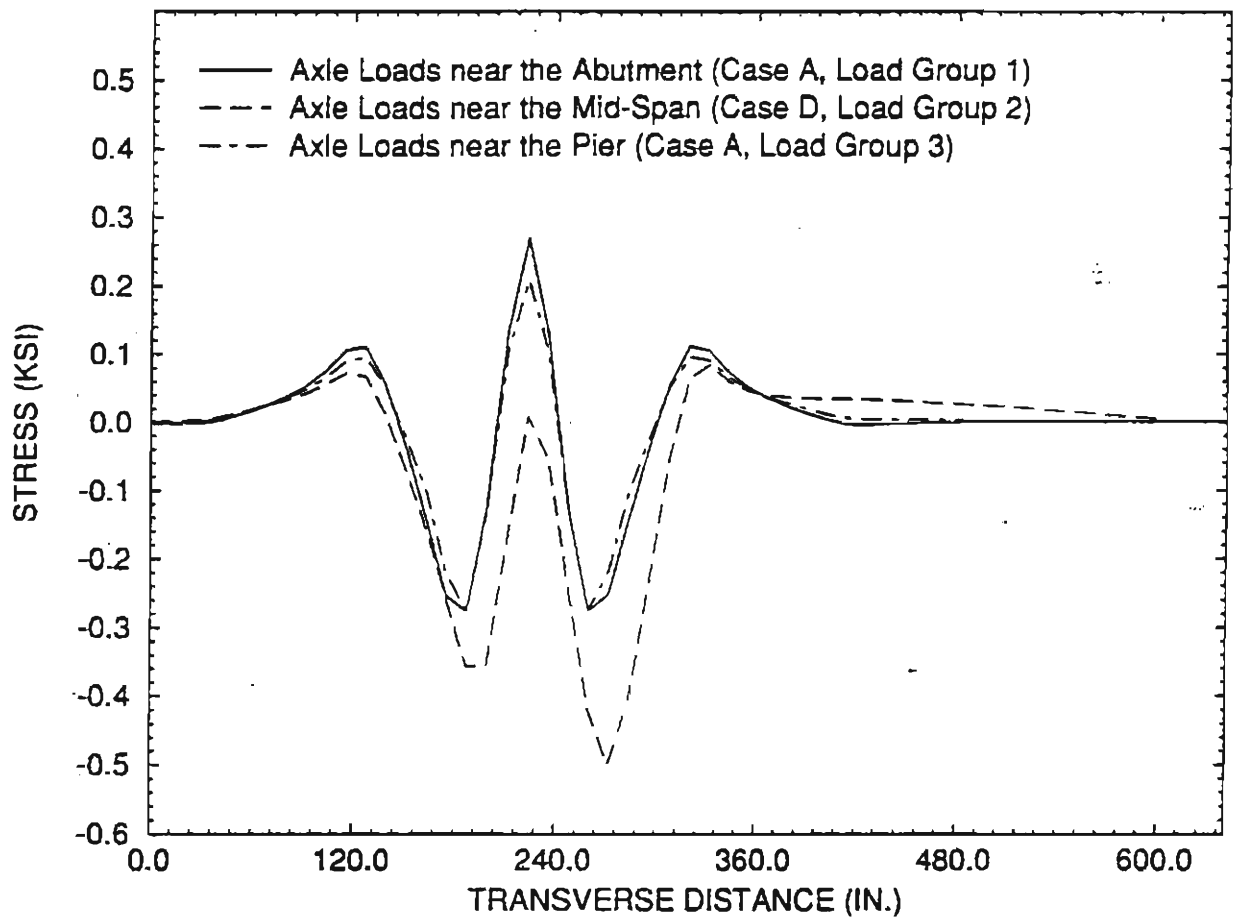


Figure 4.9: Critical Transverse Bending Stresses at Top of the Deck under Three Load Groups

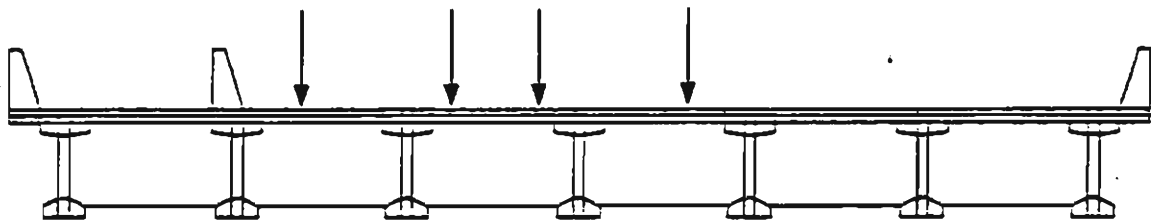
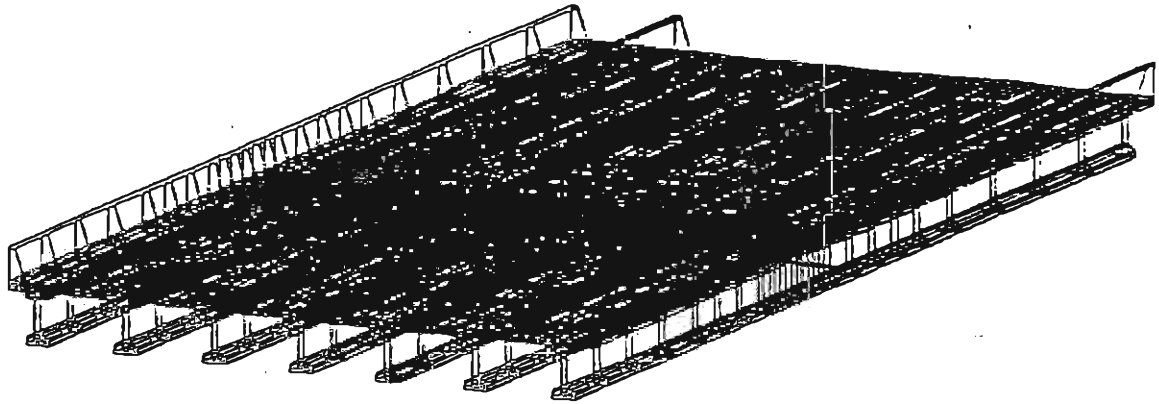


Figure 4.10: Bridge Deck with Concrete Railings

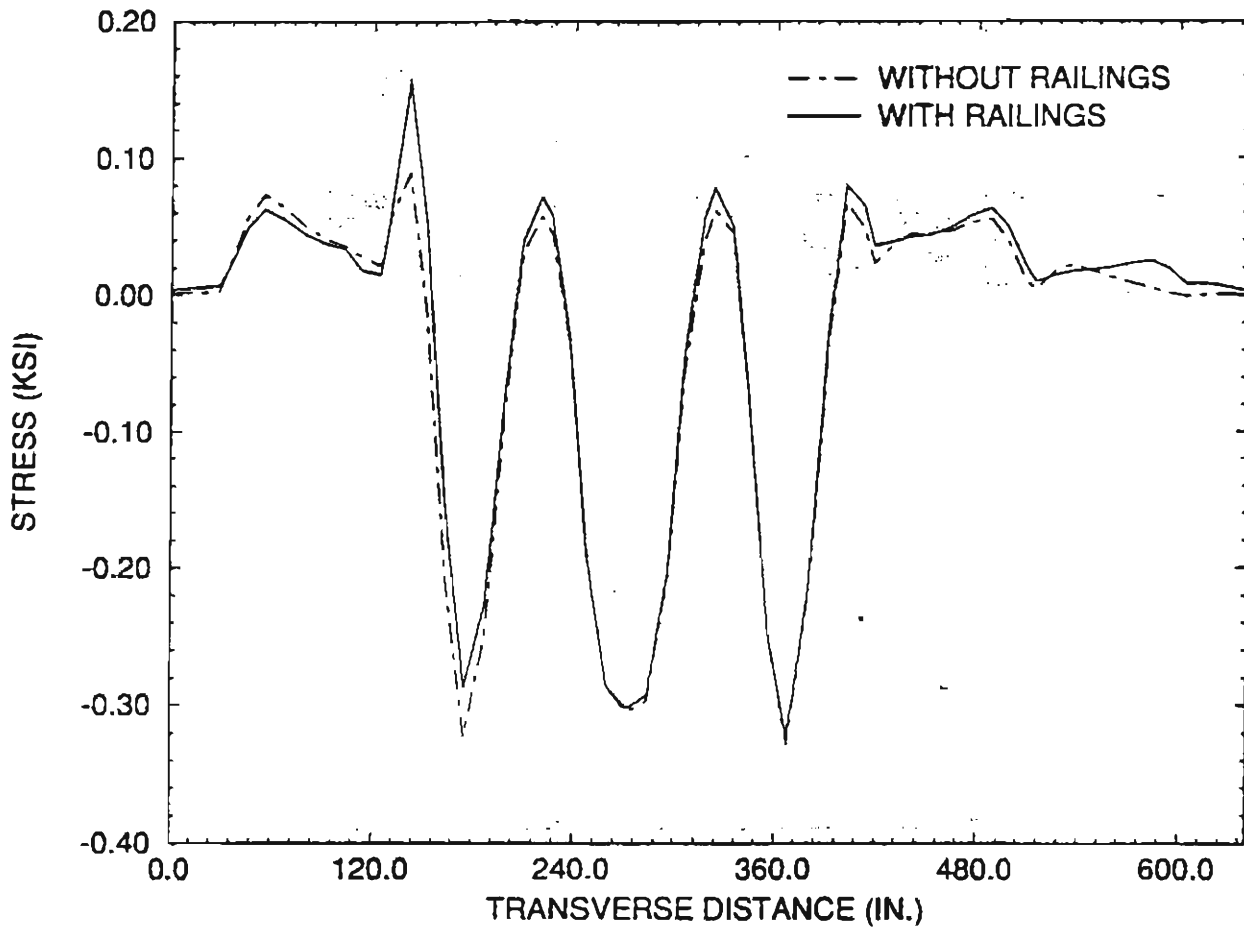


Figure 4.11: Comparison of Transverse Bending Stresses at Top of the Deck along Critical Transverse Section with and without Railings (Case B of Load Group 2)

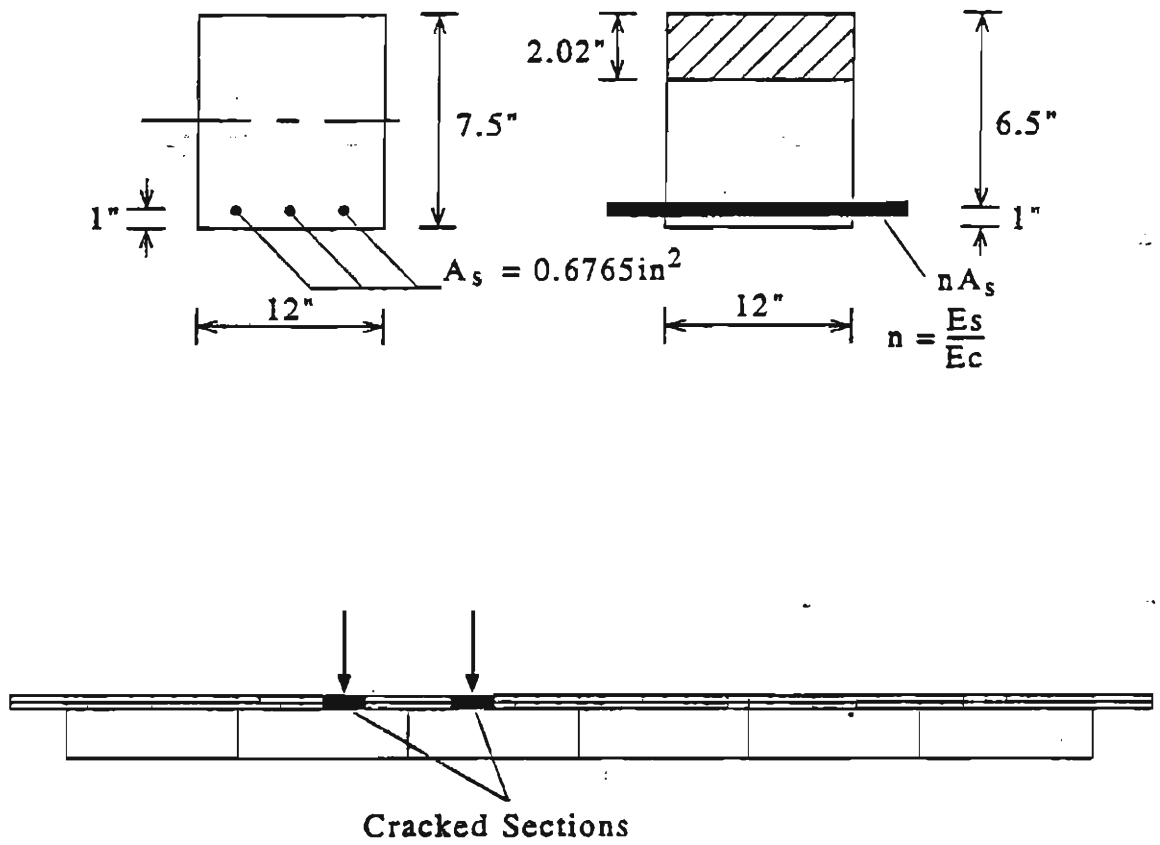


Figure 4.12: Cracked Transformed Section of the Bridge Deck

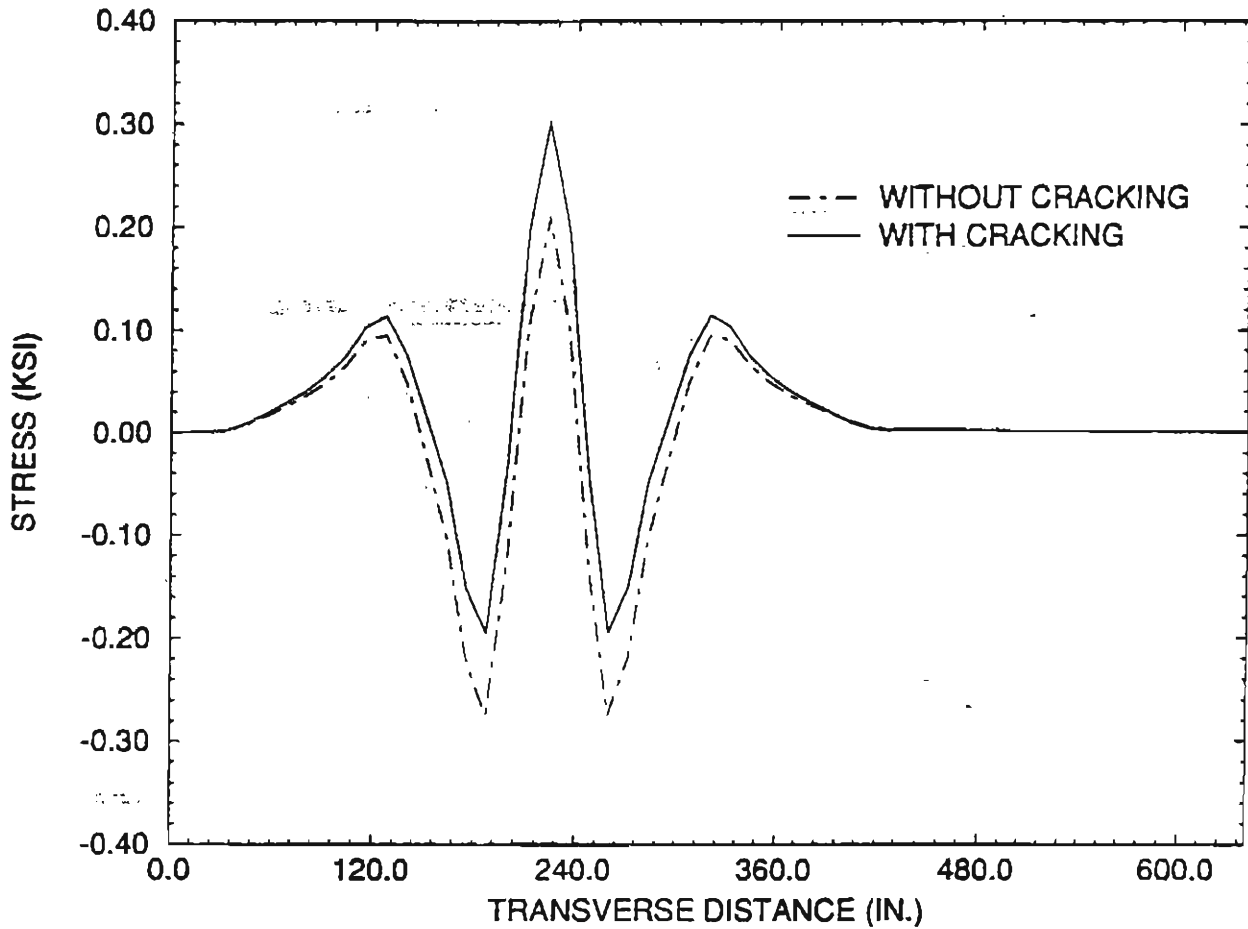


Figure 4.13: Comparison of Transverse Bending Stresses at Top of the Deck along Critical Transverse Section with and without Cracking (Case A of Load Group 3)

Chapter 5

CONCLUSIONS

The elastic behavior of a four-span slab-girder bridge deck has been analyzed with a finite element model. The response of the deck under fifteen different truck load cases has been investigated. The following conclusions have been reached.

1) A finite element model consisting of solid and 3-D beam elements is suitable for the analysis of slab-girder bridge decks. This has been validated by laboratory test results.

2) The flexibility of girders can significantly reduce the tensile stresses at the top of a concrete bridge deck. It has been found that the transverse tensile stresses at the top of the prototype bridge deck are well below the design tensile strength of deck concrete under the fifteen truck load cases. The maximum transverse tensile stress reached is 286 psi, which is only 61 percent of the design tensile strength (470 psi) of deck concrete and 68 percent of the tensile stress (420 psi) obtained with the AASHTO design moment. Hence, it is possible to eliminate the top reinforcing bars in the bridge deck.

3) The maximum transverse positive bending moment is increased due to girder deflection. It has been found that the maximum transverse tensile stress (520 psi) at the bottom of the prototype bridge deck is 24 percent greater than the tensile stress (420 psi) obtained with the AASHTO design moment.

4) The concrete railings on a bridge can increase the transverse tensile stress by about 76 percent at the top of the deck in the vicinity of the interior railing, but it is still only 33 % of the expected tensile strength of deck concrete. At locations far away from the interior railing, the effect of concrete railings is not significant. Hence, the effect of the concrete railings can be ignored in the analysis of the prototype bridge deck.

5) When the effect of deck cracking due to positive bending moment is considered, the maximum top transverse tensile stresses in the deck can increase. However, the effect of deck cracking on the top tensile stress in the deck needs further investigation.

For further studies, it will be informative to conduct non-linear stress analysis of the prototype bridge deck, considering the cracking of concrete. Such studies will provide a better understanding of the behavior of concrete bridge decks under extreme traffic loads. Furthermore, it may be useful to investigate the dynamic effect of truck loads in a more realistic fashion.

The finite element model proposed here will be further validated by field tests of the prototype bridge. Once validated, further parametric studies can be conducted with the model to develop rational design guidelines that incorporate the flexibility of deck girders.

The prototype bridge utilized for this case study is a relatively stiff structure. More flexible bridges such as steel-girder bridges can be more significantly affected by girder deflections. Hence, AASHTO design bending

moments may be unconservative for the positive moment region and over-conservative for the negative moment region of these bridges.

REFERENCES

Allen, J. H. (1991). "Cracking, Serviceability and Strength of Concrete Bridge Decks", Third Bridge Engineering Conference, *Transportation Research Record No. 1290*, Transportation Research Board, National Research Council, Washington, D.C., 152-171.

Beal, D. B. (1982). "Load Capacity of Concrete Bridge Decks", *Journal of Structural Engineering*, ASCE, Vol. 108, No. 4, 814-832.

Building Code Requirements for Reinforced Concrete (*ACI 318-89*) (1989), American Concrete Institute.

Cracking of Concrete Members in Direct Tension (*ACI 224.2R-92*) (1992), American Concrete Institute.

Fang, I. K., Worley, J. A., Burns, N. H. and Klingner, R. E. (1990). "Behavior of Isotropic R/C Bridge Decks on Steel Girders", *Journal of Structural Engineering*, ASCE, Vol. 116, No. 5, 659-678.

Lin, J. J. et al. (1991). "Nonlinear Analysis of Composite Bridges by the Finite Element Method", *Computers & Structures*, Vol. 40, No. 3.

Memari, A. M. and West, H. H. (1991). "Computation of Bridge Design Forces From Influence Surface", *Computers & Structures*, Vol. 38, No. 5/6.

Minutes of AASHTO Bridge Subcommittee (1957-1961), Federal Highway Administration Files, AASHTO.

Mufie, A. A. et al. (1991). "Fiber Reinforced Concrete Deck Slabs without Steel Reinforcements", *Technical Report*, Technical University of Nova Scotia, July.

Newmark, N. M. (1949). "Design of I-Beam Bridges", A Symposium of Highway Bridge Floors, *ASCE Transactions*, Vol. 114, 979-1072.

Razaqpur, A. G. and Nofal, M. (1989). "A Finite Element for Model-

ing the Nonlinear Behavior of Shear Connectors in Composite structures",
Computers & Structures, Vol. 32, No. 1.

· *Standard Specifications for Highway Bridges (1935)*, 2nd ed., AASHTO,
Washington, D.C..

· *Standard Specifications for Highway Bridges (1989)*, 14th ed., AASHTO,
Washington, D.C..

· Westergaard, H. M. (1930). "Computations of Stresses in Bridge Slabs
Due to Wheel Loads", *Public Roads*, pp. 1-23, March.

· Wilson, E. L. et al. (1989). *SAP90 Program User's Manual*, Computers
& Structures, Inc.

Appendix A

STRESS CONTOURS AT THE TOP OF THE BRIDGE DECK



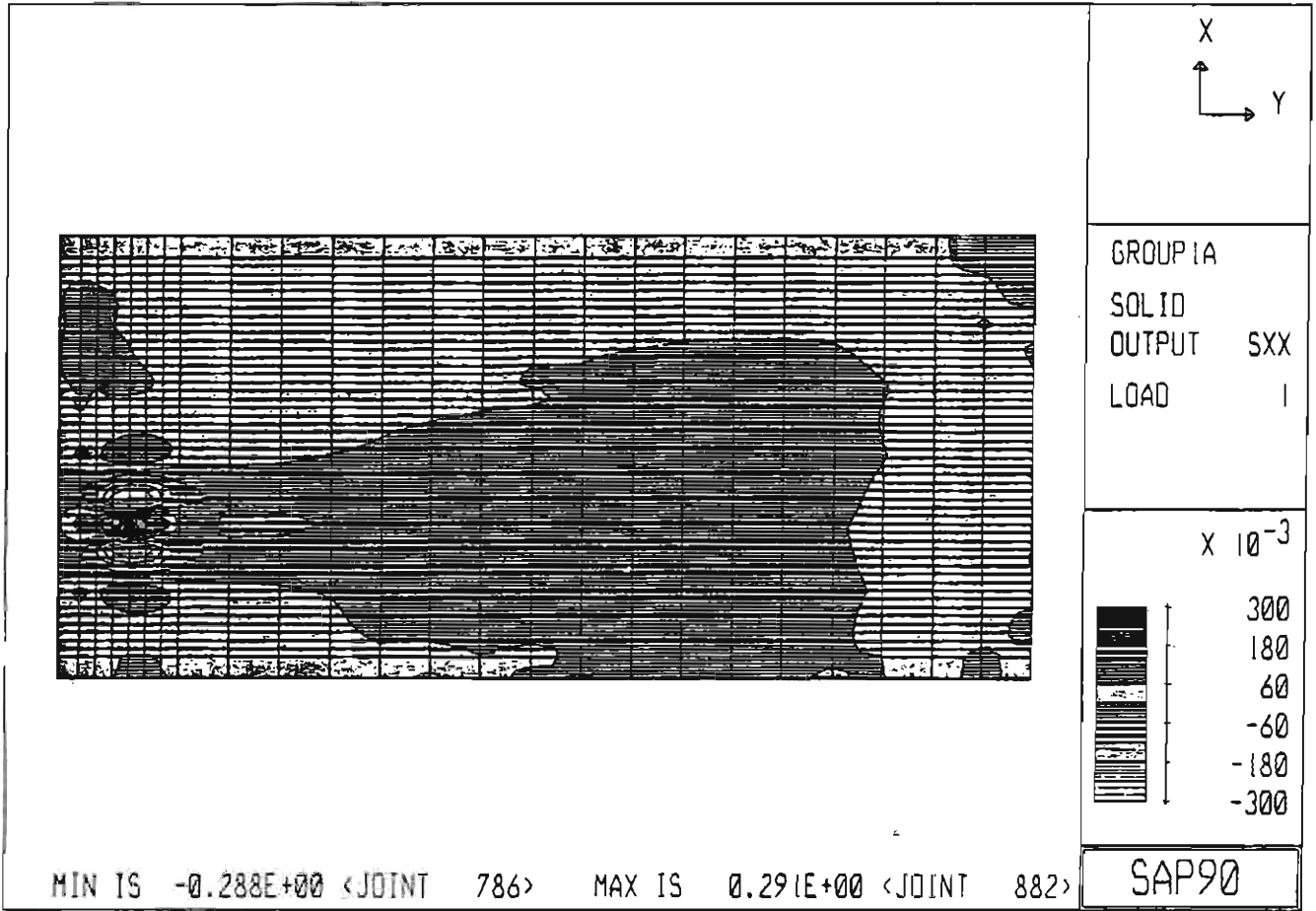


Fig A.1 Stress Contour of Top Transverse Stress
 (Case A of Load Group 1)

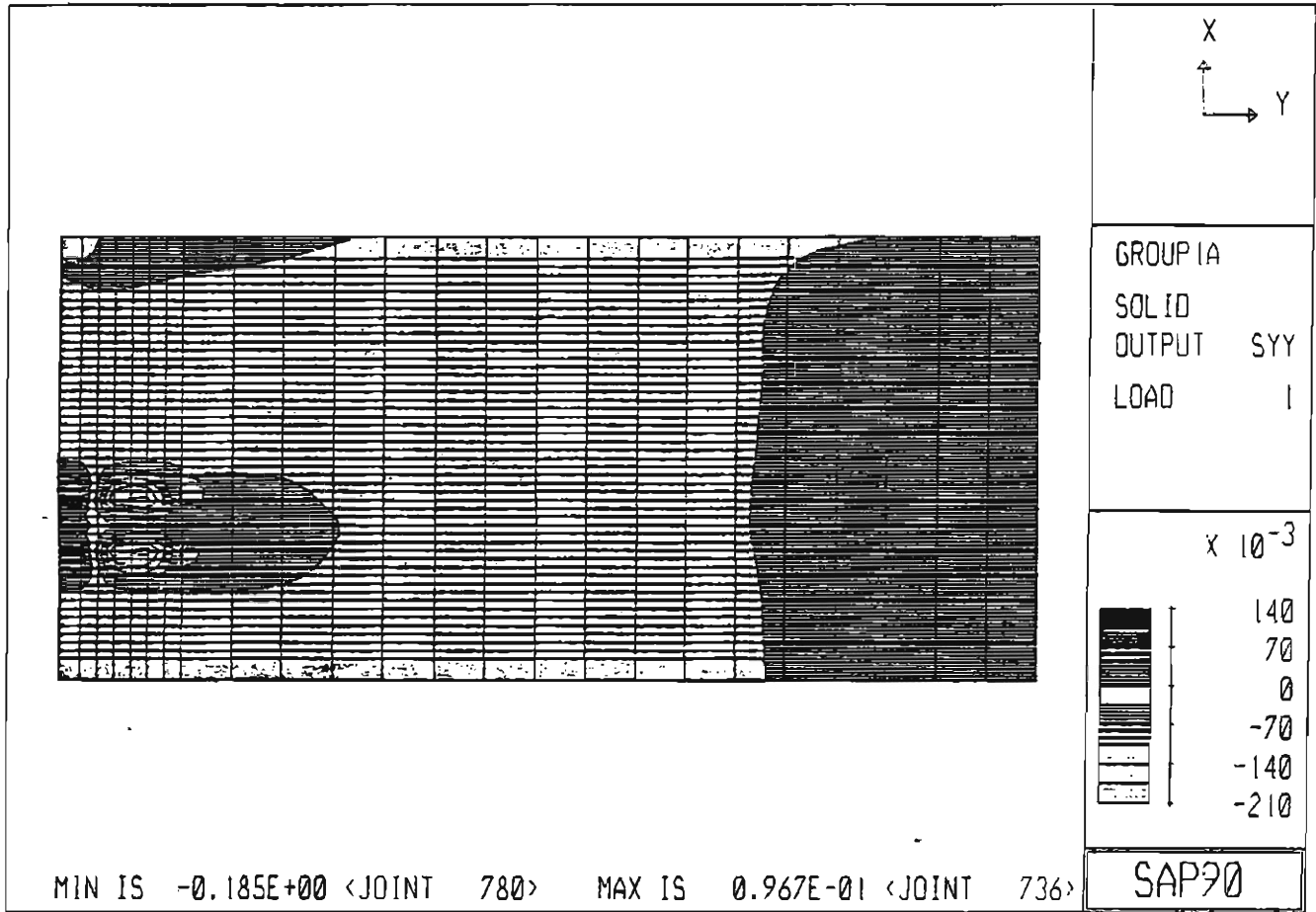


Fig. A.2 Stress Contour of Top Longitudinal Stress
(Case A of Load Group 1)

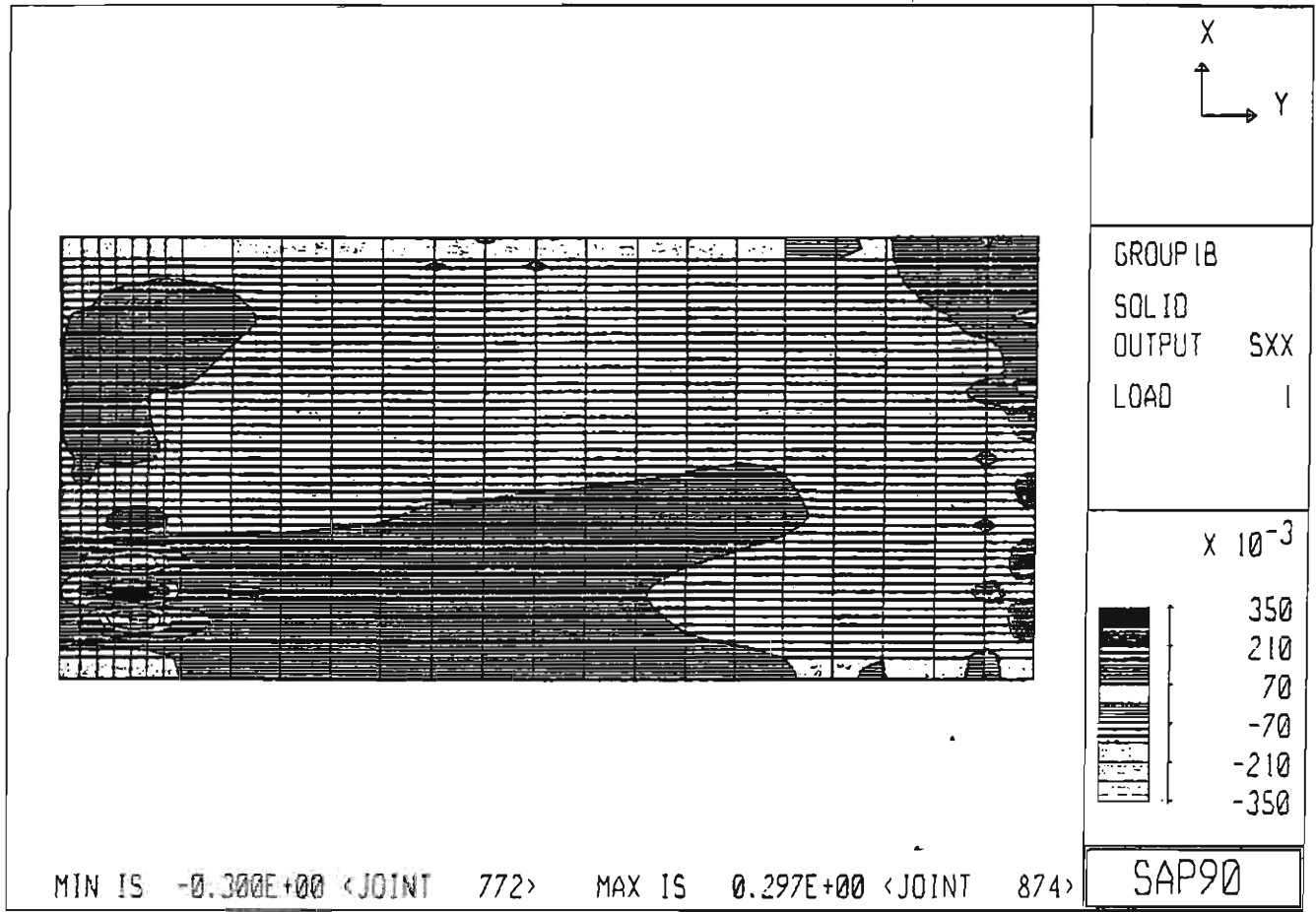


Fig. A.3 Stress Contour of Top Transverse Stress
 (Case B of Load Group 1)

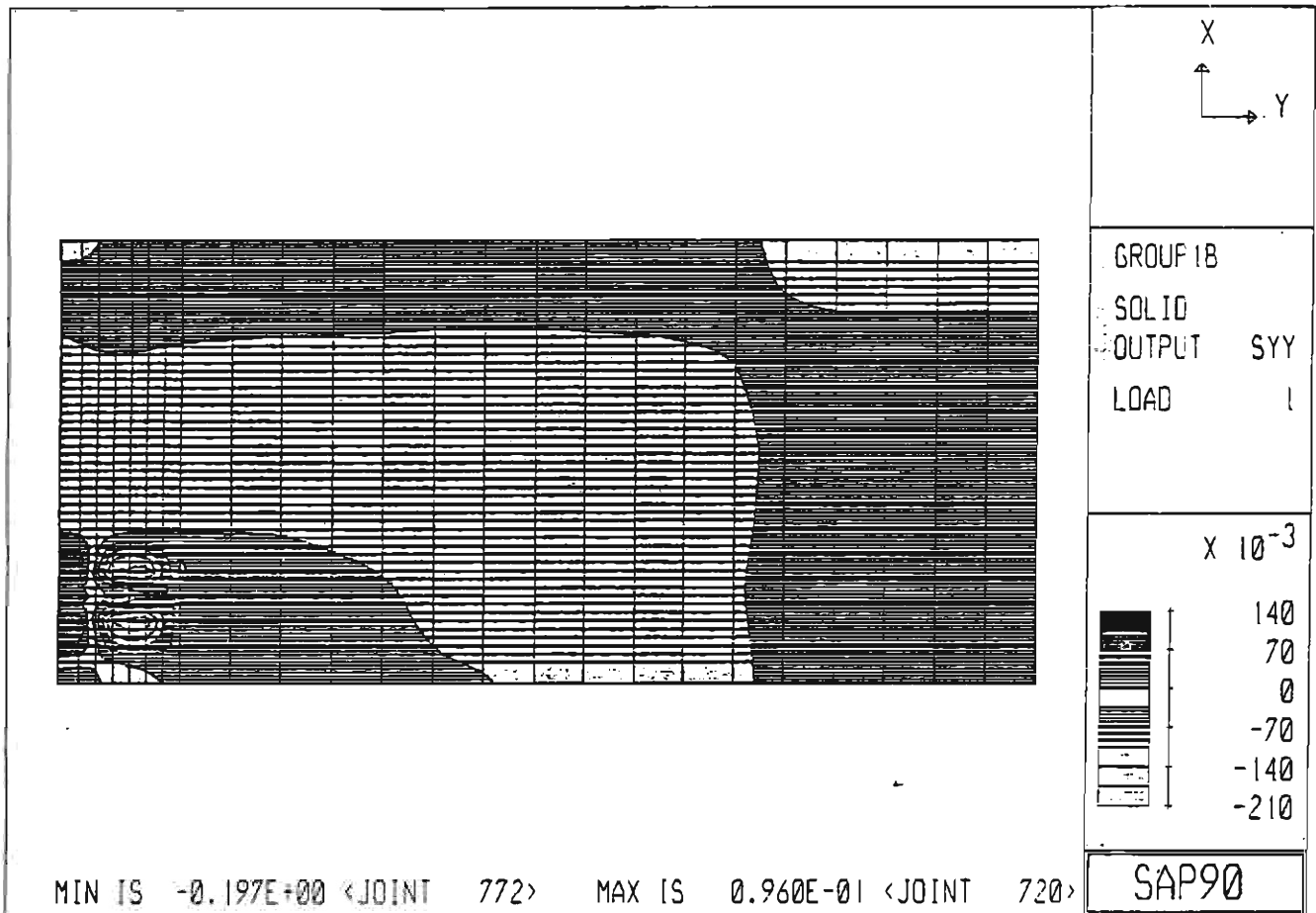


Fig. A.4 Stress Contour of Top Longitudinal Stress
(Case B of Load Group 1)

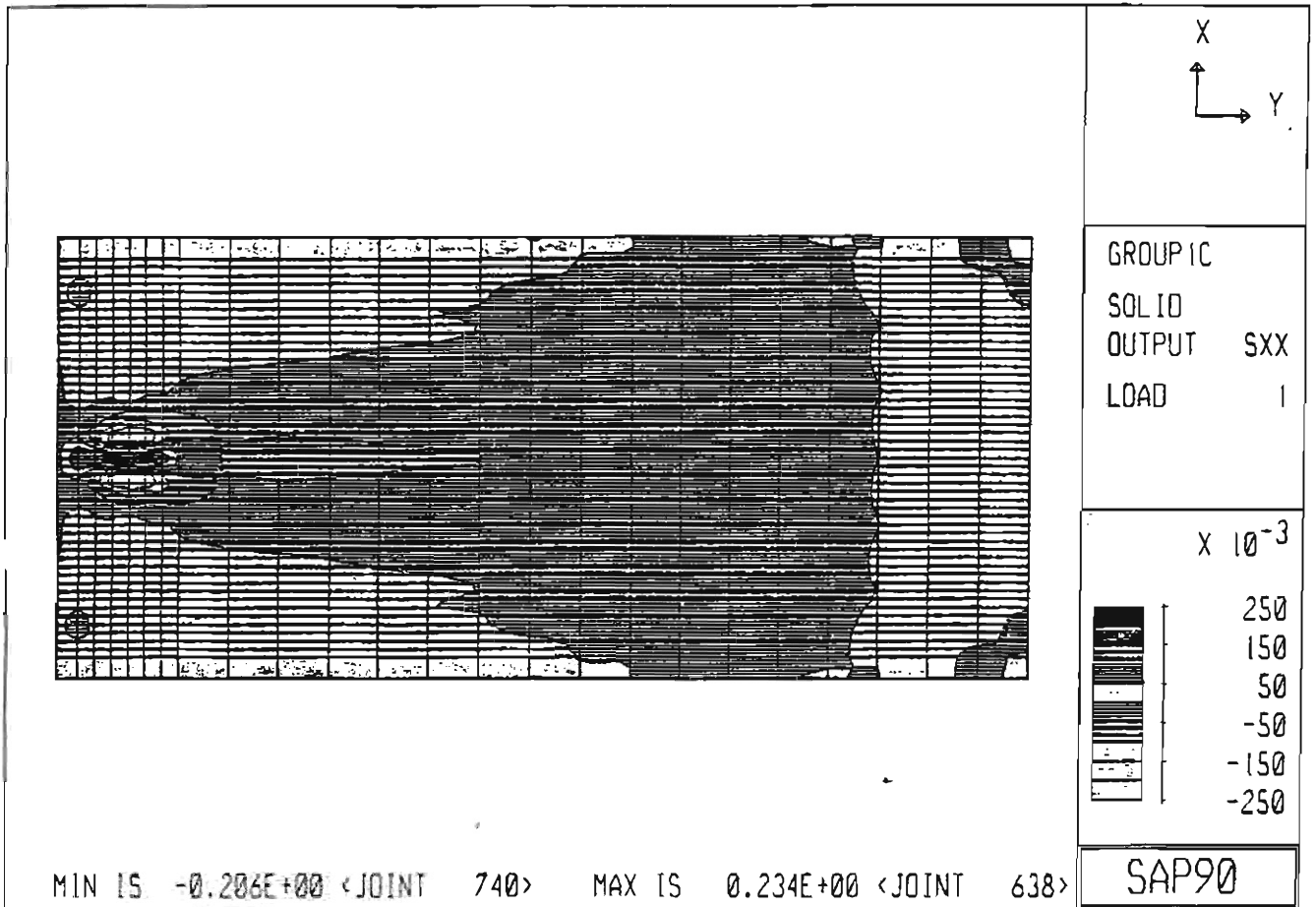


Fig. A.5 Stress Contour of Top Transverse Stress
(Case C of Load Group 1)

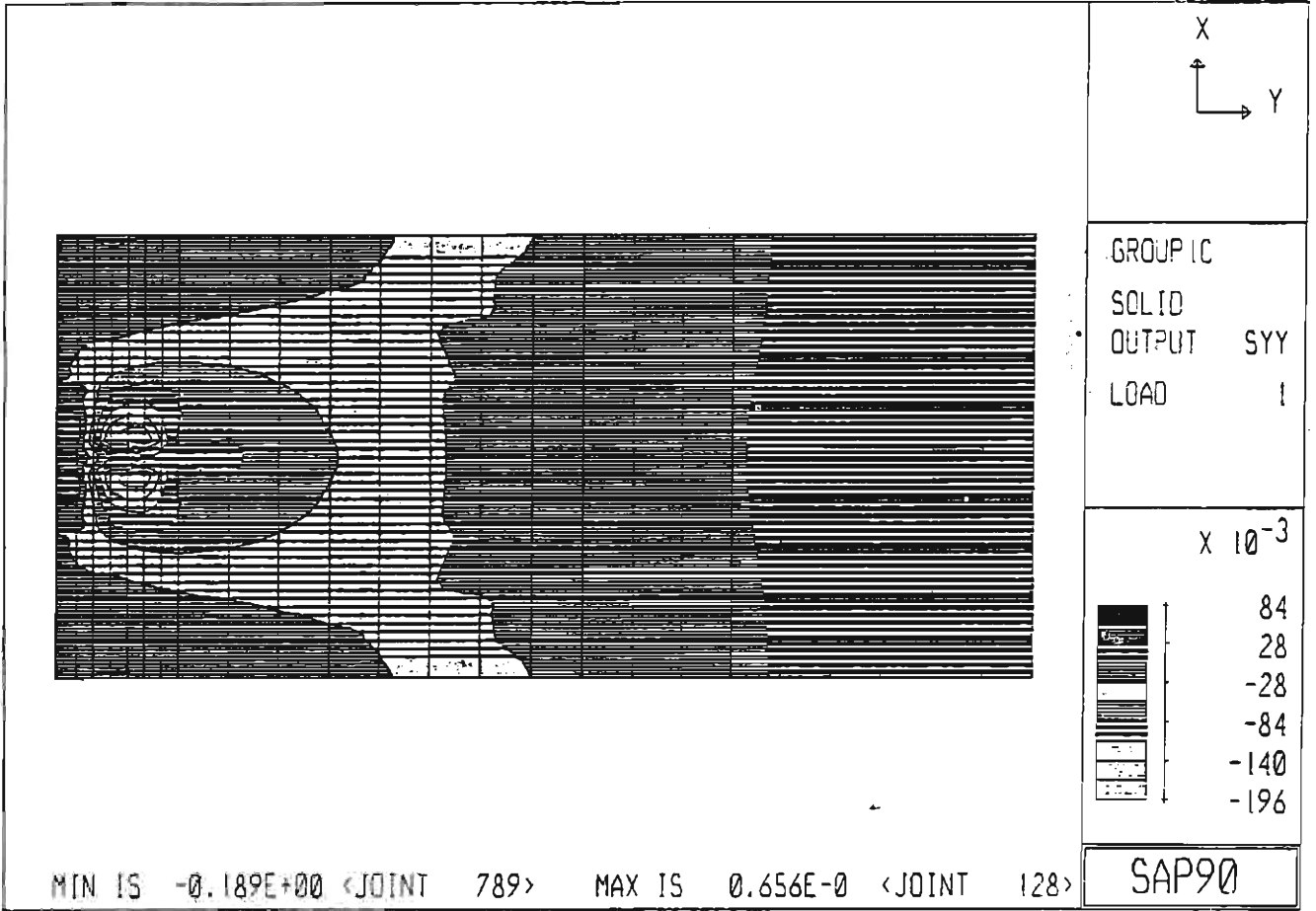


Fig. A.6 Stress Contour of Top Longitudinal Stress
(Case C of Load Group 1)

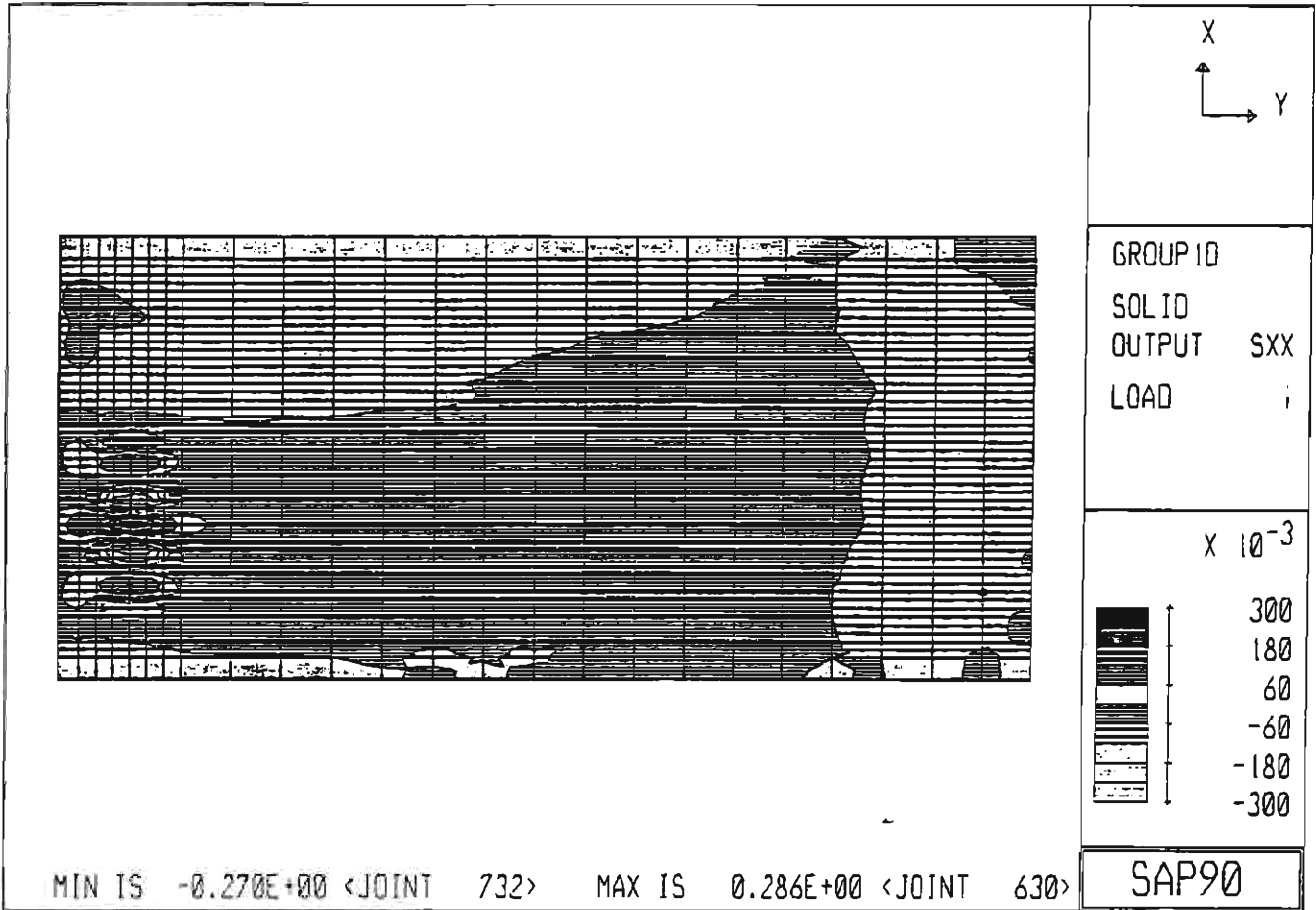


Fig. A.7 Stress Contour of Top Transverse Stress
 (Case D of Load Group 1)

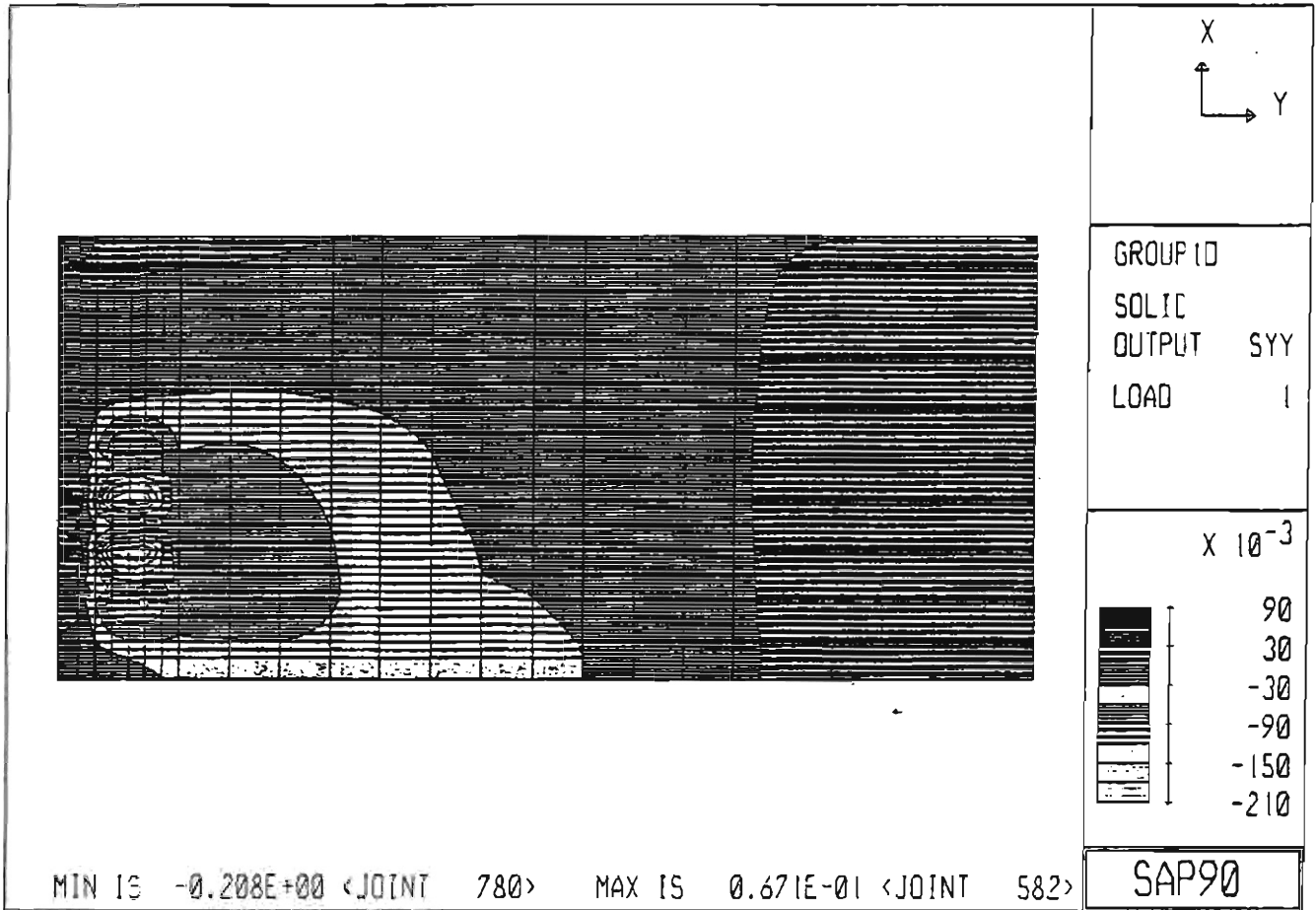


Fig. A.8 Stress Contour of Top Longitudinal Stress
(Case D of Load Group 1)

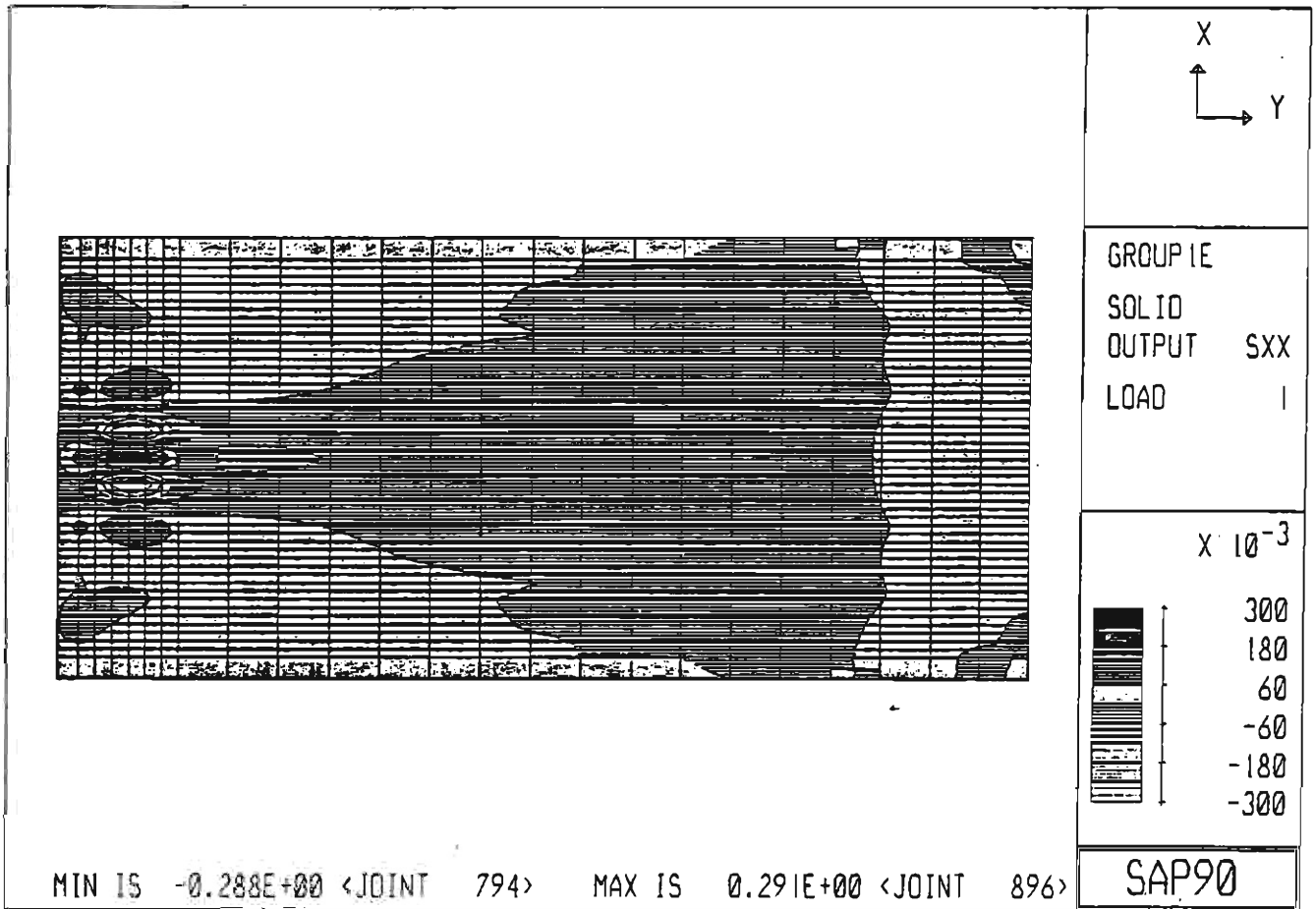


Fig. A.9 Stress Contour of Top Transverse Stress
(Case E of Load Group 1)

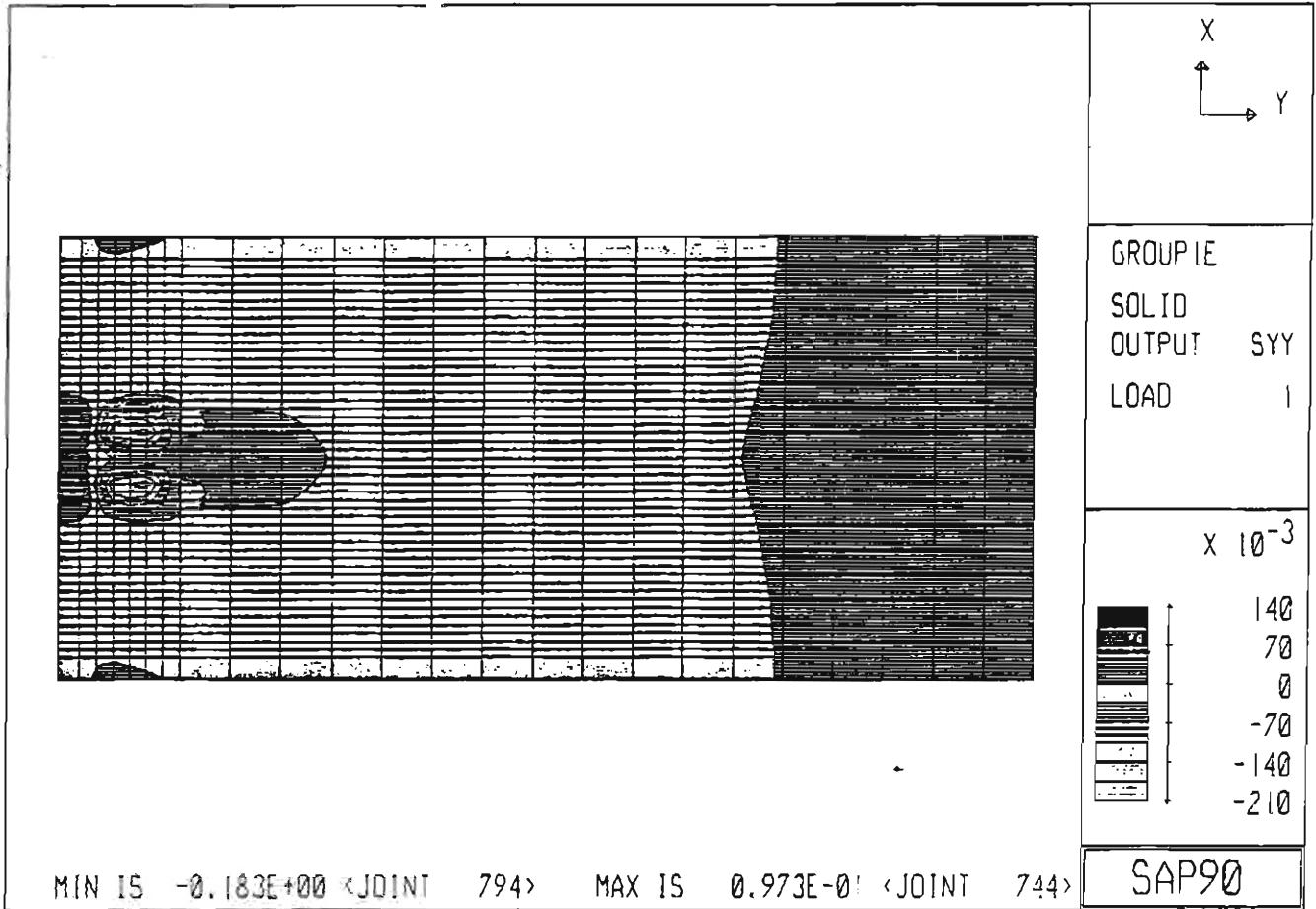


Fig. A.10 Stress Contour of Top Longitudinal Stress
(Case E of Load Group 1)

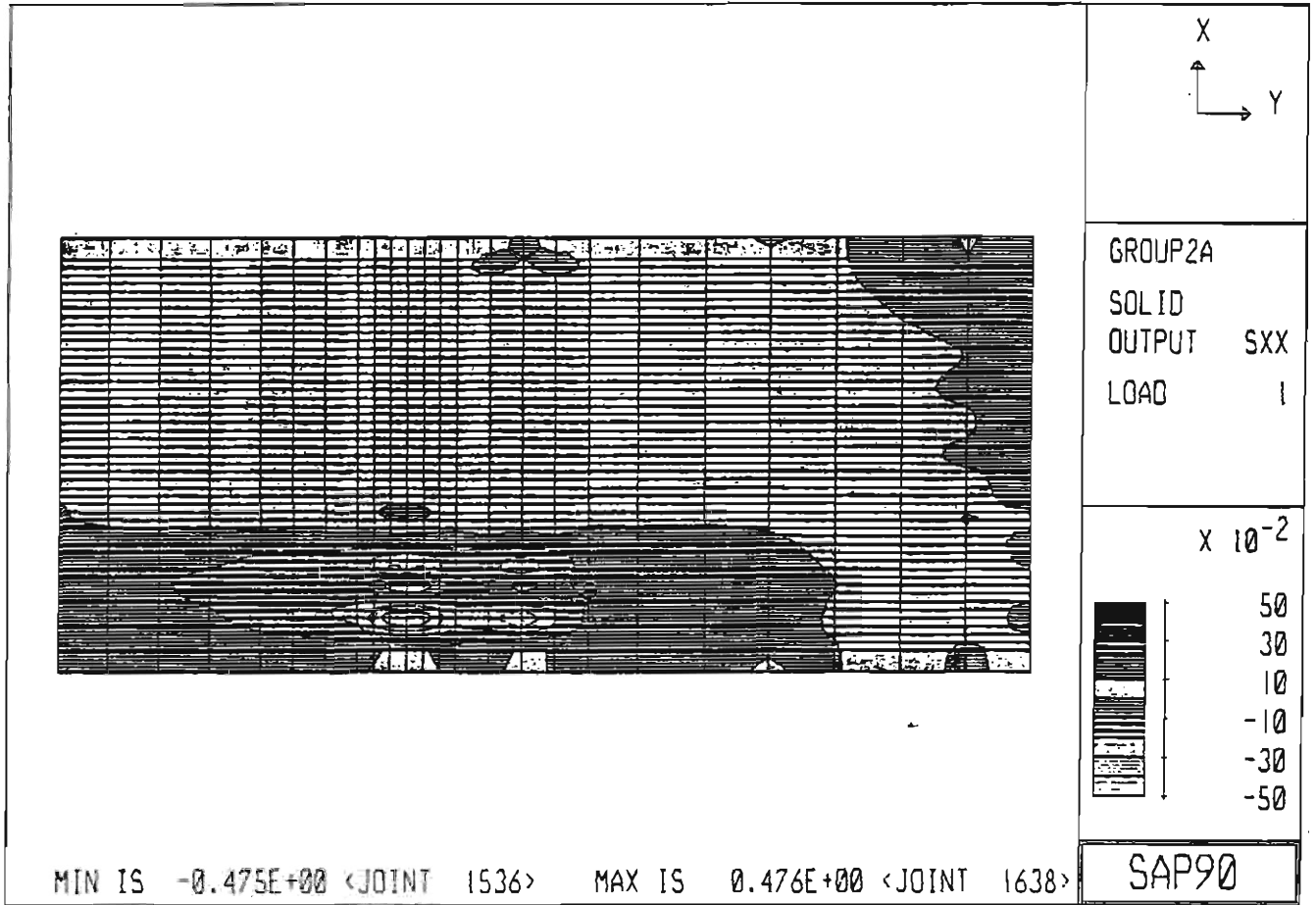


Fig. A.11 Stress Contour of Top Transverse Stress
 (Case A of Load Group 2)

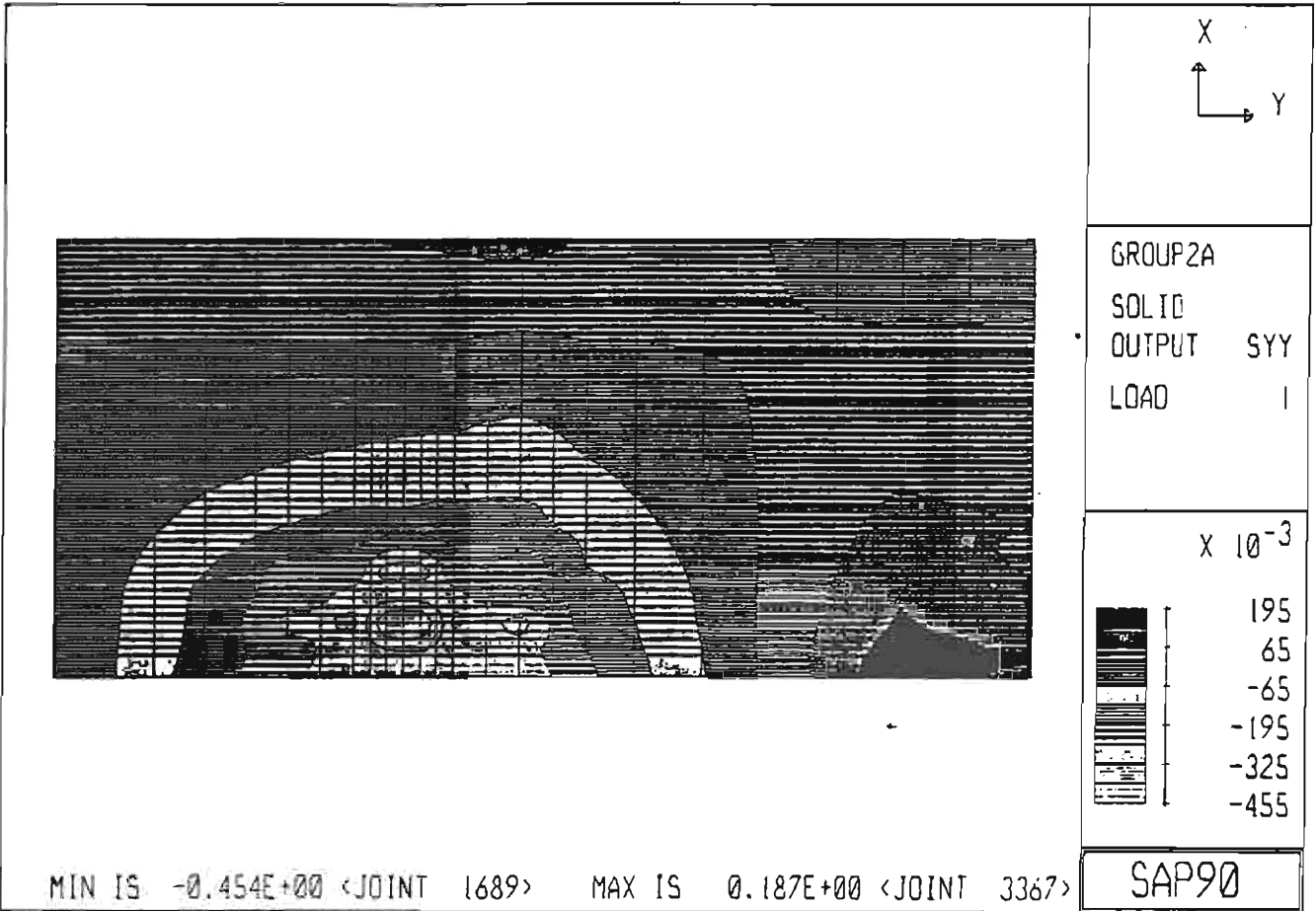


Fig. A.12 Stress Contour of Top Longitudinal Stress
 (Case A of Load Group 2)

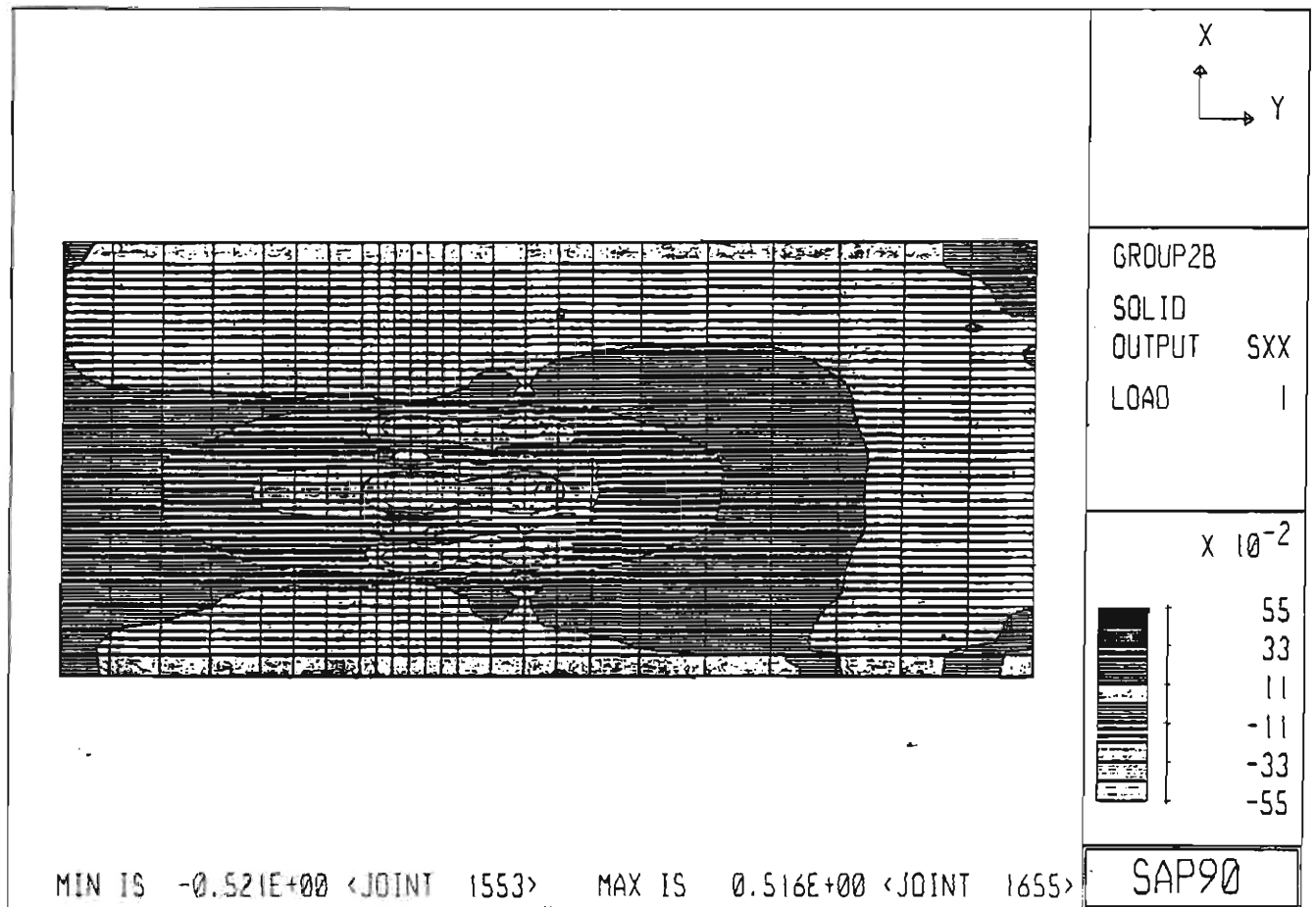


Fig. A.13 Stress Contour of Top Transverse Stress
(Case B of Load Group 2)

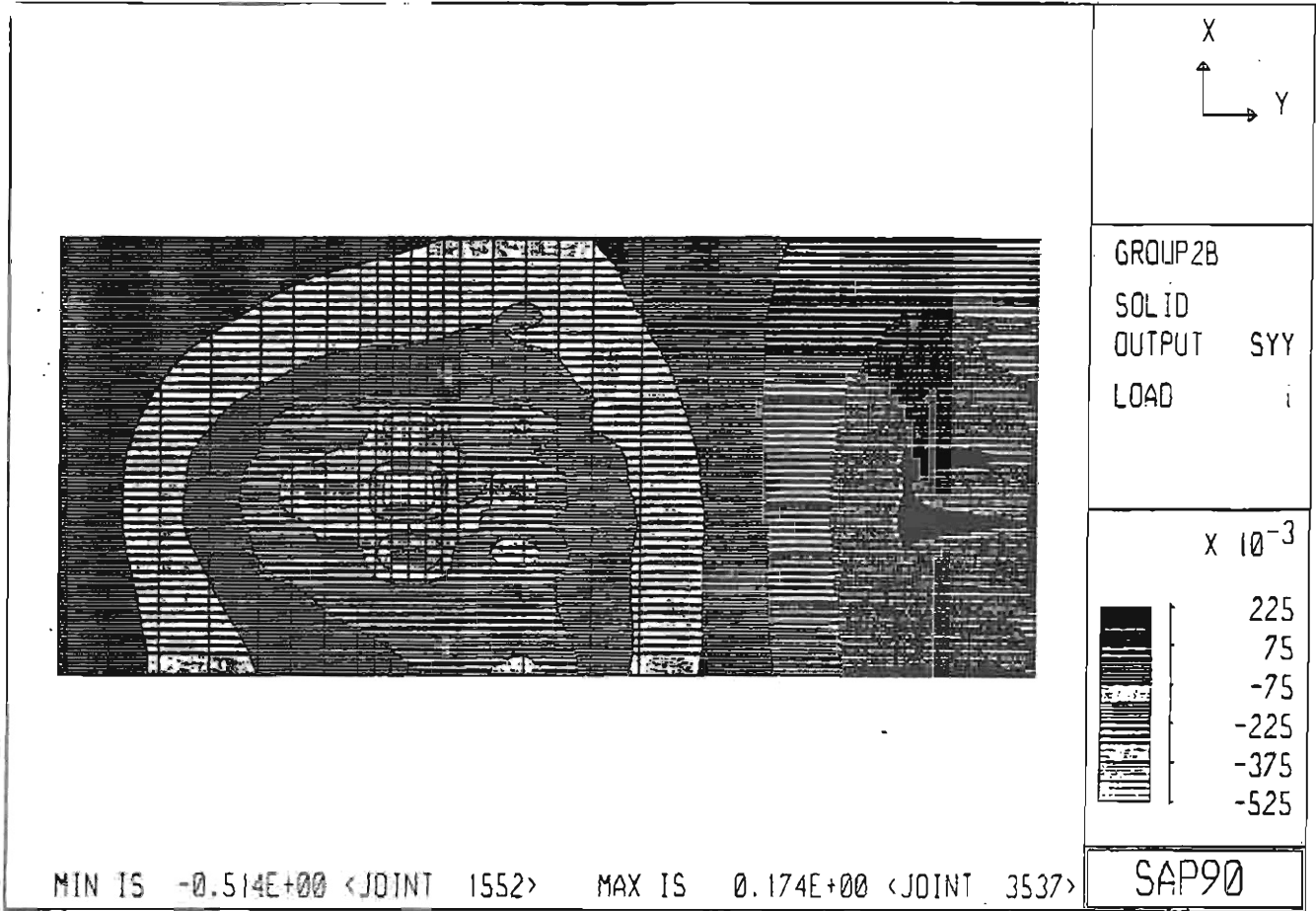


Fig. A.14 Stress Contour of Top Longitudinal Stress
 (Case B of Load Group 2)

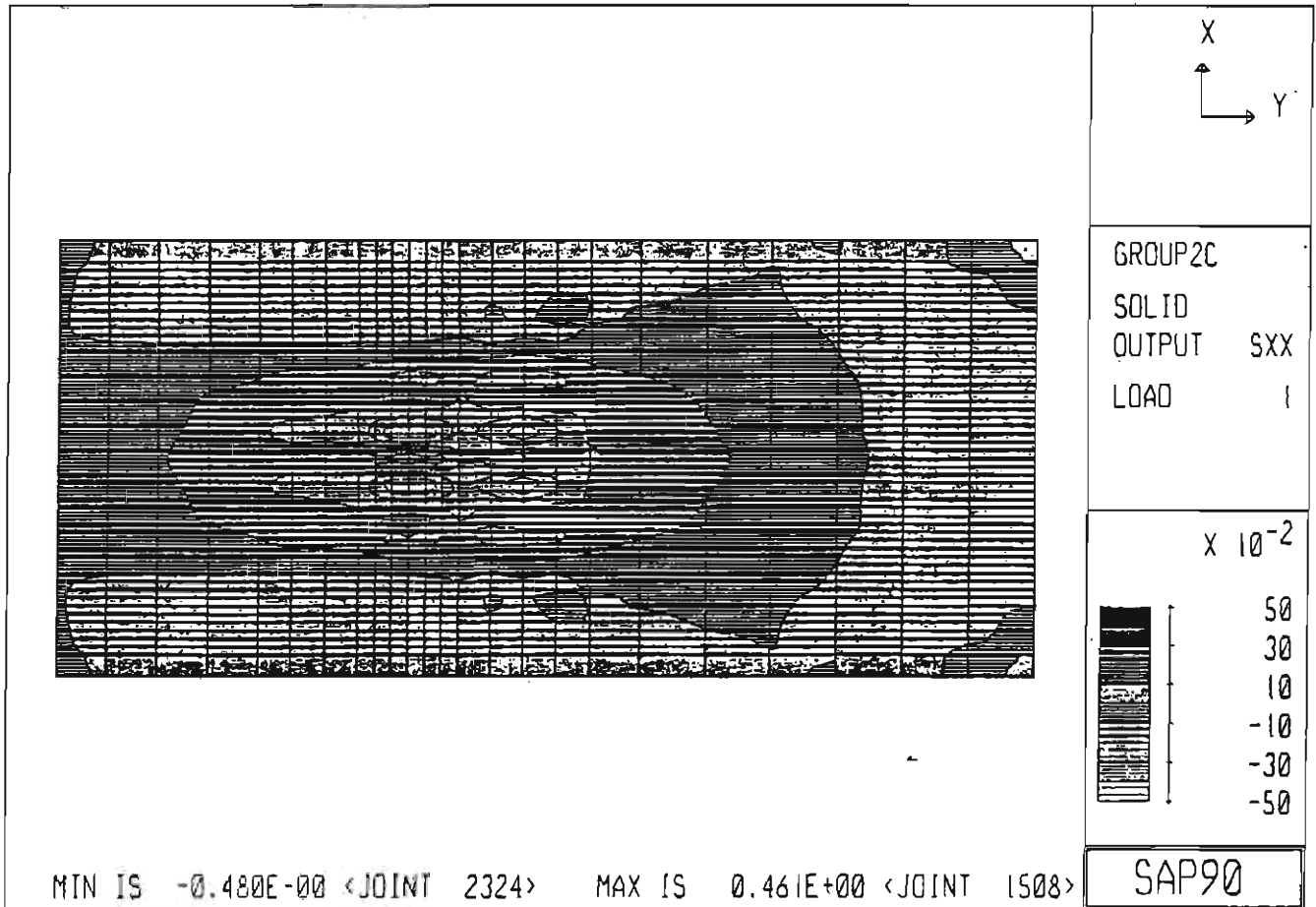


Fig. A.15 Stress Contour of Top Transverse Stress
 (Case C of Load Group 2)

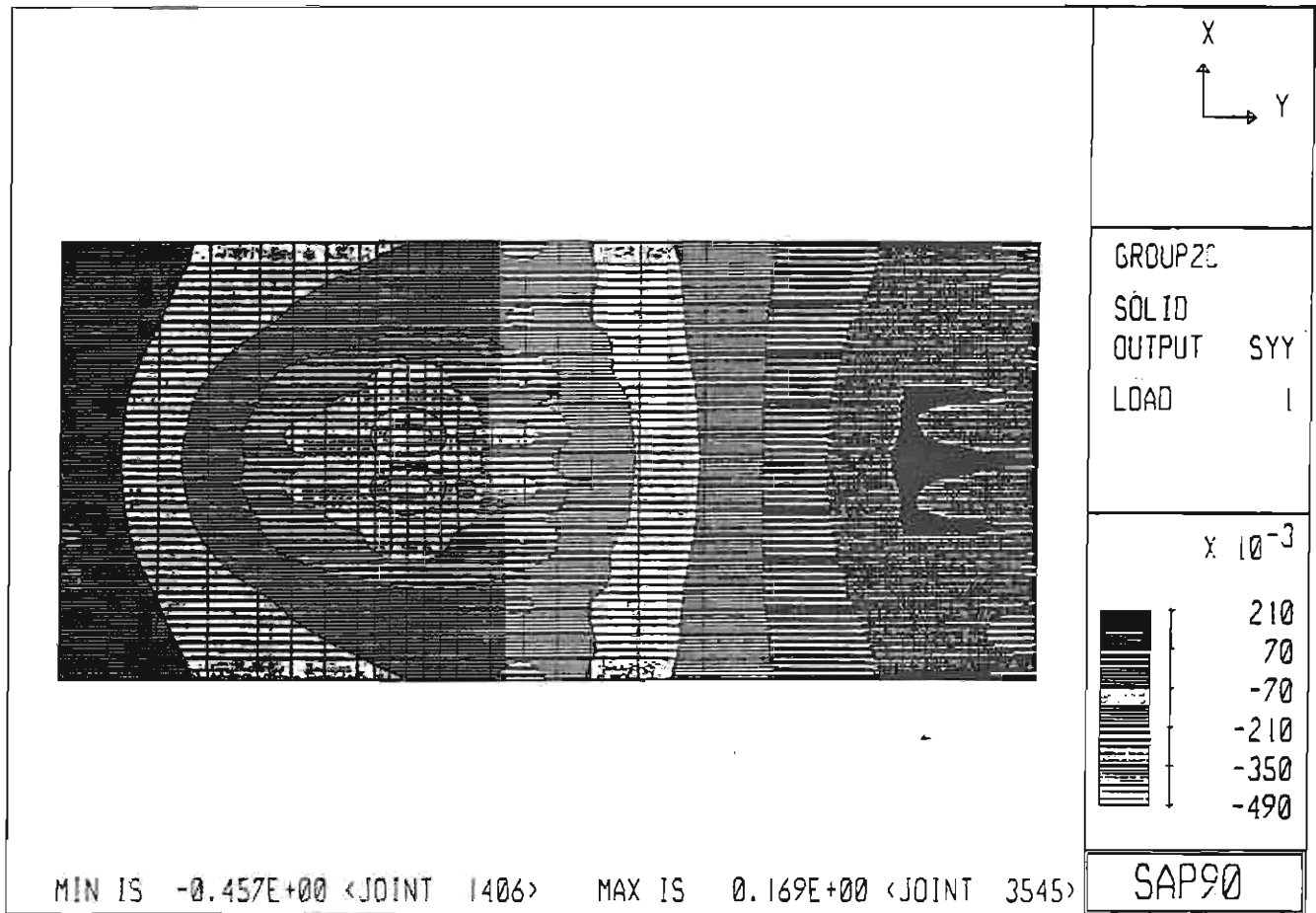


Fig. A.16 Stress Contour of Top Longitudinal Stress
 (Case C of Load Group 2)

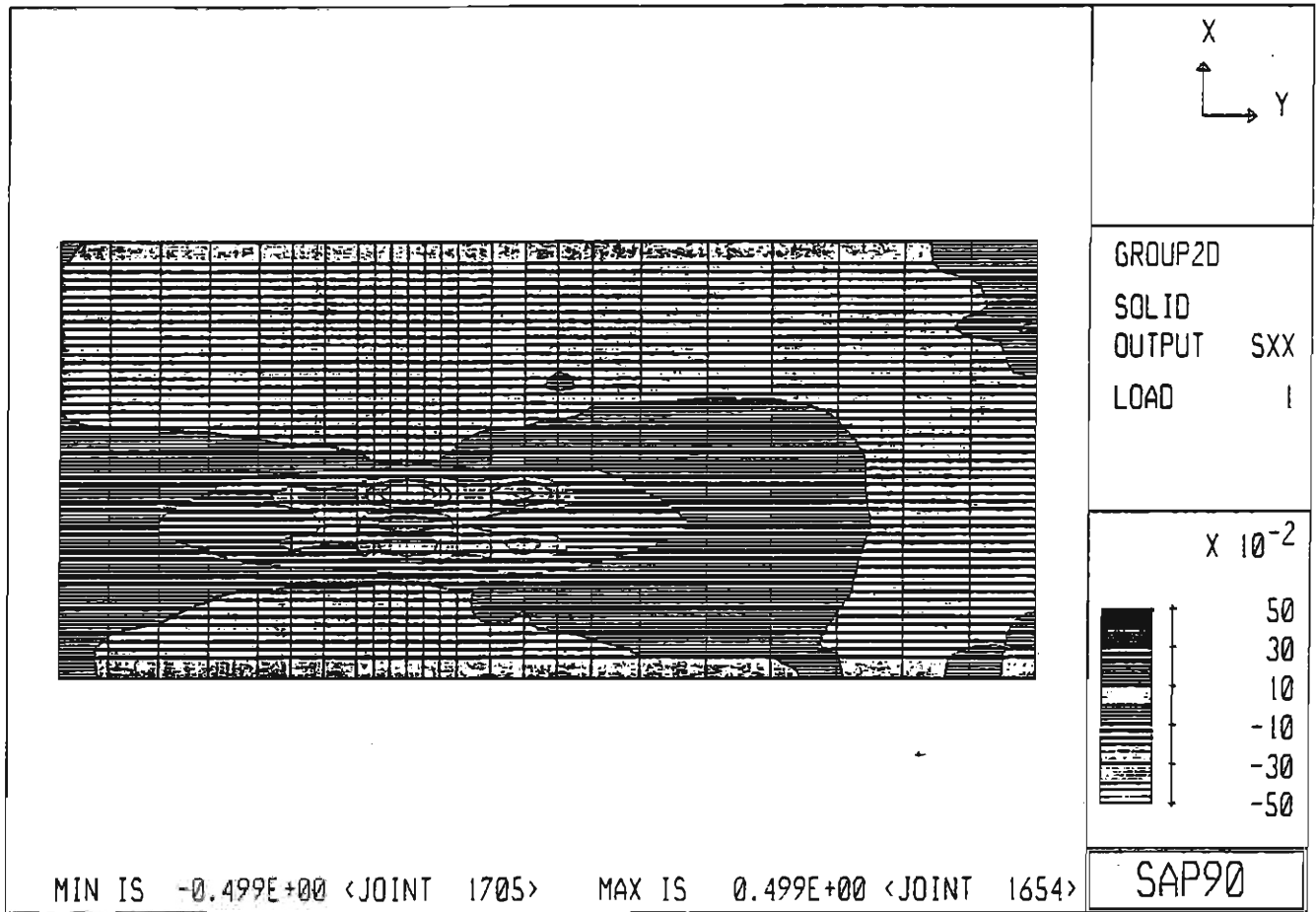


Fig. A.17 Stress Contour of Top Transverse Stress
 (Case D of Load Group 2)

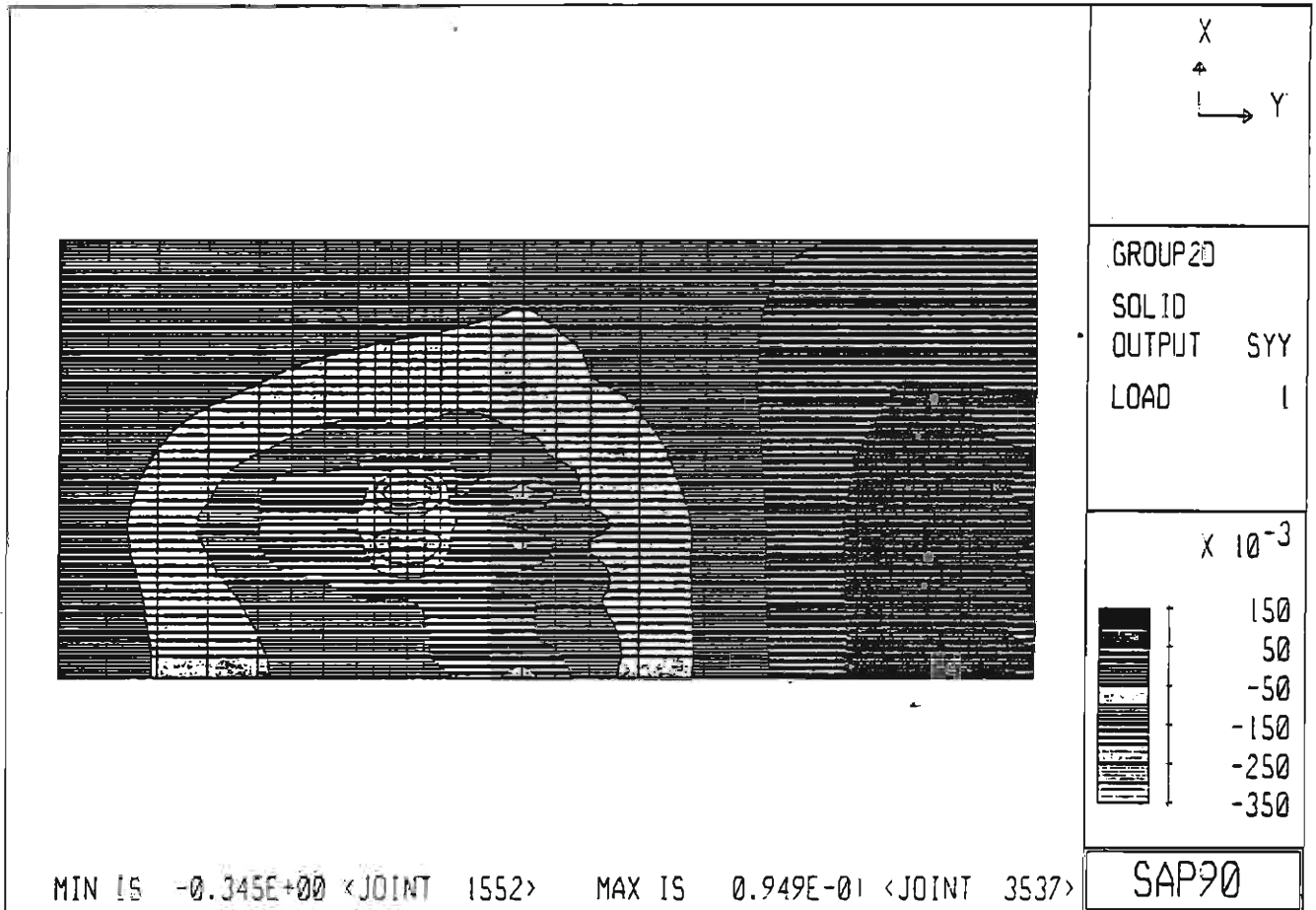


Fig. A.18 Stress Contour of Top Longitudinal Stress
(Case D of Load Group 2)

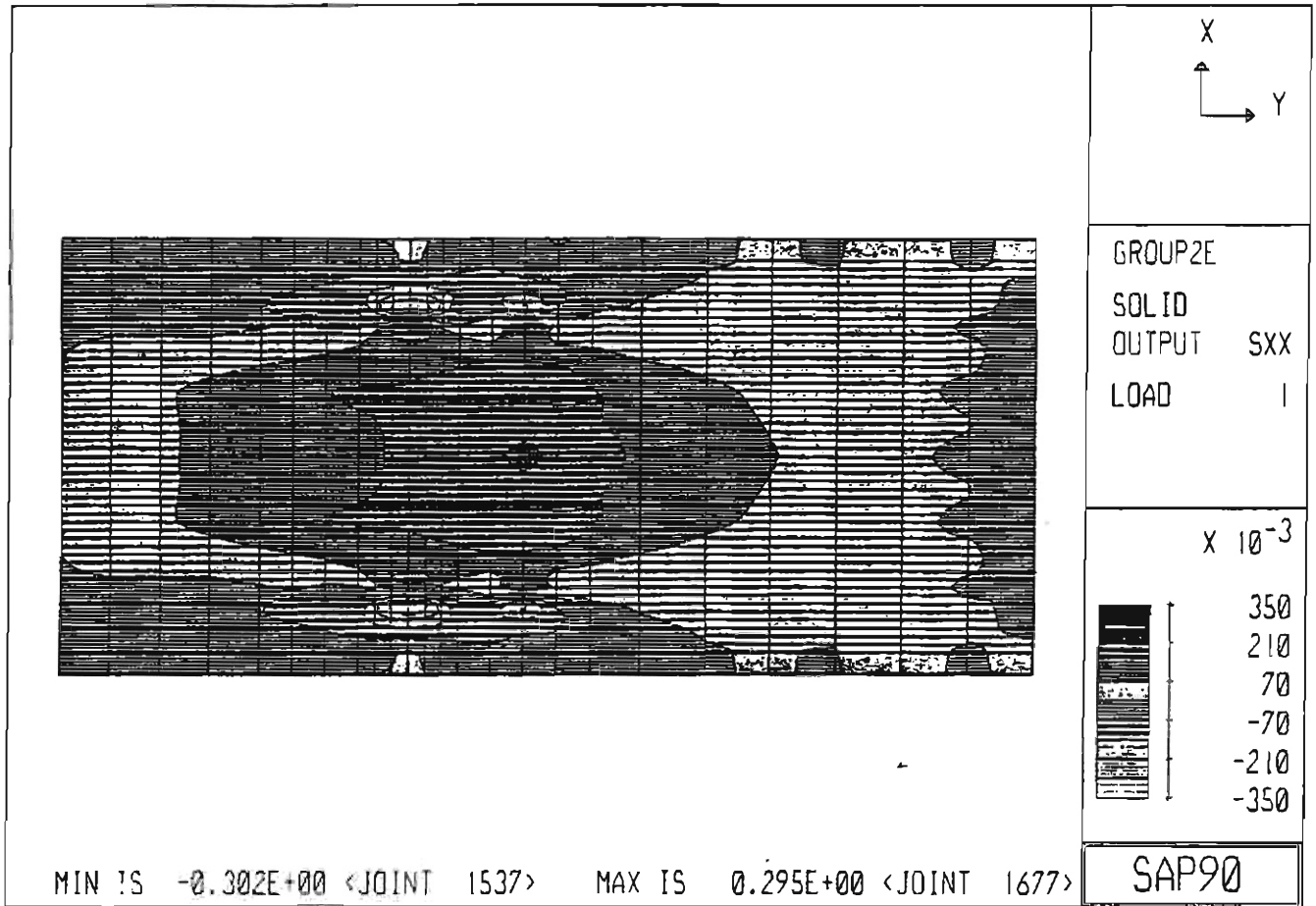


Fig. A.19 Stress Contour of Top Transverse Stress
 (Case E of Load Group 2)

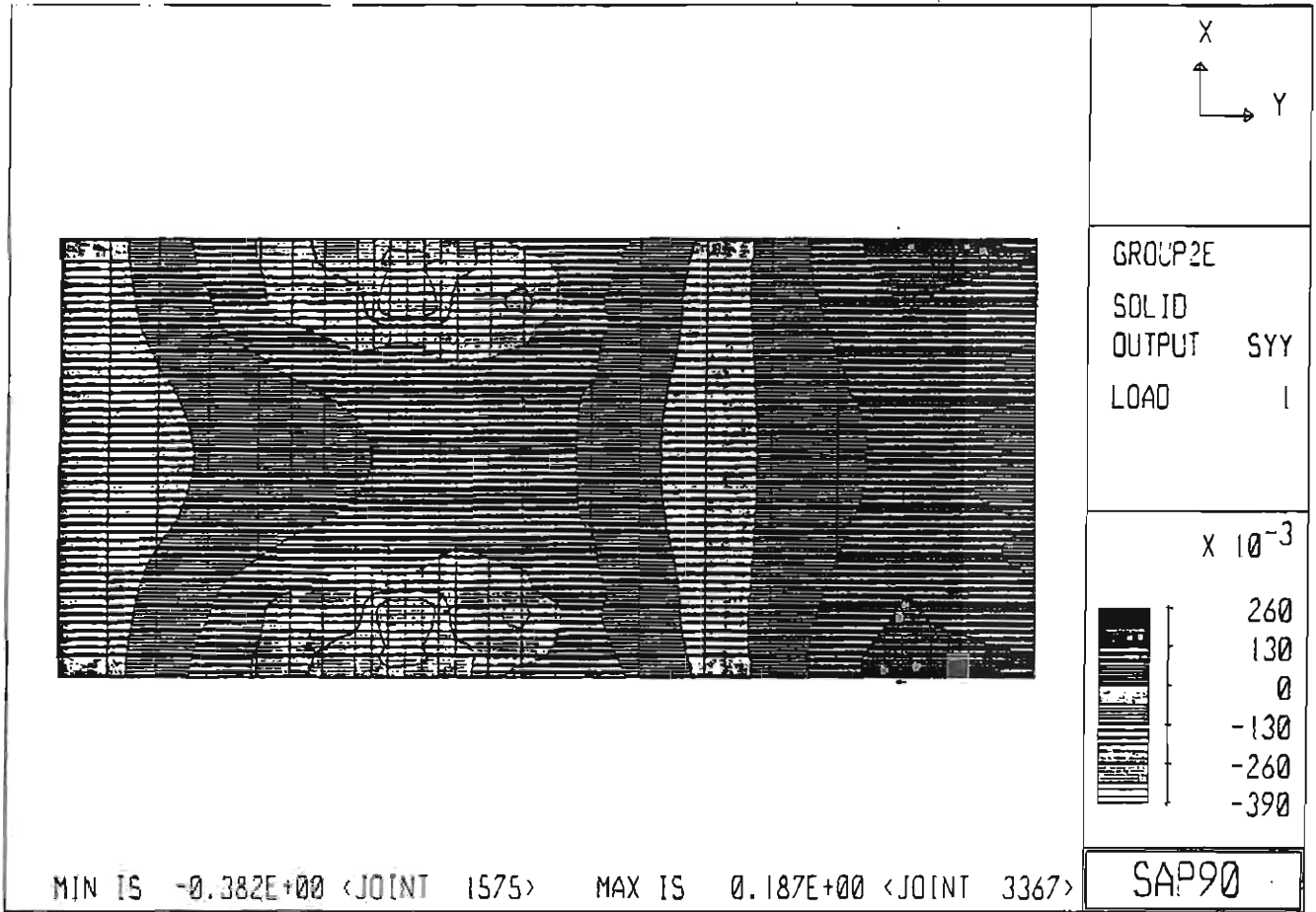


Fig. A.20 Stress Contour of Top Longitudinal Stress
 (Case E of Load Group 2)

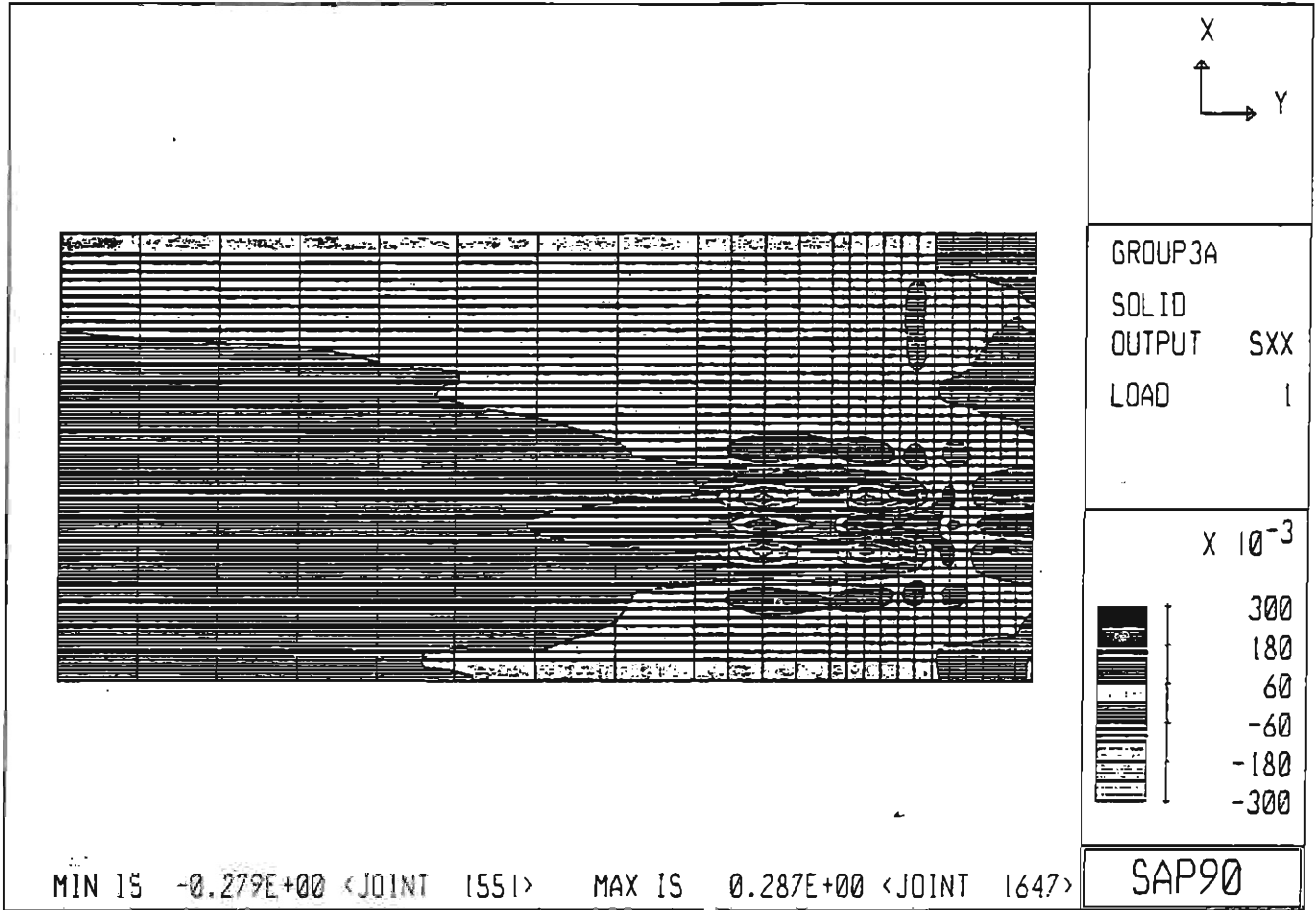


Fig. A.21 Stress Contour of Top Transverse Stress
(Case A of Load Group 3)

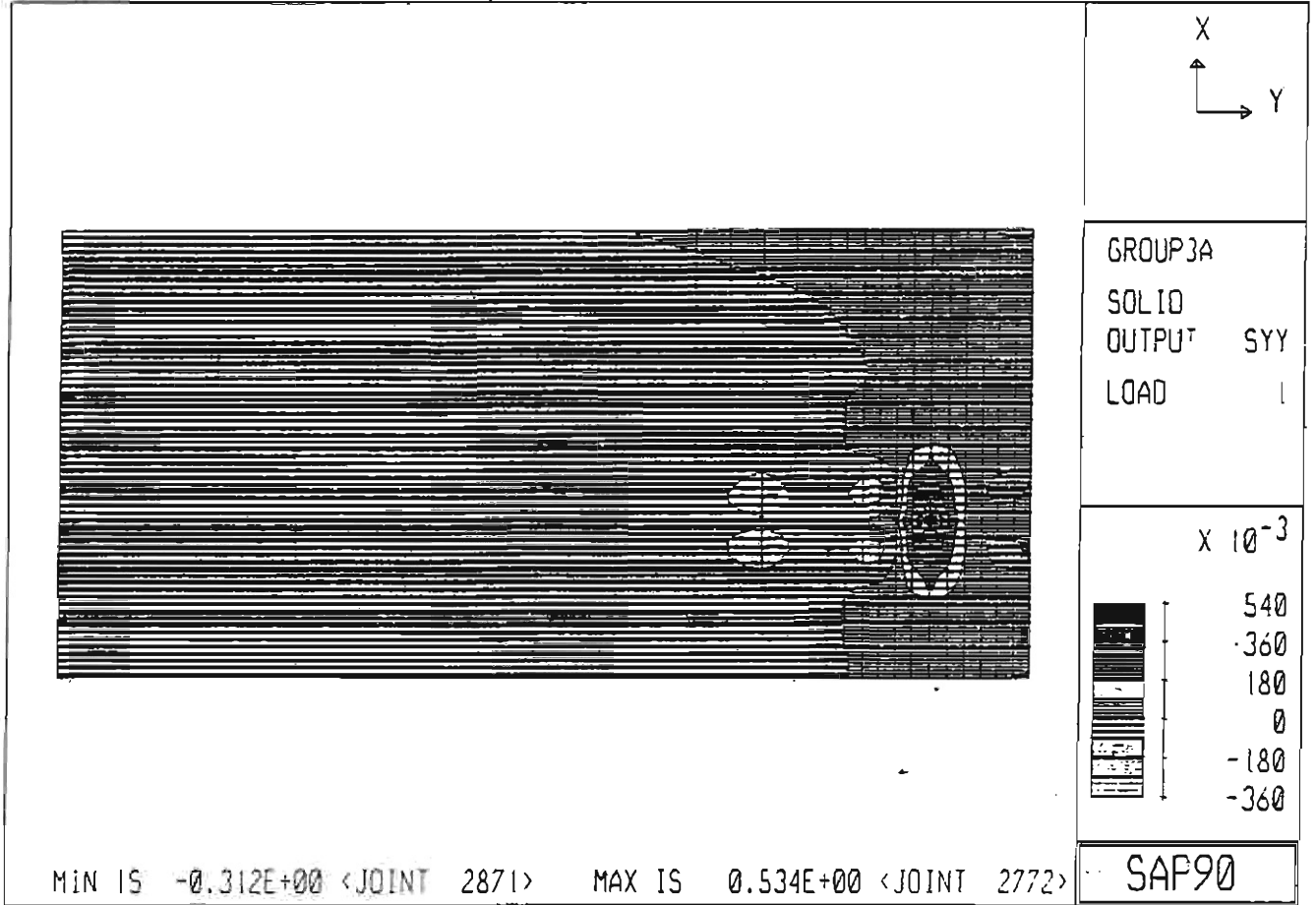


Fig. A.22 Stress Contour of Top Longitudinal Stress
 (Case A of Load Group 3)

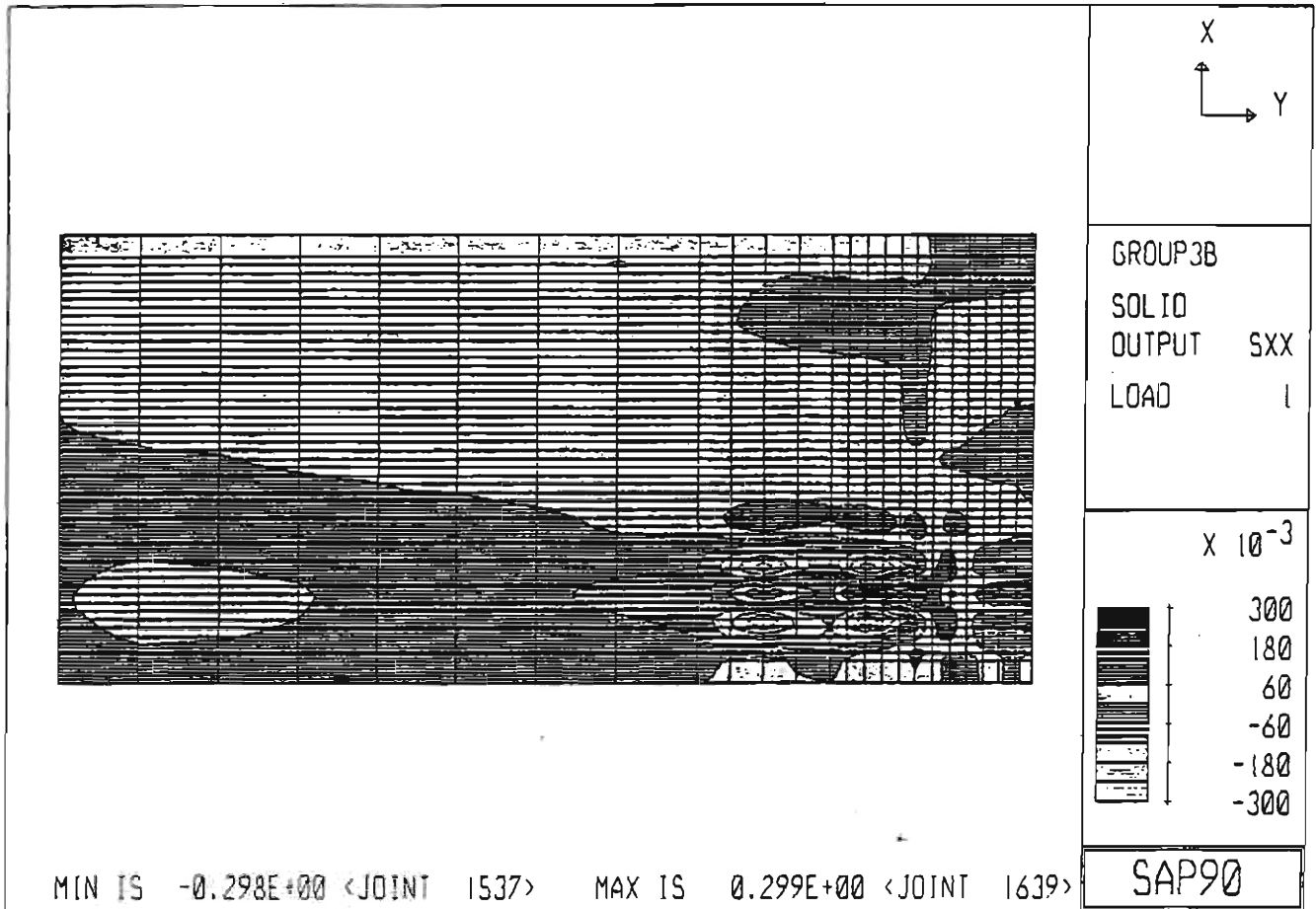


Fig. A.23 Stress Contour of Top Transverse Stress
(Case B of Load Group 3)

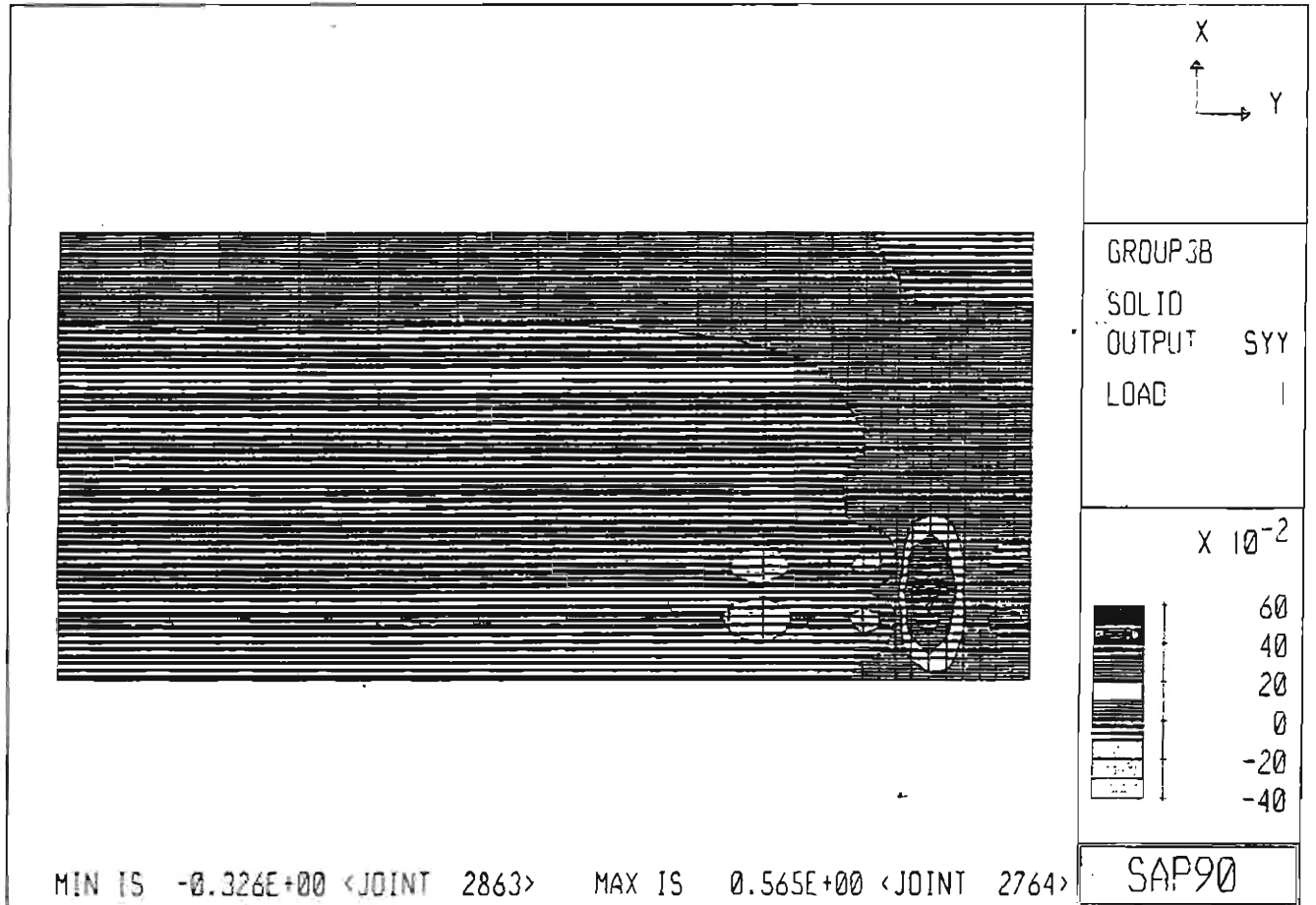


Fig. A.24 Stress Contour of Top Longitudinal Stress
 (Case B of Load Group 3)

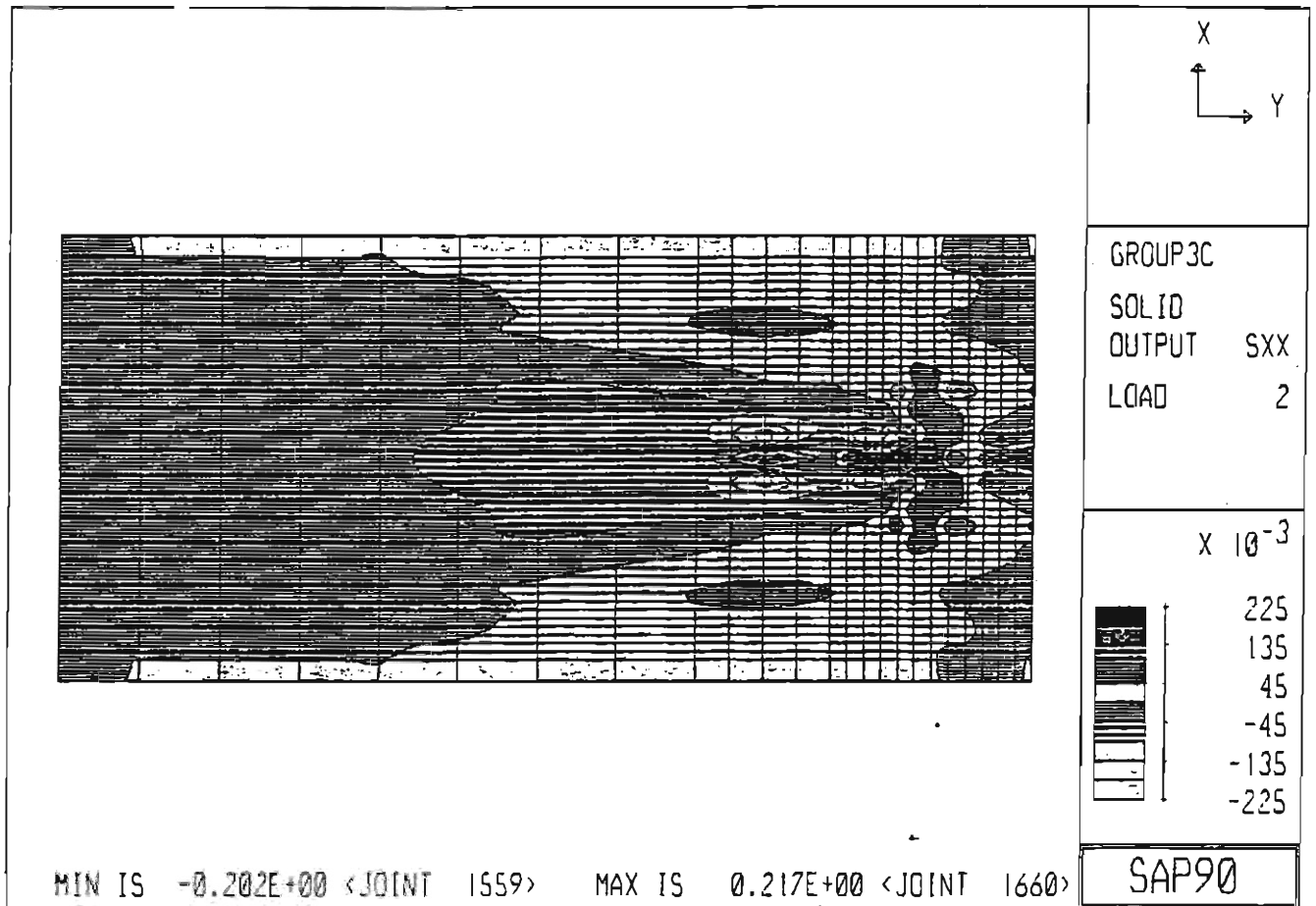


Fig. A.25 Stress Contour of Top Transverse Stress
 (Case C of Load Group 3)

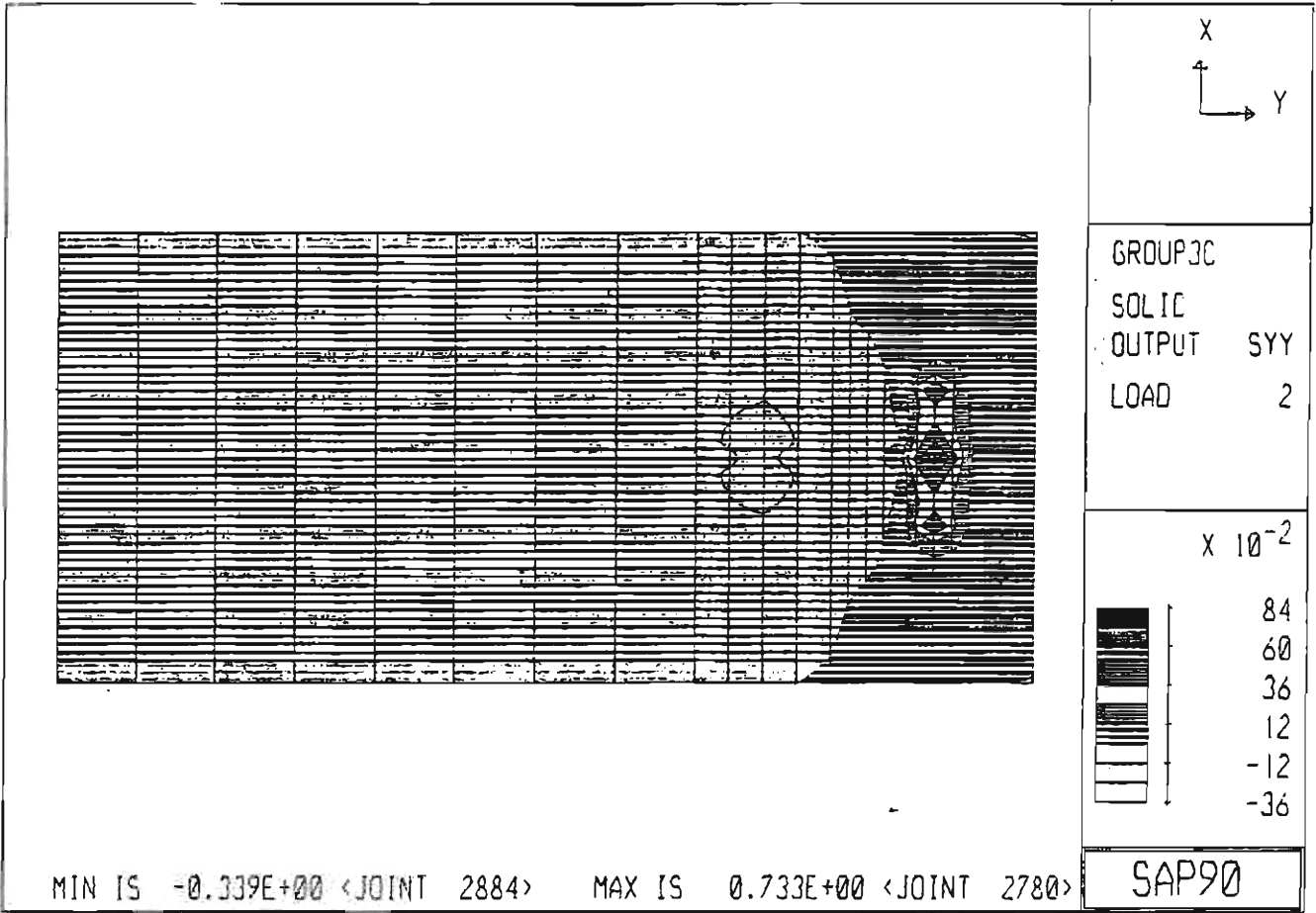


Fig. A.26 Stress Contour of Top Longitudinal Stress
 (Case C of Load Group 3)

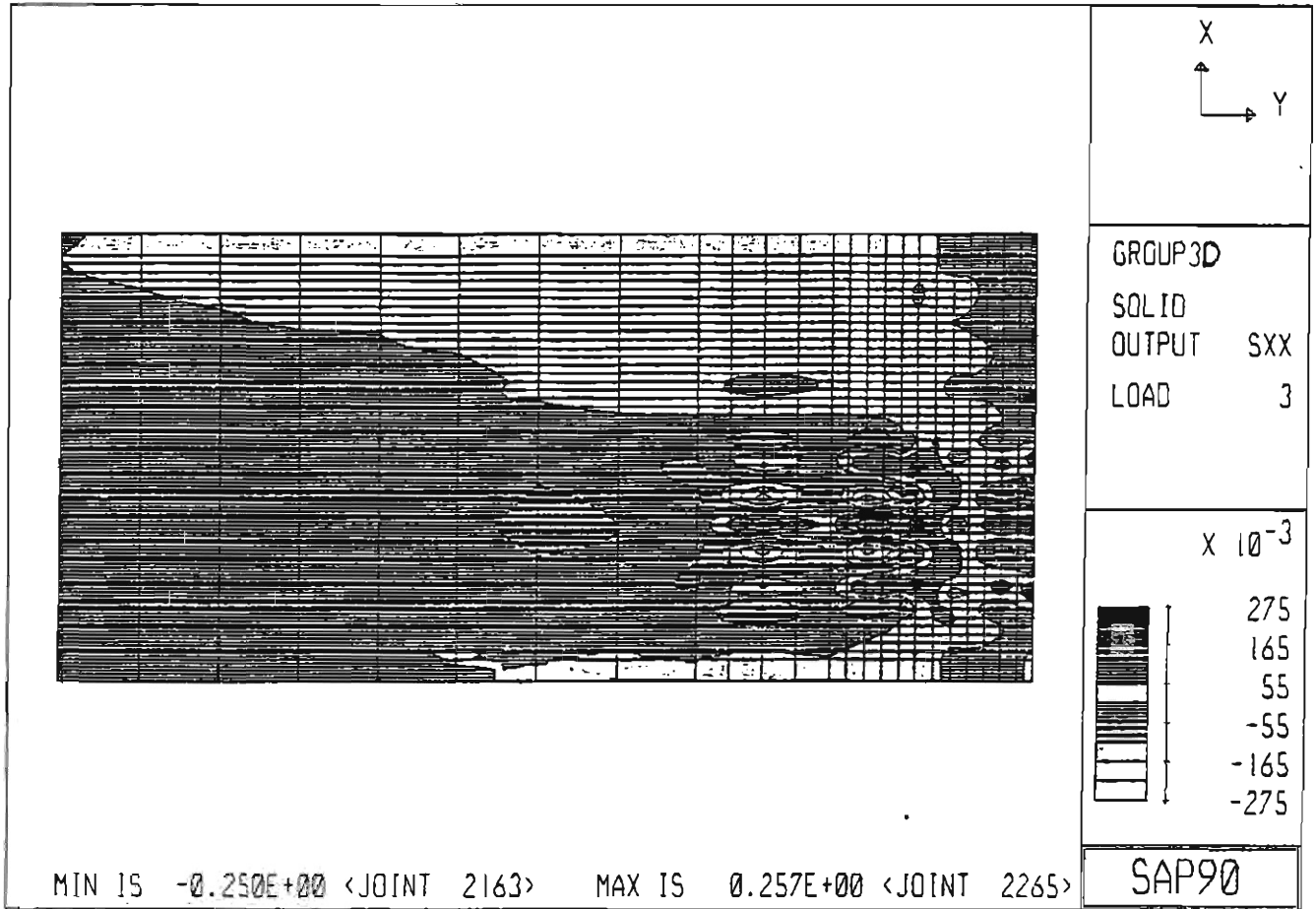


Fig. A.27 Stress Contour of Top Transverse Stress
(Case D of Load Group 3)

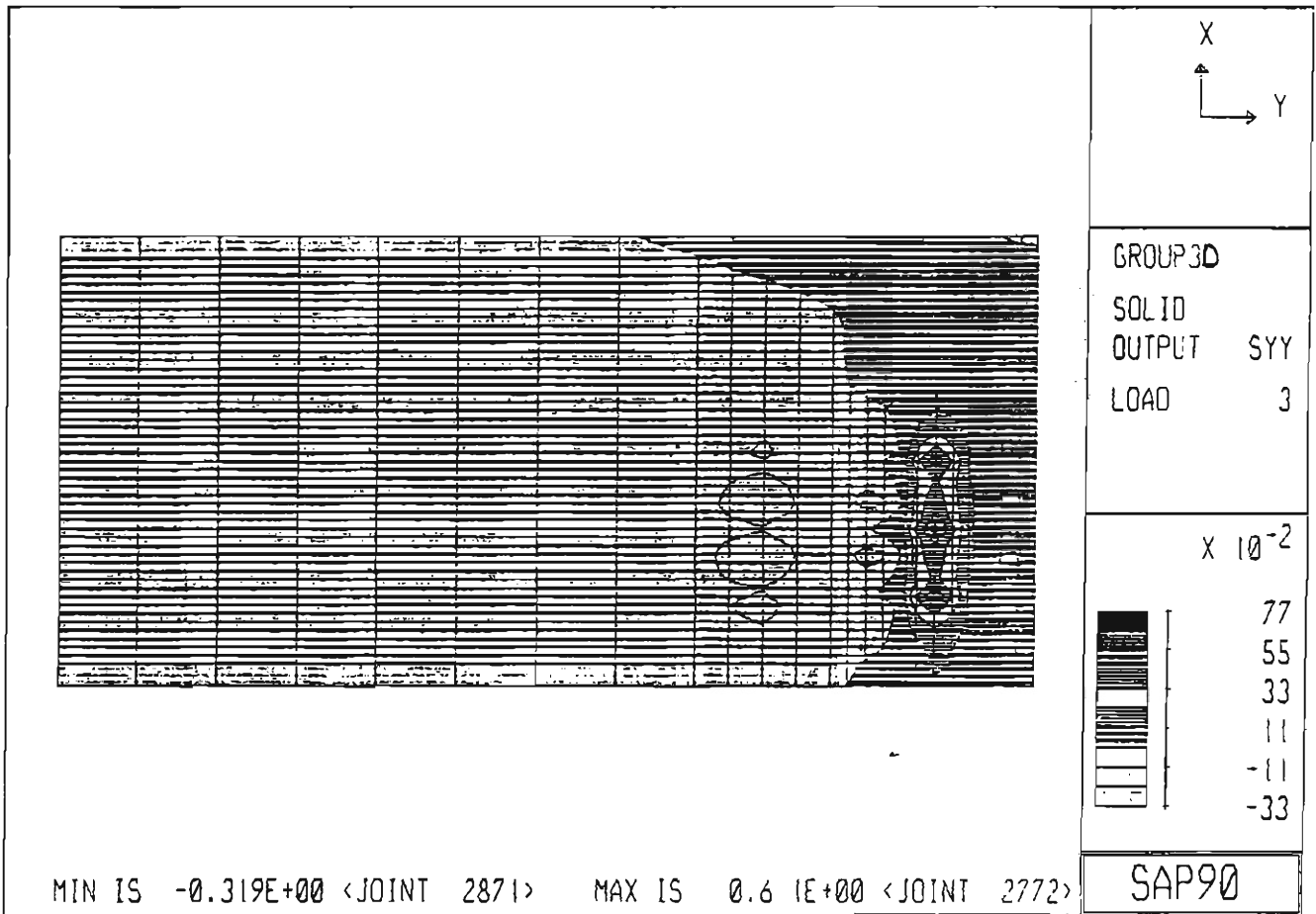


Fig. A.28 Stress Contour of Top Longitudinal Stress
 (Case D of Load Group 3)

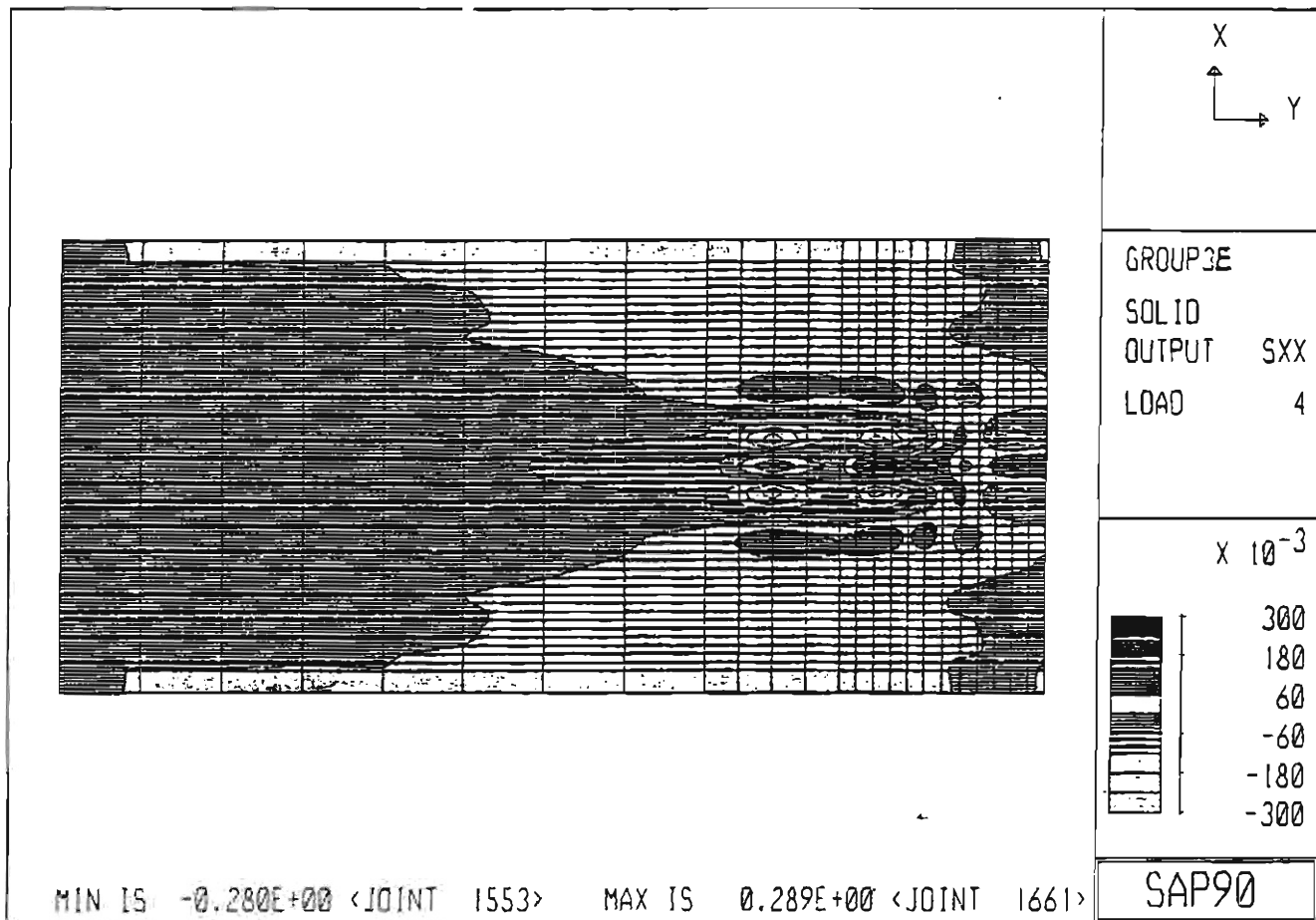


Fig. A.29 Stress Contour of Top Transverse Stress
 (Case E of Load Group 3)

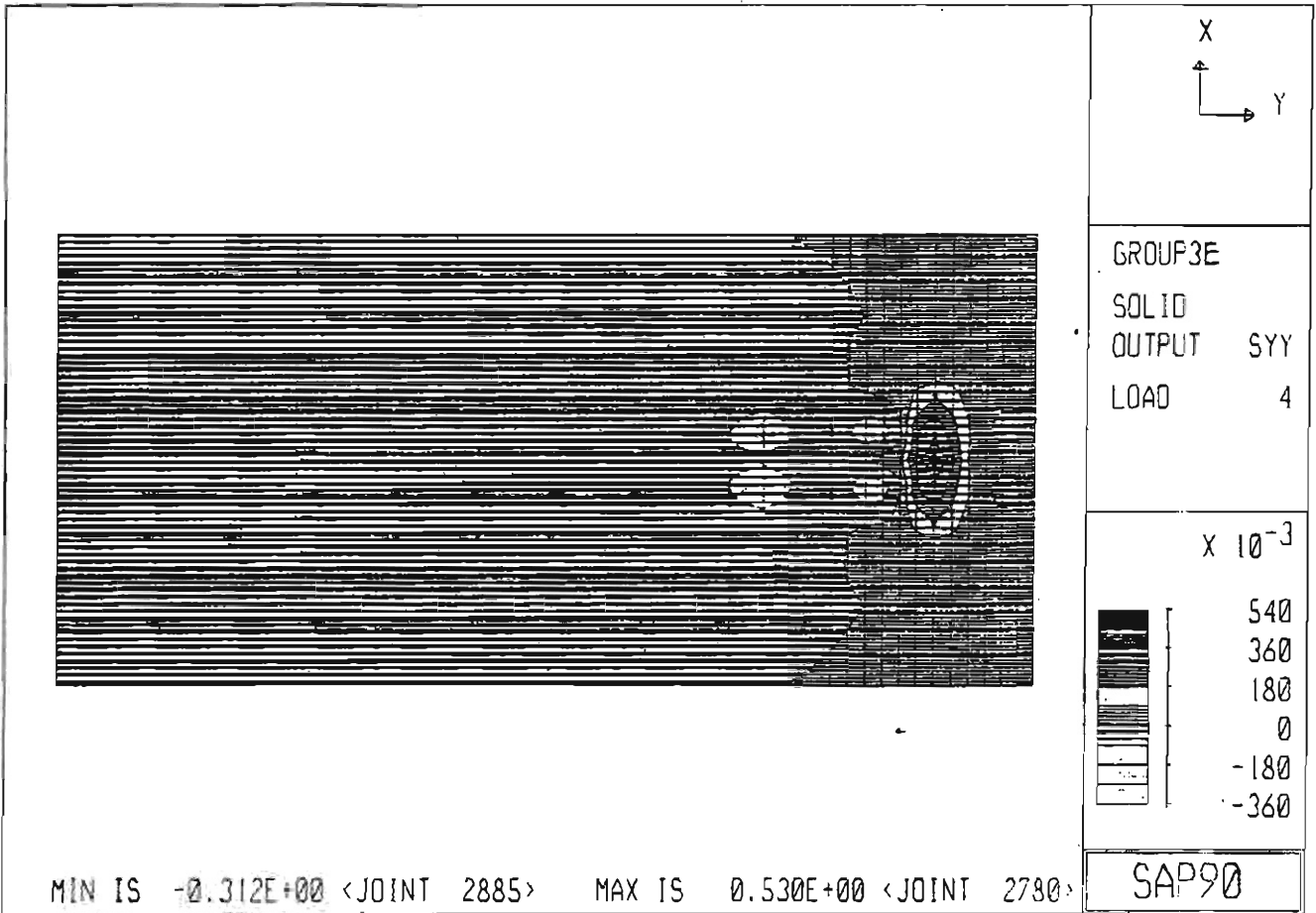


Fig. A.30 Stress Contour of Top Longitudinal Stress
 (Case E of Load Group 3)

Appendix B

DEFLECTION DIAGRAMS OF THE BRIDGE DECK

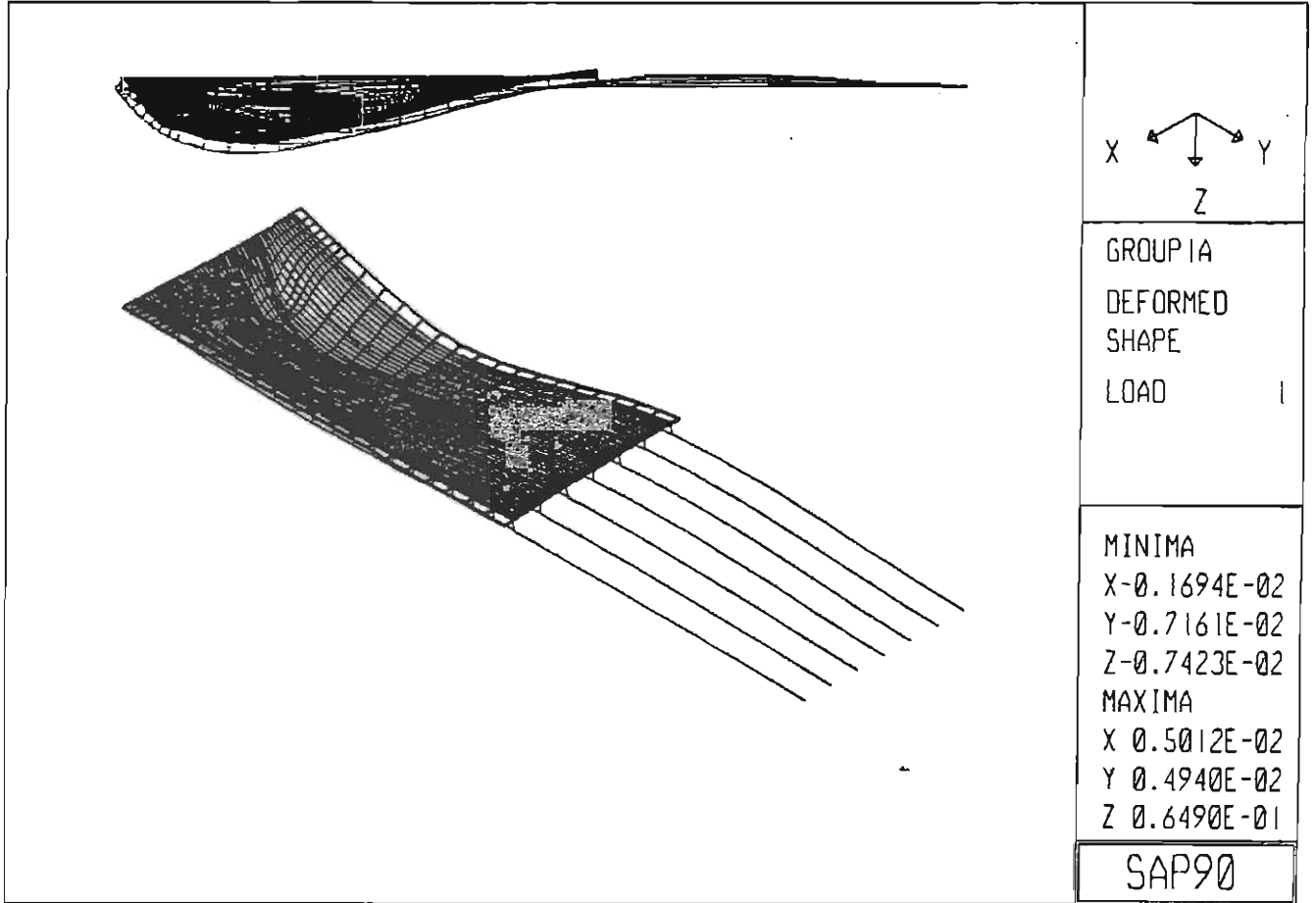


Fig. B.1 Deflection Diagram of Case A of Load Group 1

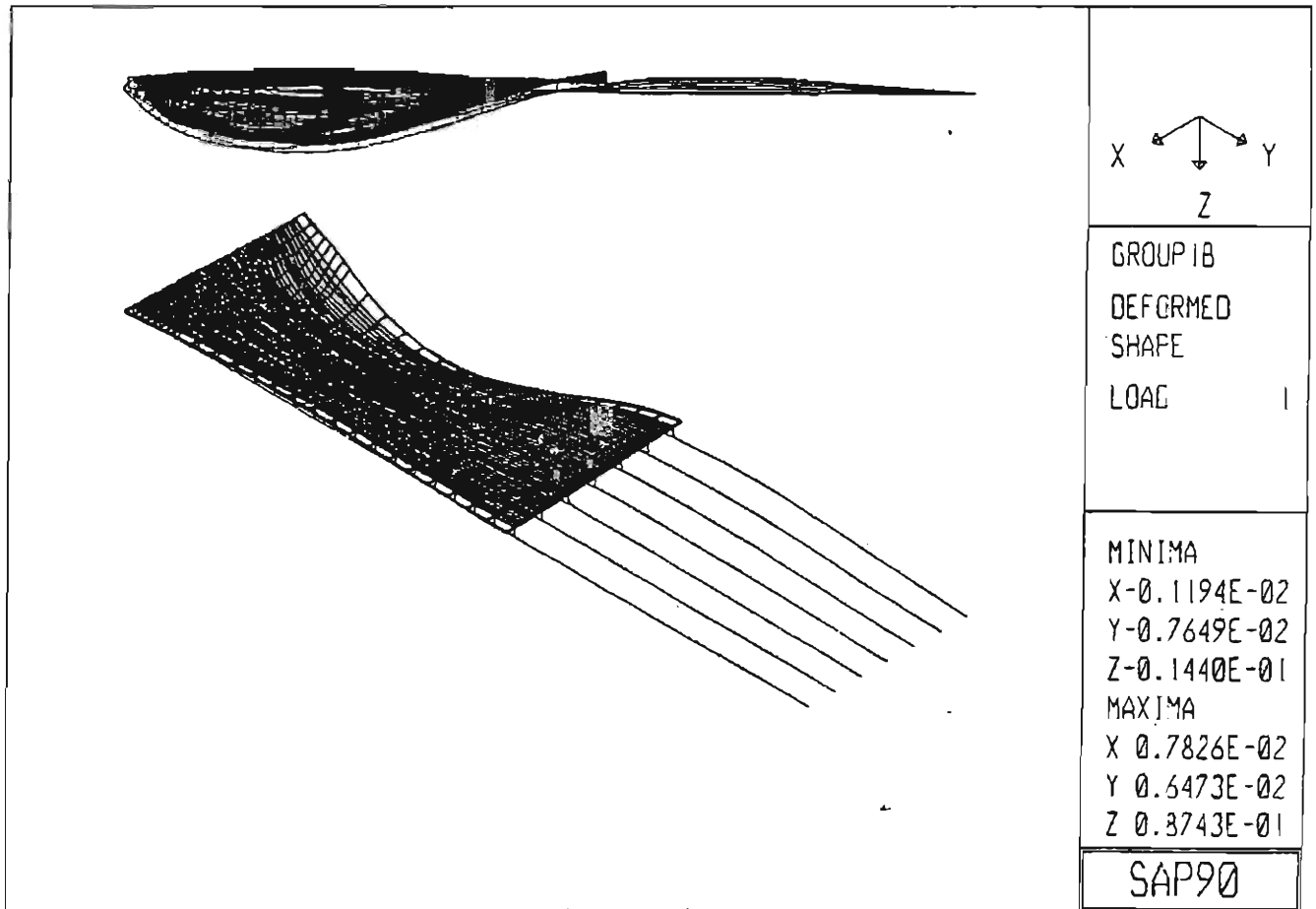


Fig. B.2 Deflection Diagram of Case B of Load Group 1

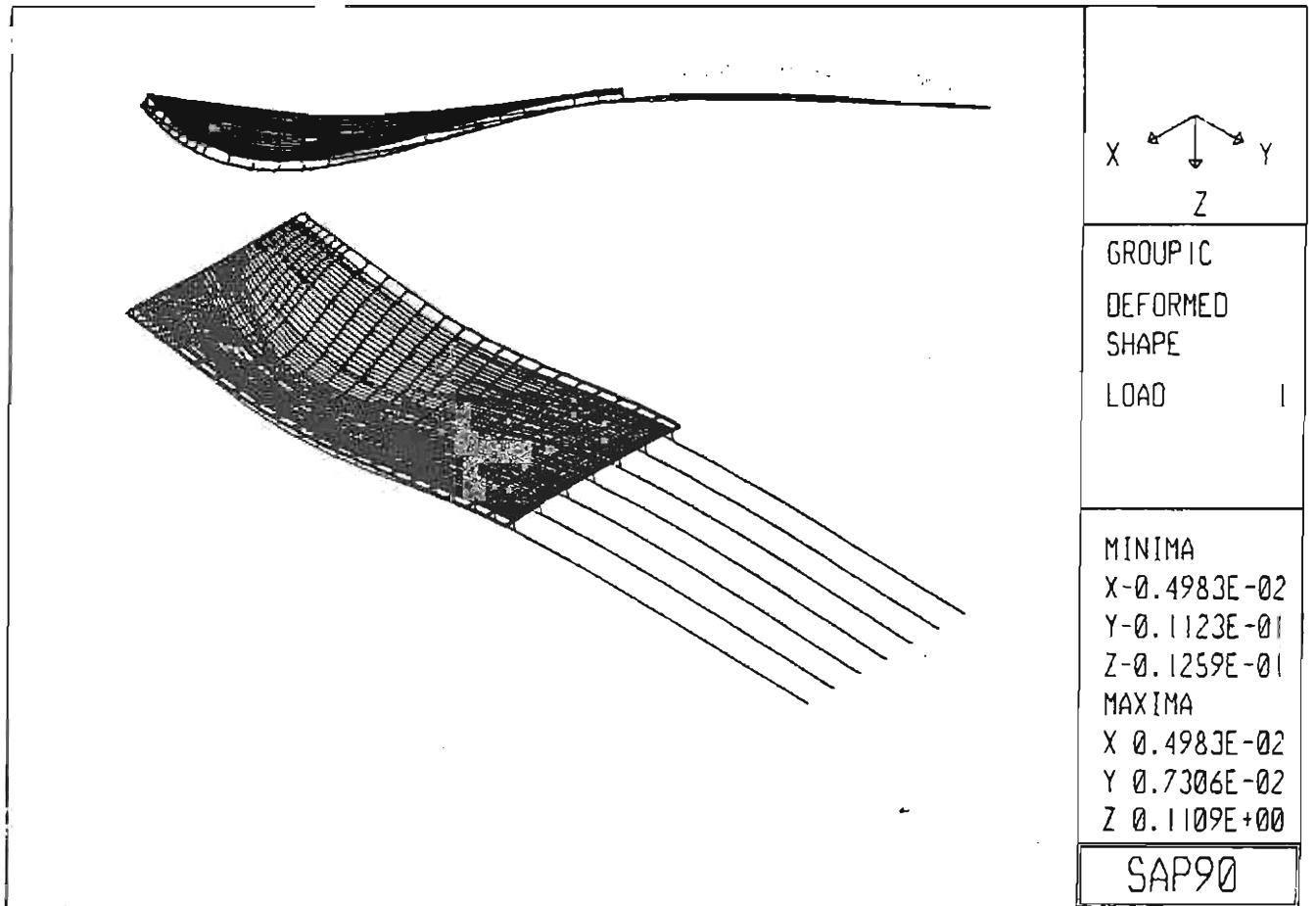


Fig. B.3 Deflection Diagram of Case C of Load Group 1

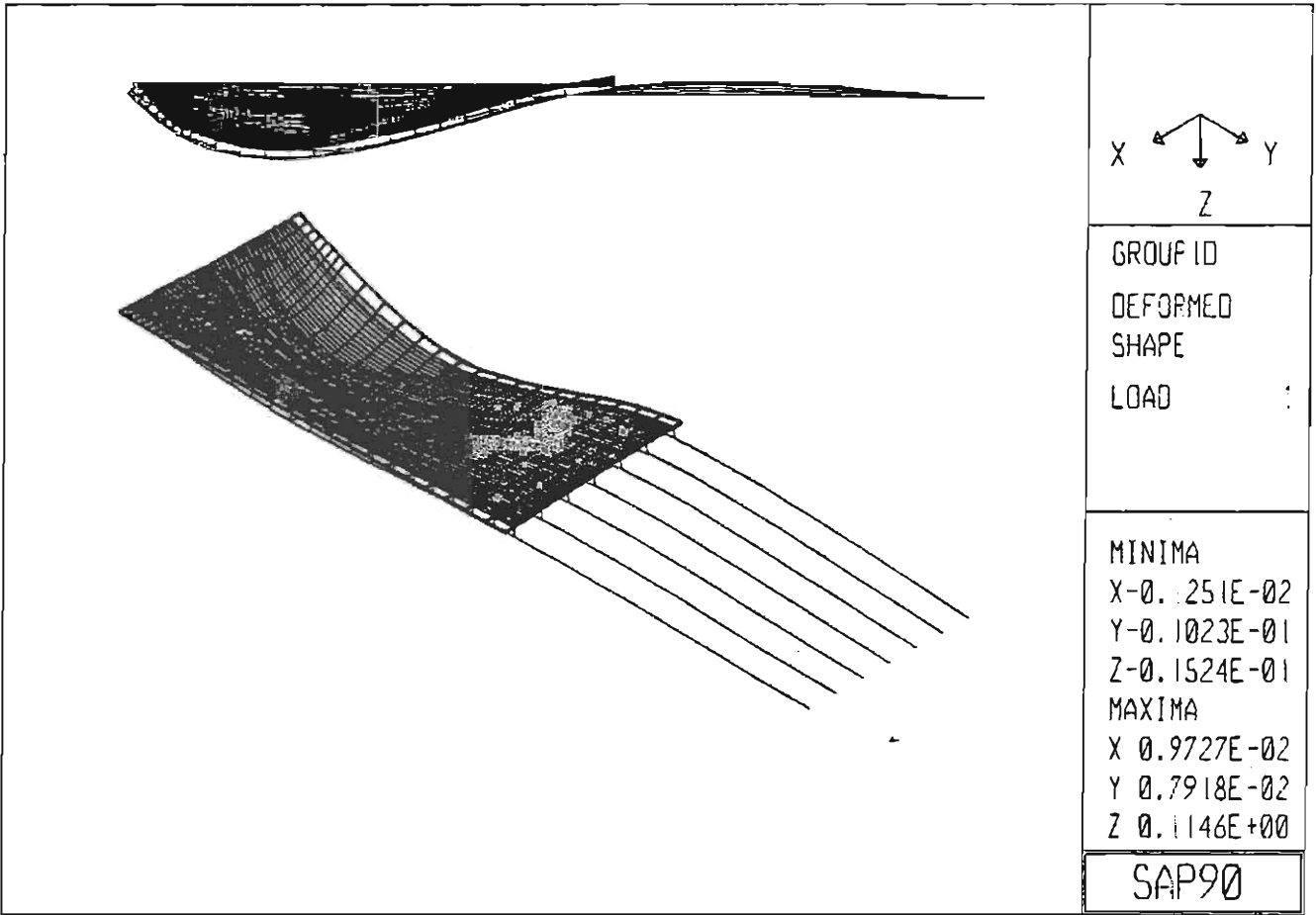


Fig. B.4 Deflection Diagram of Case D of Load Group 1

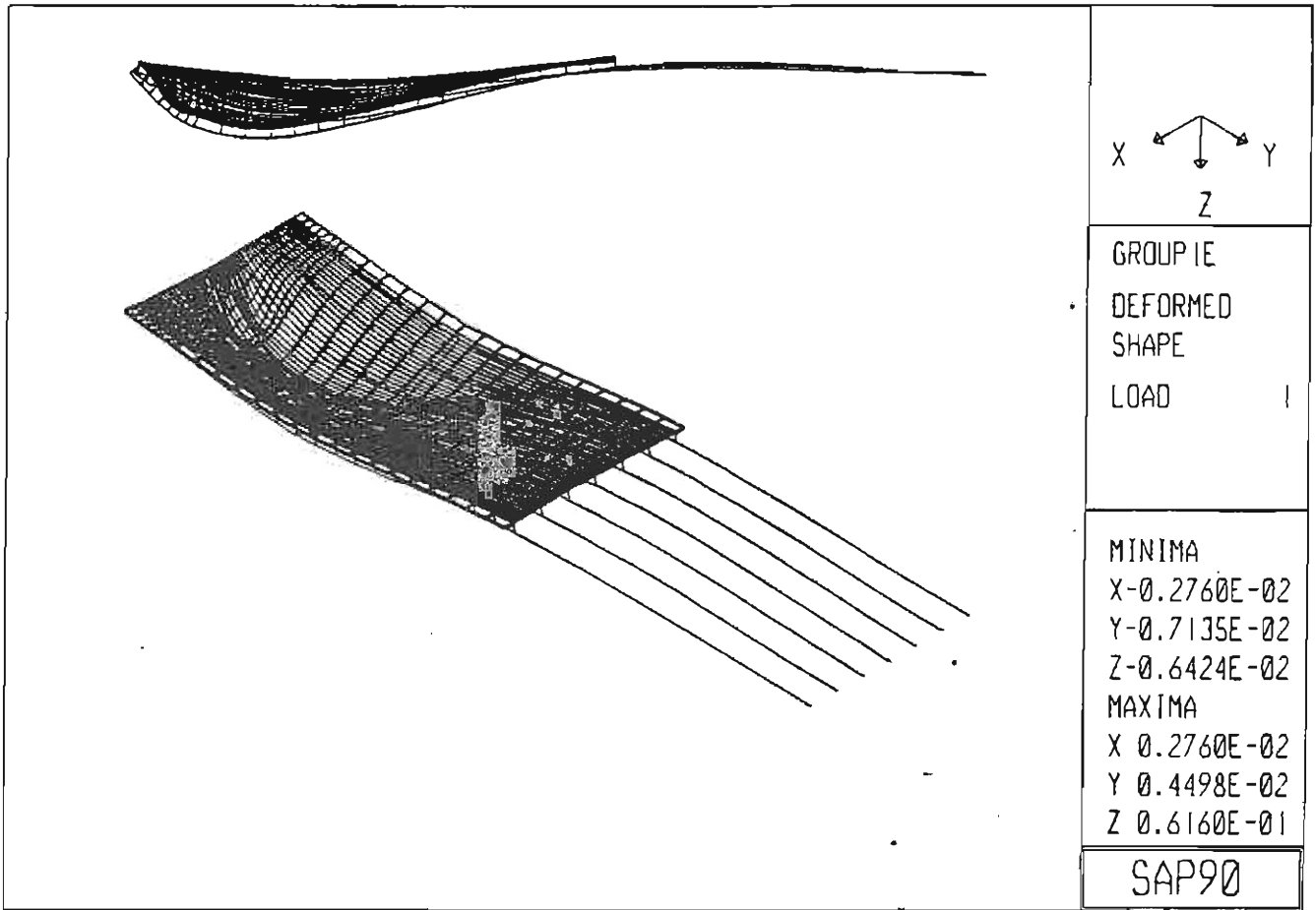


Fig. B.5 Deflection Diagram of Case E of Load Group 1

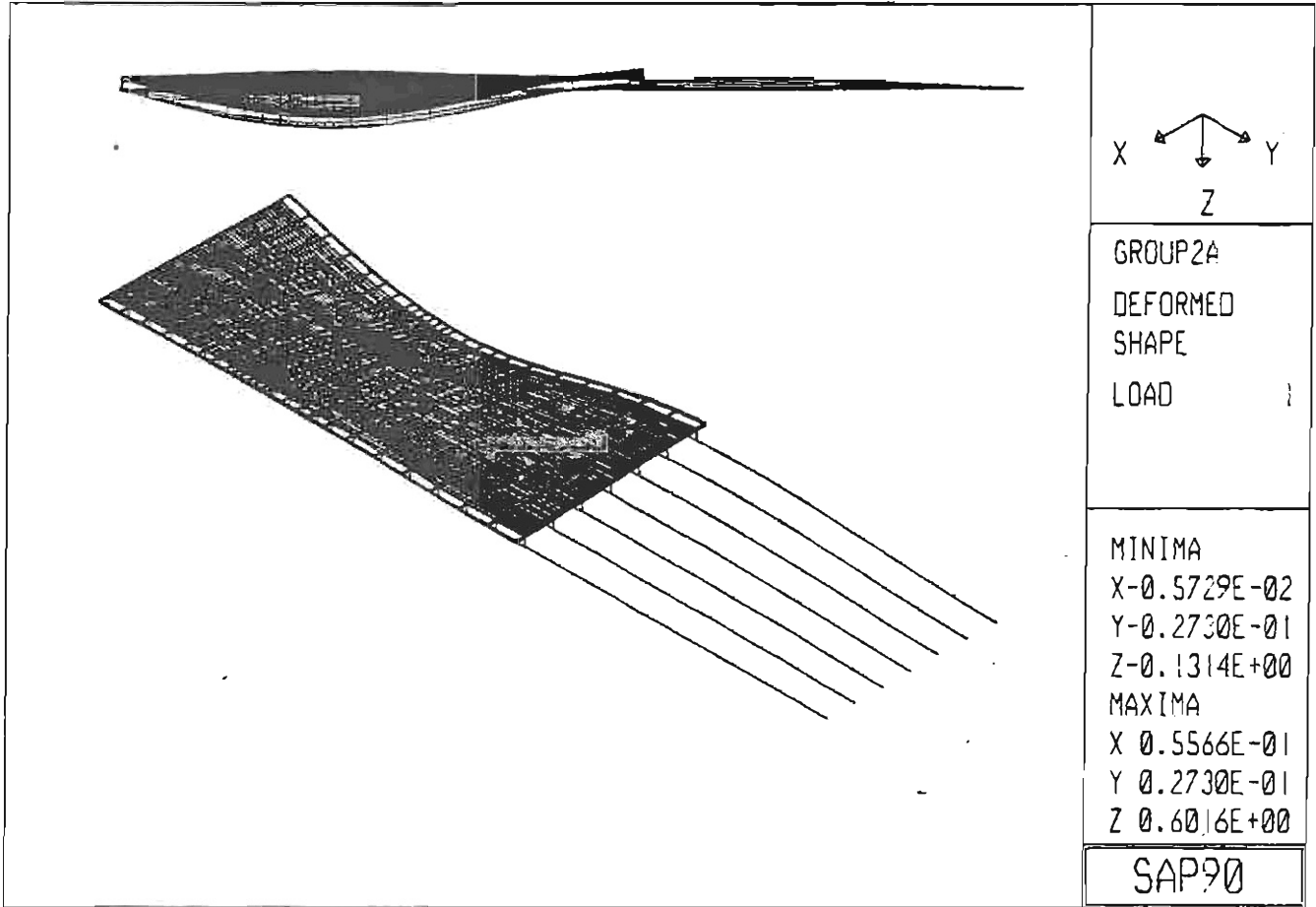


Fig. B.6 Deflection Diagram of Case A of Load Group 2

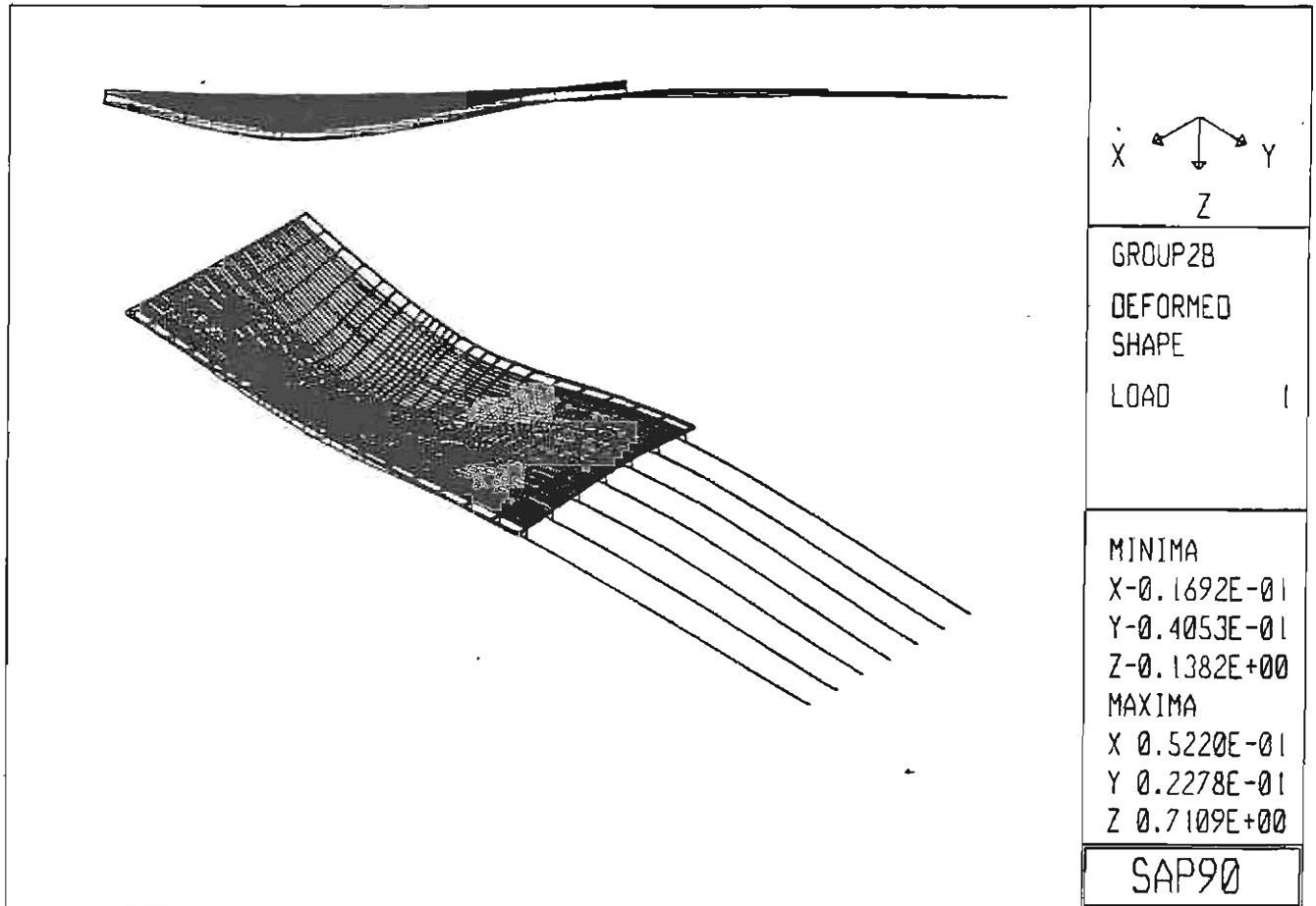


Fig. B.7 Deflection Diagram of Case B of Load Group 2

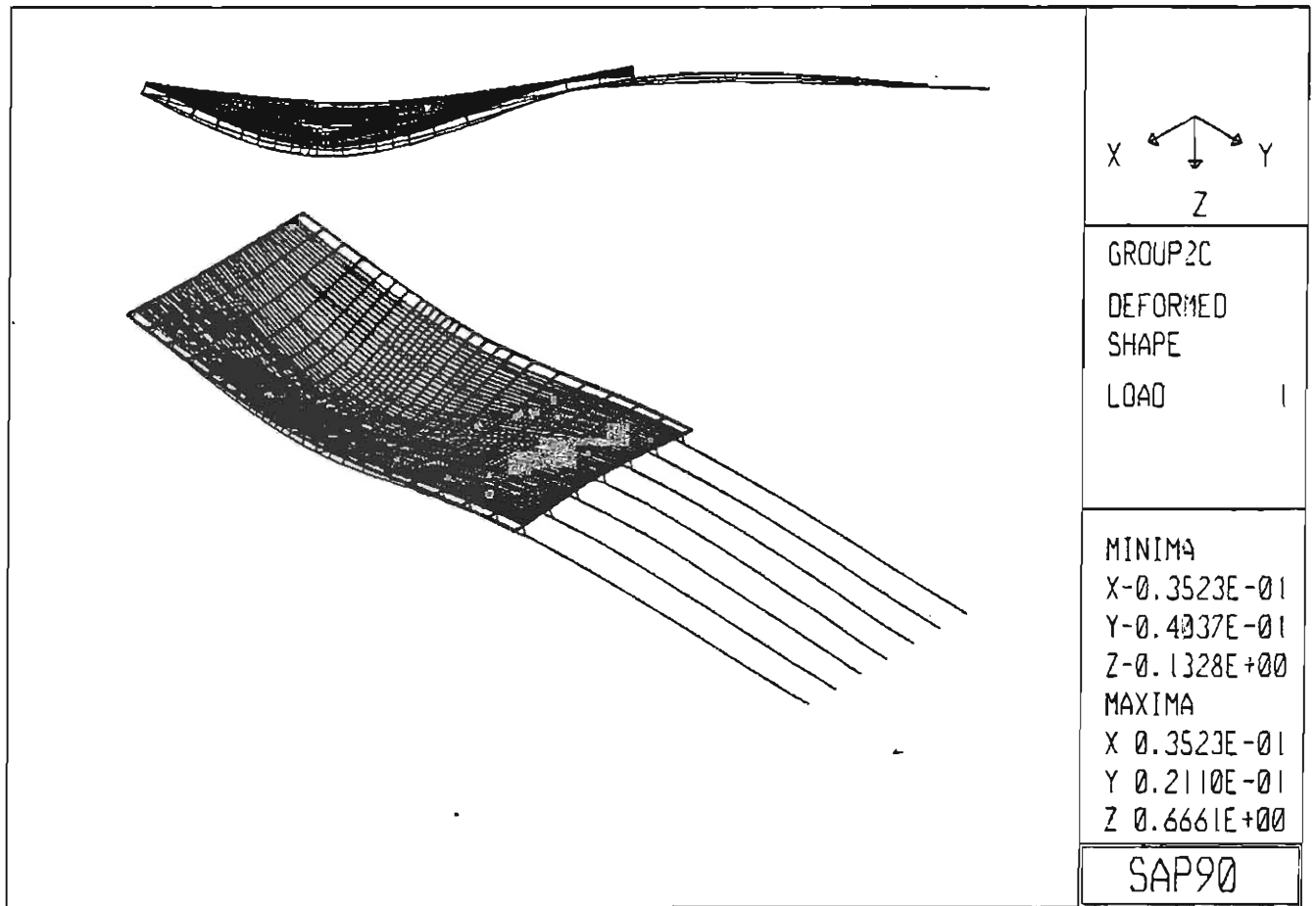


Fig. B.8 Deflection Diagram of Case C of Load Group 2

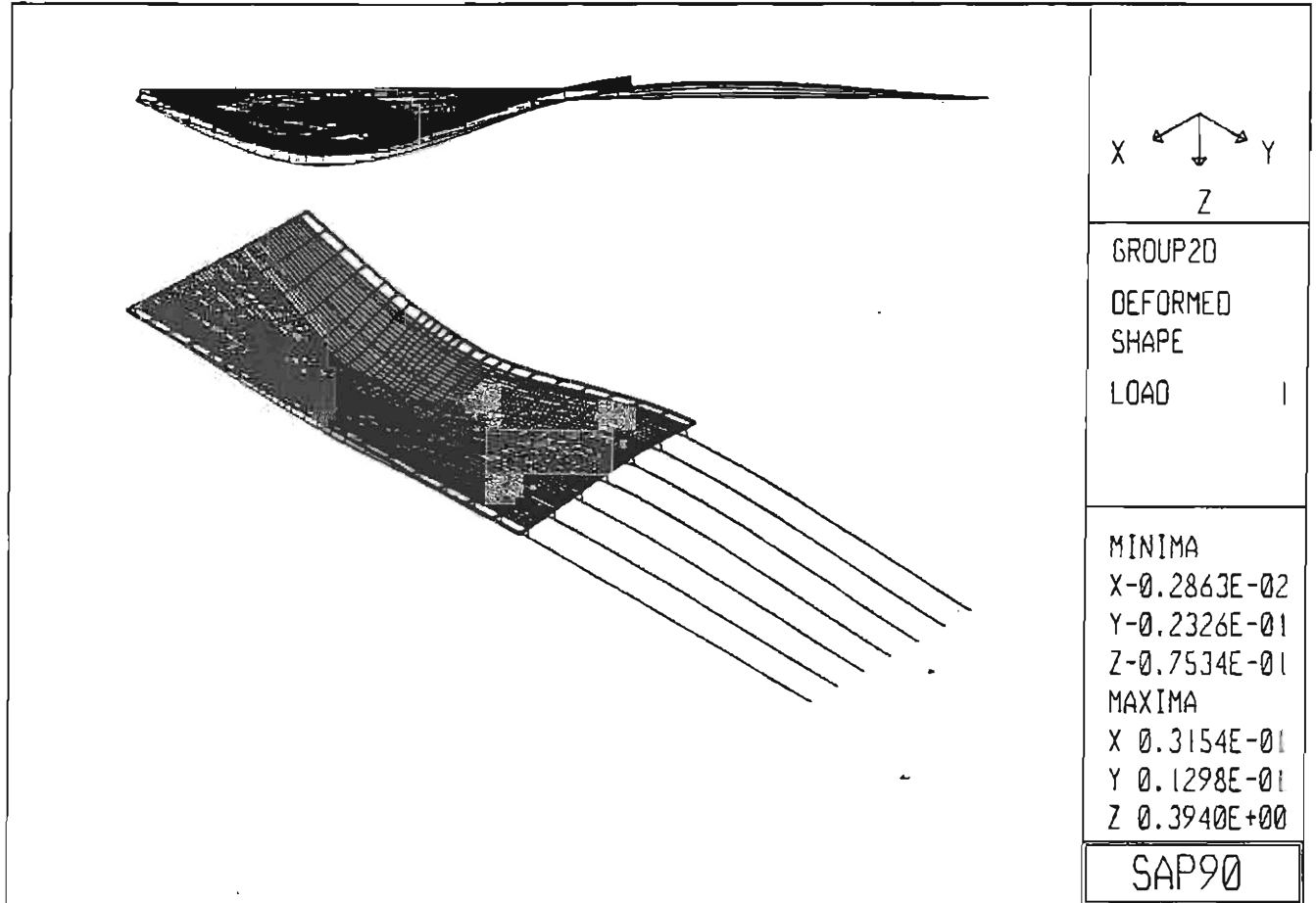


Fig. B.9 Deflection Diagram of Case D of Load Group 2

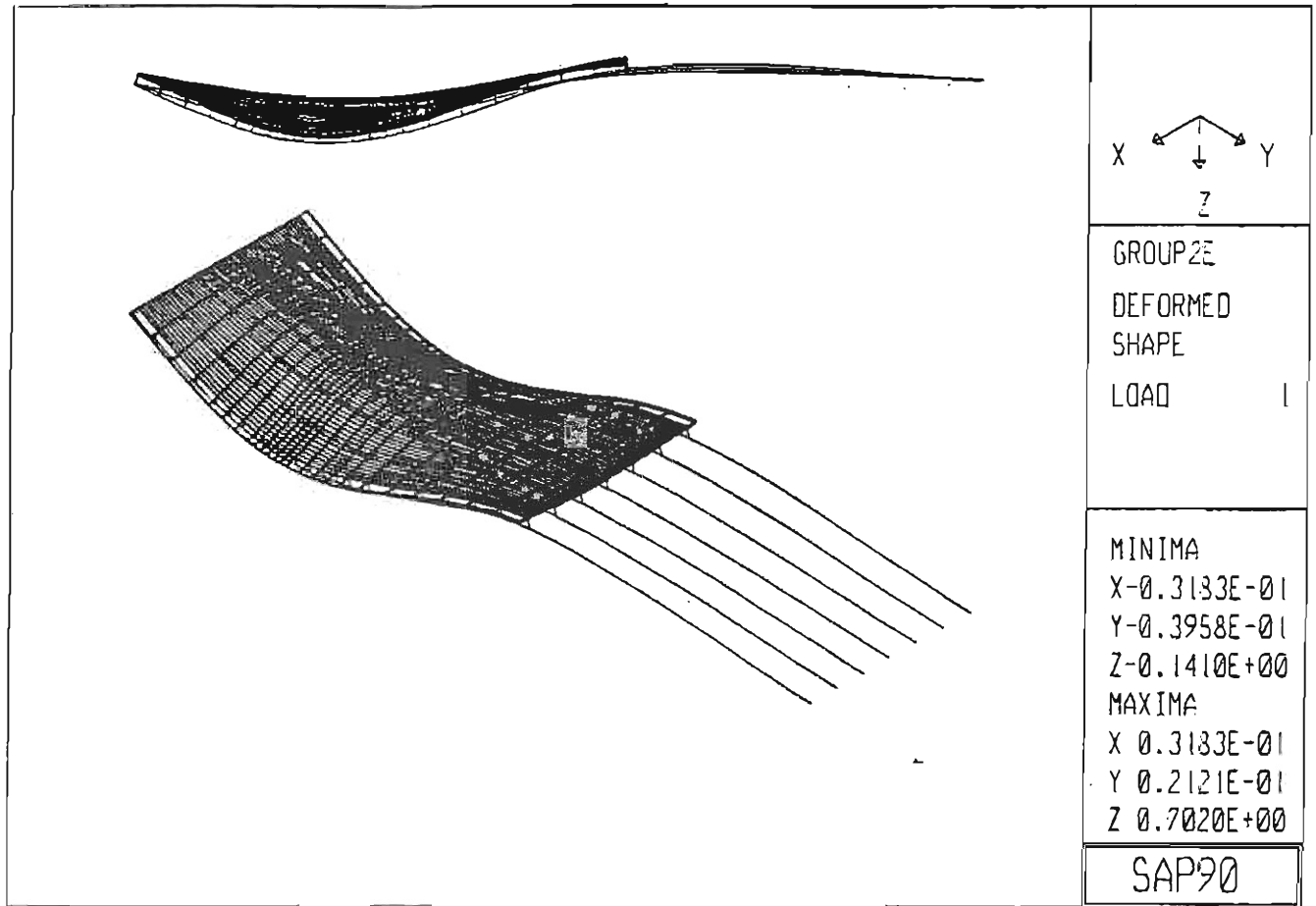


Fig. B.10 Deflection Diagram of Case E of Load Group 2

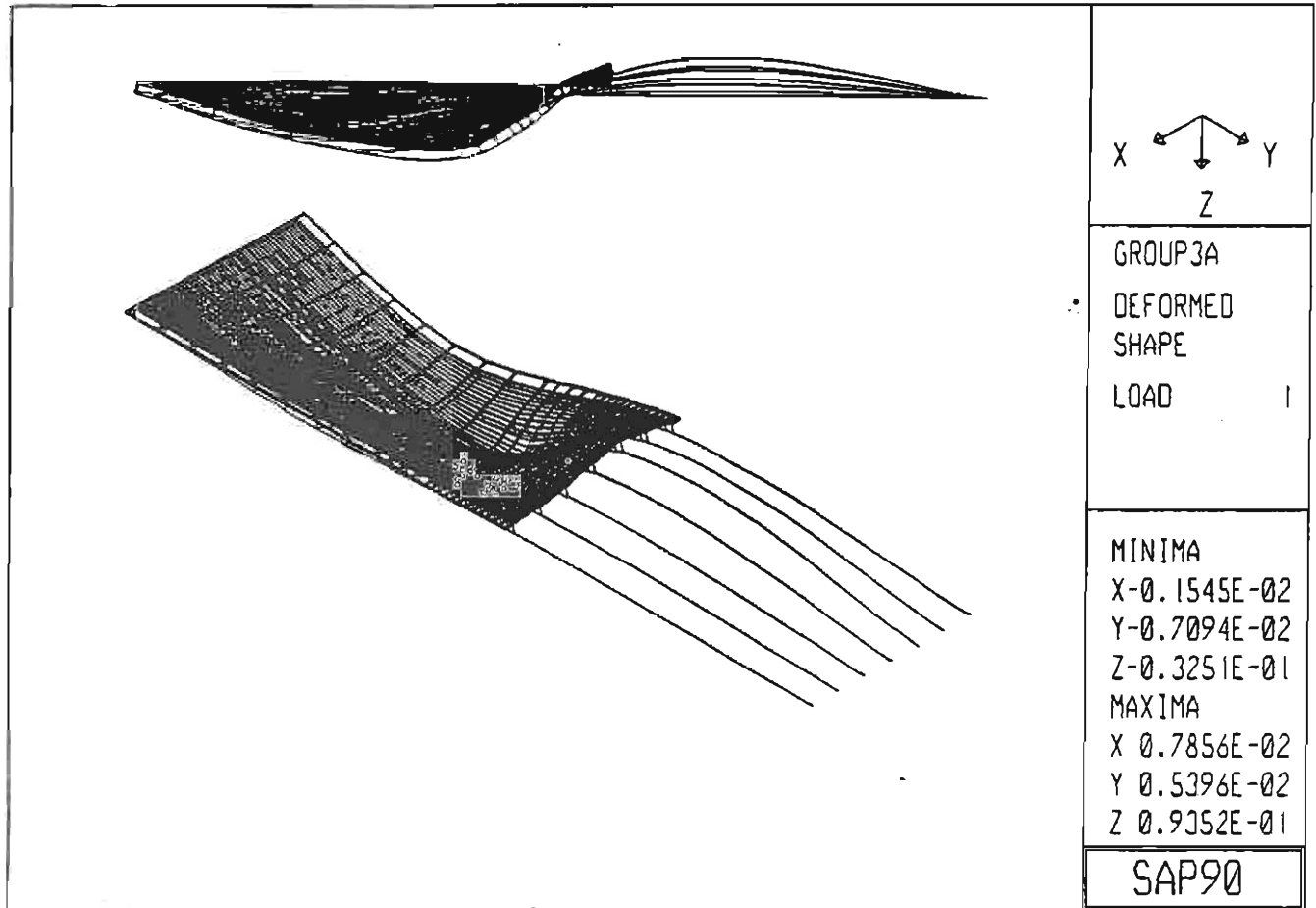


Fig. B.11 Deflection Diagram of Case A of Load Group 3

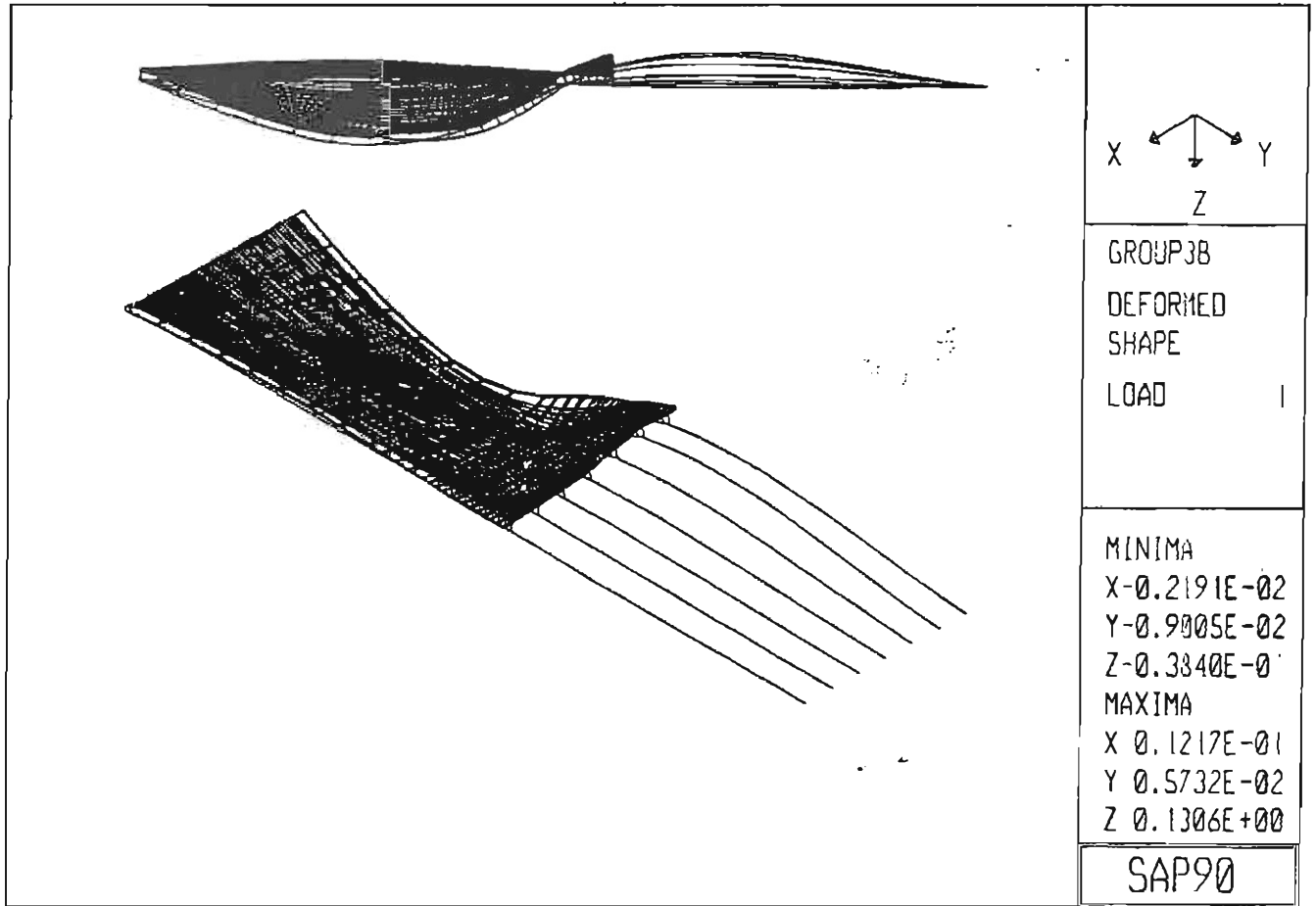


Fig. B.12 Deflection Diagram of Case B of Load Group 3

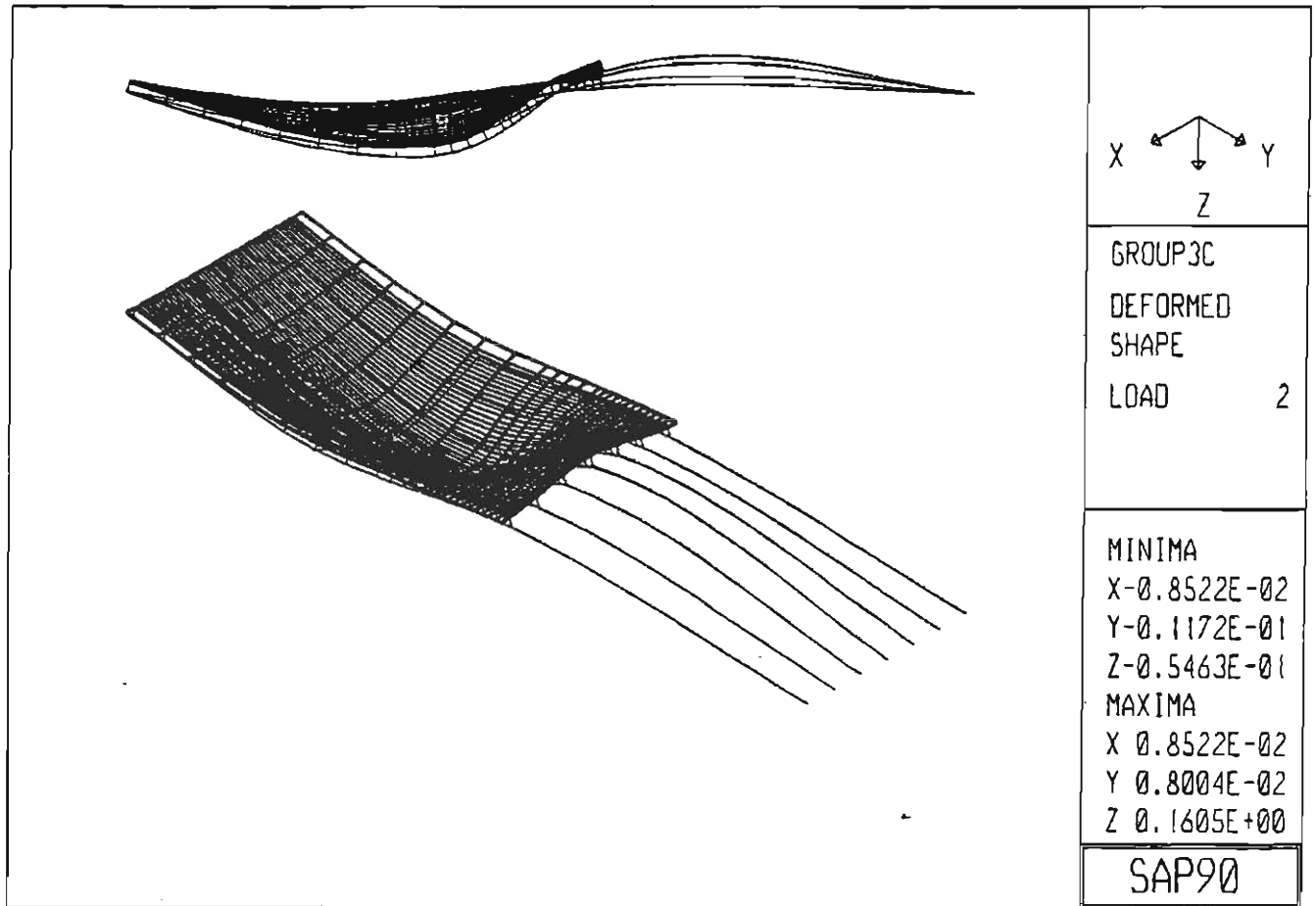


Fig. B.13 Deflection Diagram of Case C of Load Group 3

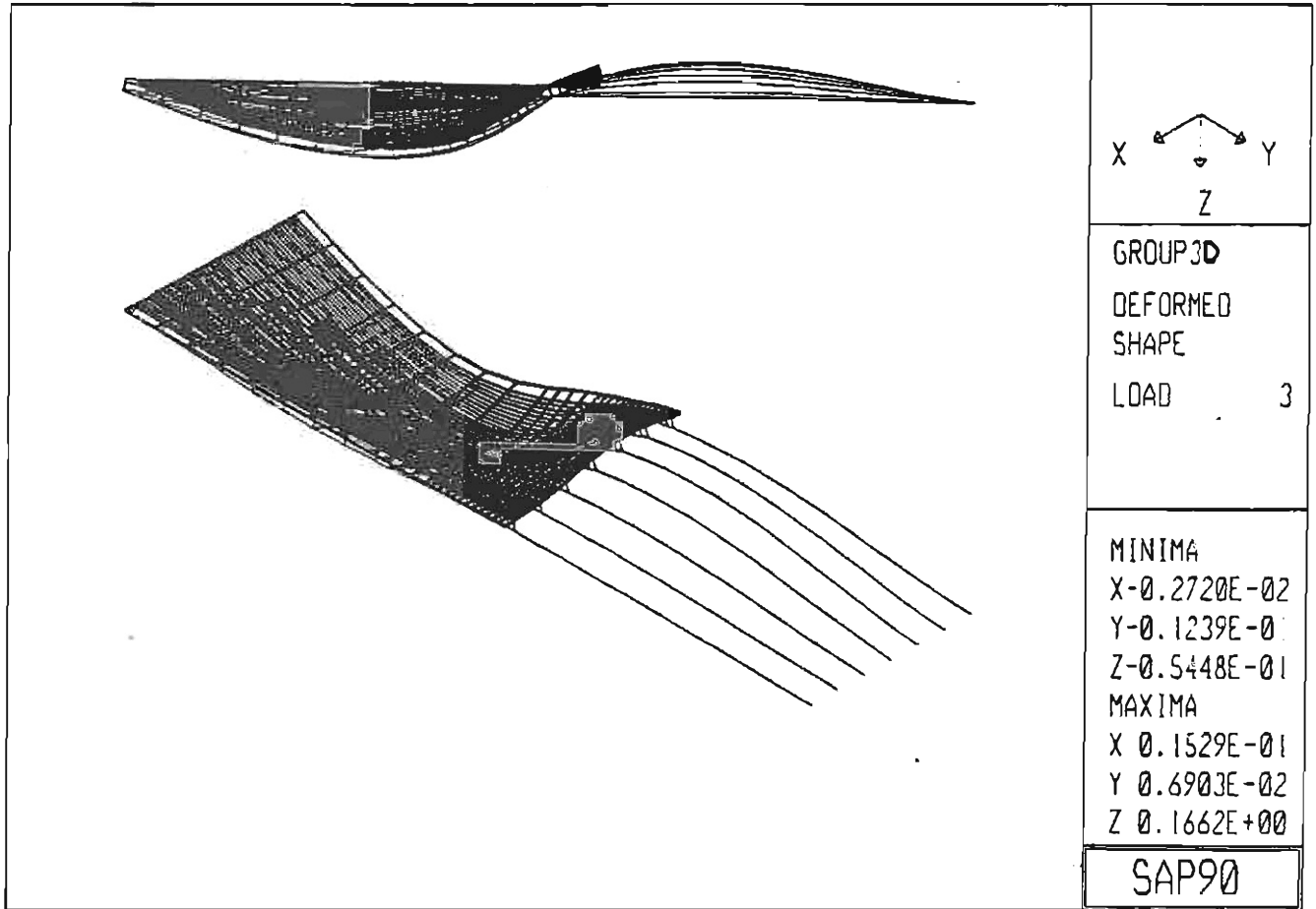


Fig. B.14 Deflection Diagram of Case D of Load Group 3

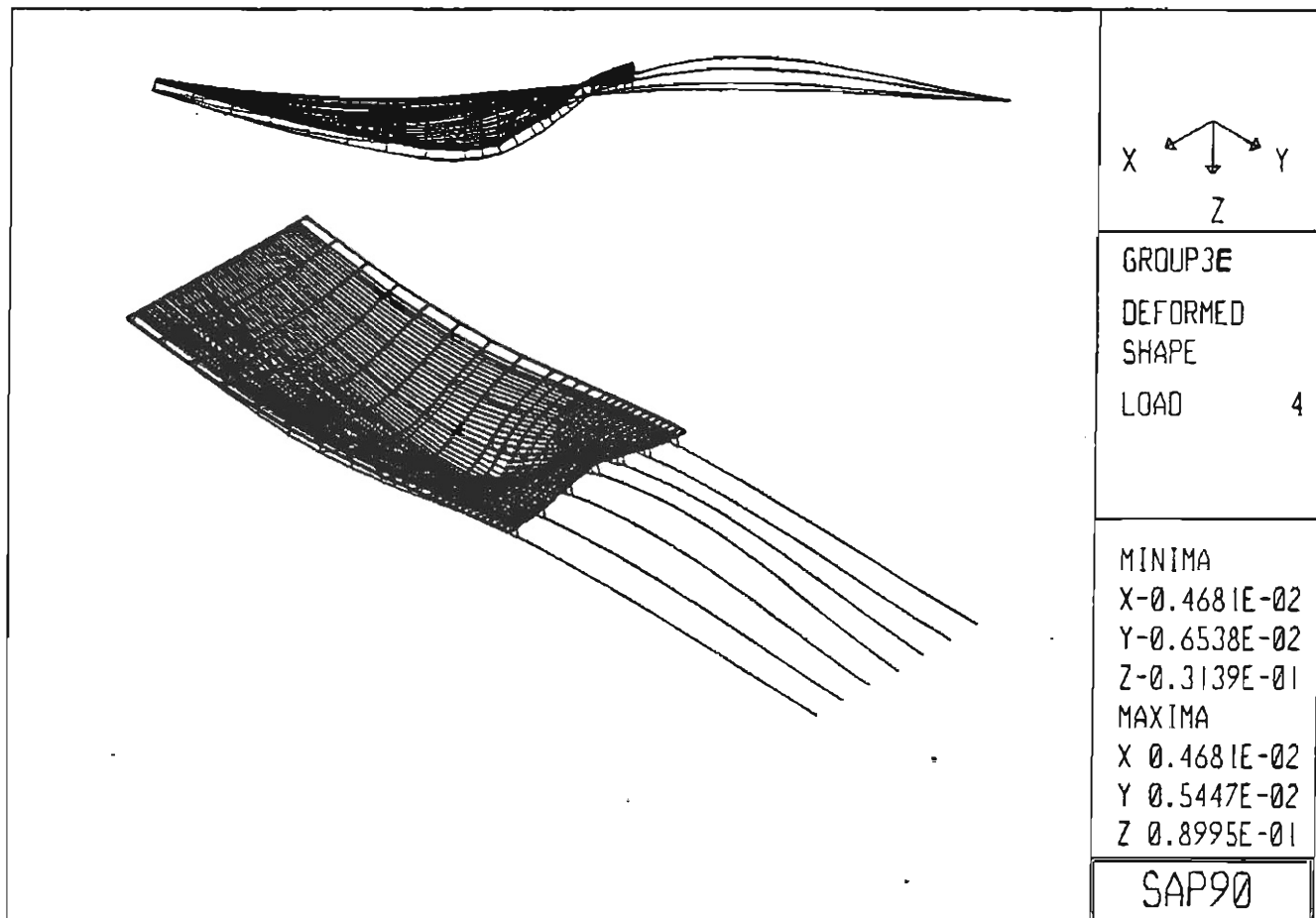


Fig. B.15 Deflection Diagram of Case E of Load Group 3